The Effect of Splice Length and Distance between Lapped Reinforcing Bars in Concrete Block Specimens

A Thesis Submitted to the College of Graduate Studies and Research

In Partial Fulfillment of the Requirements for the Degree of

Master of Science

In the Department of Civil & Geological Engineering

University of Saskatchewan

Saskatoon

By

Denise Stefania Sanchez Contreras

PERMISSION TO USE

In presenting this thesis in partial fulfilment of the requirements for a Postgraduate degree from the University of Saskatchewan, I agree that the Libraries of this University may make it freely available for inspection. I further agree that permission for copying of this thesis in any manner, in whole or in part, for scholarly purposes may be granted by the professor or professors who supervised my thesis work (Dr. Lisa R. Feldman) or, in their absence, by the Head of the Department or the Dean of the College in which my thesis work was done. It is understood that any copying or publication or use of this thesis or parts thereof for financial gain shall not be allowed without my written permission. It is also understood that due recognition shall be given to me and to the University of Saskatchewan in any scholarly use which may be made of any material in my thesis.

Requests for permission to copy or to make other use of material in this thesis in whole or part should be addressed to:

Head of the Department of Civil and Geological Engineering
University of Saskatchewan
Engineering Building
57 Campus Drive
Saskatoon, Saskatchewan, S7N 5A9
Canada

ABSTRACT

The tensile resistance of No. 15 lap spliced reinforcing bars with varying transverse spacing and lap splice length was evaluated in full-scale concrete block wall splice specimens. The range of the transverse spacing between bars was limited to that which allowed the bars to remain within the same cell, and included the evaluation of tied spliced bars in contact. Two-and-a-half block wide by three course tall double pullout specimens reinforced with contact lap splices were initially used to determine the range of lap splice length values to be tested in the wall splice specimens such that bond failure of the reinforcement occurred. The double pullout specimens were tested in direct tension with six replicates per arrangement. Three values of lap splice length: 150, 200, and 250 mm, were selected from the testing of the double pullout specimens and tested in the wall splice specimens in combination with three values of transverse spacing: 0, 25, and 50 mm, with three replicates per configuration. A total of twenty-seven two-and-a-half block wide by thirteen course tall wall splice specimens reinforced with two lap splices were tested in four-point loading. Both the double pullout and the wall splice specimens were constructed in running bond with all cells fully grouted.

The tensile resistance of the lap spliced bars in the double pullout specimens was measured directly. The contact lap splices with a 150, 200, and 250 mm lap splice length developed approximately 38, 35 and 29% of the theoretical yield load of the reinforcement, respectively. The difference between the mean tensile resistances of the three reinforcement configurations tested in the double pullout specimens was found to be statistically significant at the 95% confidence level. Different than expected, the tensile resistance of the lap spliced reinforcing bars in the double pullout specimens was inversely proportional to the lap splice

length provided. For the short lap splice lengths used in this investigation, the linear but not proportional relationship between bond force and lap splice length known from reinforced concrete is believed to have caused this phenomenon.

An iterative sectional analysis using moment-curvature response was used to calculate the tensile resistance of the lap spliced reinforcement in the wall splice specimens. The calculated mean tensile resistance of the reinforcement increased with increasing lap splice length, and was greater when the bars were in contact. Securing the bars in contact may have influenced the tensile capacity of the contact lap splices as higher stresses are likely to develop as a result of the bar ribs riding over each other with increasing slip. Results of the data analysis suggest that the tensile resistance of non-contact lap splices within the same cell is generally independent of the spacing between the bars. A comparison of the experimental results for the wall splice specimens with the development and splice length provisions in CSA S304.1-04 and TMS 402-11 indicate that both the Canadian and U.S. design standards are appropriate for both contact and non-contact lap splices located within the same cell given the limited test database included in this investigation.

CO-AUTHORSHIP

The experimental and analytical work presented in this thesis was conducted by Denise S. Sanchez Contreras and reviewed by Dr. Lisa Feldman. The test results for the wall splice specimens reported in the experimental program were published in the proceedings of the 12th Canadian Masonry Symposium in Vancouver, Canada, June 2013. A paper summarizing the test and analysis results for the wall splice specimens has been accepted for publication in the ASCE Journal of Structural Engineering.

ACKNOWLEDGEMENTS

First, the author would like to thank God for the blessings, wisdom, and perseverance that He has been bestowed upon her during this research project.

The author would like to express her deepest appreciation and gratitude to Dr. Lisa R. Feldman for her guidance and engagement throughout the learning process of this master thesis. The author also thanks her committee members, Dr. Bruce Sparling and Dr. Moh Boulfiza for their valuable input and support in the preparation of this thesis.

A special thanks goes to Brennan Pokoyoway and Dale Pavier, Structures Laboratory technicians, and journeyman Kim Parenteau and Roy Nicolas from Gracom Masonry, for their assistance with the execution of the experimental program. The author is also thankful to her fellow graduate students for their friendship and help in the construction and testing of the specimens.

Financial support provided by the Saskatchewan Masonry Institute (SMI), the Saskatchewan Centre for Masonry Design (SCMD), the Natural Sciences and Engineering Research Council of Canada (NSERC), and the University of Saskatchewan is also gratefully acknowledged.

Finally, the author would like to thank her parents, Irma Contreras Lopez and Ruben Sanchez Solis, brother, Ruben Aubin, and boyfriend, Carlos Mondragon for their endless love and support – there are no words to convey how much I love you all.

TABLE OF CONTENTS

LIST OF TABLES

LIST OF FIGURES

LIST OF SYMBOLS

A_n	Average net area of the concrete block units
A_s	Cross-sectional area of a reinforcing bar
b	Width of the wall splice specimen
c	Neutral axis depth from the top face
C	Compressive force in the masonry
D	Oven-dry density of the masonry units
d_b	Nominal diameter of a reinforcing bar
d_{eff}	Effective depth of the reinforcing bars
E_m	Modulus of elasticity for masonry
E_s	Modulus of elasticity of the reinforcing steel
E_{sh}	Slope at the initiation of strain hardening of steel
f'_{gr}	In-situ compressive strength of grout
f'_m	Compressive strength of masonry
f_{mi}	Compressive stress at the i^{th} segment
f_s	Tensile stress in the reinforcing steel
f_{ult}	Ultimate stress of the reinforcing steel
f_y	Yield strength of the reinforcement
I	Denotes bar size, as shown, in imperial units
I_{cr}	Cracked moment of inertia of the wall splice specimens
I_{eff}	Effective moment of inertia of the wall splice specimens
I_g	Gross moment of inertia of the wall splice specimens

k_1	Bar location factor (from CSA S304.1-04)
k_2	Bar coating factor (from CSA S304.1-04)
k_3	Bar size factor (from CSA S304.1-04)
K	Accounts for the cover to the reinforcing bar, and the spacing between the bars (from TMS 402-11)
L	Span length of the wall splice specimens
l_d	Development length
L_{eff}	Effective splice length of the reinforcement
L_s	Lap splice length
M_a	Applied moment
M_{cr}	Cracking moment
P	Applied load
P_y	Applied load at yielding of the reinforcement
R	Reaction at support
s_t	Transverse spacing of the reinforcement
T	Tensile force in the reinforcement
u	Average bond stress
V_n	Net volume of the masonry units
x	Distance along the length of a reinforcing bar
Z	Constant for the falling stress-strain curve segment for the masonry prisms
γ	Bar size factor (from TMS 402-11)
Δ_{mid}	Midspan deflection
ε_c	Compressive strain in masonry

ε_{sh} Strain at the initiation of strain hardening

ε_s Tensile strain in the reinforcing steel

ε_{ult} Strain in the steel reinforcement at ultimate stress

ε_x Compressive strain at the extreme fibre

ε_y Strain in the steel reinforcement at yielding

ϕ Curvature

Φ_{cr} Curvature of the cracked section of the wall splice specimen

Φ_{eff} Effective curvature

Φ_g Curvature of the gross section of the wall splice specimen

Φ_i Curvature in the i^{th} segment

ϕ_{uc} Curvature of the uncracked section of the wall splice specimen

CHAPTER 1

INTRODUCTION

1.1 Background

Masonry construction involves the use of small modular units such as clay brick, concrete block, or stone, that are mortared together to form structural elements (Hatzinikolas, 2005). Its use dates back more than 10,000 years, and some very sophisticated structures built by early civilizations are still in existence. In North America, masonry has been used for approximately 500 years; however, the use of reinforced masonry is very recent. Historically, the addition of reinforcement started as an attempt to improve the strength and ductility of masonry, particularly in areas of high seismic activity. The addition of the tensile and shear resistance of the steel, combined with the compressive resistance of the masonry, results in an efficient and cost effective system that is appropriate for modern construction (Hamid, 2005).

To be effective, the steel reinforcement and surrounding cementitious materials must be fully composite. This action is dependent upon bond. Bond can be defined, to a certain extent, as the property achieved by mechanical interlocking and sliding friction between the components of a structure or member (i.e. the steel reinforcement, grout, and concrete block) by means of force transfer between them (Hamid, 2005). Full composite action is assumed in the design of reinforce masonry components, though the mechanisms of force transfer are complicated and not fully understood.

In Canada, the provisions for the design of masonry structures are defined in CSA Standard S304.1-04 (CAN/CSA, 2004a). Most of these provisions, including those for the development and splicing of reinforcement, have been copied directly from the provisions used for reinforced concrete as defined in CSA Standard A23.3-04 (CSA, 2004): Design of Concrete Structures, or determined empirically from the evaluation of existing masonry structures. Certainly, there are similarities between concrete and masonry, but there are also important differences. Unlike reinforced concrete, in which reinforcement can be accurately placed with stirrups and ties at any required location in a member, reinforcement in masonry is limited to the block cell size, making positioning the bars more complicated. In concrete, as in masonry, bond depends upon the diameter and the development or splice length of the reinforcing bars, the spacing between reinforcement, the compressive stress of the cementitious material, the cover distance to reinforcement, confinement, and the effect of transverse reinforcement. However, in masonry, variables such as the type of block, the block pattern (i.e. running versus stack), the strength of the mortar joints, and the strength of the masonry units add uncertainty to the bond and stress transfer known from concrete (Ahmed & Feldman, 2012).

In masonry structures, lap splicing is a common practice in cases when a structure is taller or longer than the typically produced reinforcing bars. Spliced bars provide the required continuity of the reinforcement along the length or height of the member. Such spliced bars are usually not located in direct contact as they are not typically tied together. An insufficient lap splice length or an excessive transverse spacing between lapped reinforcing bars may lead to a potential bond failure at the location of the splice if their resistance is less than in cases where continuous reinforcement is provided. Although previous research of non-contact lap splices in

reinforced concrete specimens suggests that the spacing between spliced bars actually enhances the bond performance of the reinforcement (Hamad and Mansour, 1996), a review of existing literature did not identify any similar studies related to masonry construction.

Recent research performed at the University of Saskatchewan included an evaluation of double pullout and wall splice specimens reinforced with contact and non-contact lap splices, though the scope of the project was limited to non-contact splices in adjacent cells, 300 mm lap splice lengths, and 15 mm diameter reinforcing bars (Ahmed and Feldman, 2012). The current project extends this previous work to include contact and non-contact lap splices located within the same cell, and evaluates the effect of the lap splice length and transverse bar spacing for No. 15 bars in full-scale concrete block specimens.

1.2 Objectives

The primary objective of this experimental investigation is to evaluate the mean tensile resistance of the lap spliced reinforcement, given varying lap splice lengths and transverse bar spacings, for No. 15 lapped reinforcing bars located within a same block cell in full-scale concrete block wall splice specimens. Replicate specimens were tested to validate the results, and companion specimens were cast and tested to establish the actual material properties of the concrete blocks, mortar, grout, reinforcement, and the masonry assemblage.

The specific objectives of this investigation are:

1. To initially investigate different values of lap splice length using double pullout specimens tested in direct tension, in order to determine an adequate range of values of lap splice length that ensure bond failure.
2. To investigate and compare the mean tensile resistance of the lap spliced reinforcing bars located in the same cell in wall splice specimens given varying lateral bar spacings and lap splice lengths.
3. To perform a regression analysis for the resulting test data to model the relationship between the tensile resistance of the lap spliced reinforcement and the two independent variables: splice length and transverse bar spacing of the reinforcement; and
4. To compare the obtained experimental tensile force in the lap spliced bars to the predicted tensile force as calculated in accordance with the current U.S. and Canadian code provisions for the development and splicing of reinforcement in masonry.

1.3 Methodology and Scope

A total of 18 double pullout and 27 wall splice specimens were constructed by an experienced mason for this experimental program which was divided into two construction and testing stages. In the first stage, double pullout specimens reinforced with contact lap splices were used to determine an adequate range of values of lap splice lengths to ensure that the specimens would fail in bond. Three values of splice length as obtained from the first stage were then tested in full-scale wall specimens using three different transverse bar spacings including bars in contact. Six of the wall splice specimens were constructed as part of the first phase, while the remaining twenty one wall splice specimens were constructed in the second phase.

The double pullout and the wall splice specimens were tested in direct tension and four-point loading arrangements, respectively. The tensile resistance was directly obtained from the load versus displacement relationship for the double pullout specimens, while a numerical analysis, which incorporated the material properties of the actual construction materials, was performed to obtain the lap splice tensile resistance from the load versus midspan deflection relationship as obtained for the wall splice specimens. Crack propagation patterns and failure modes were also compared for the different reinforcement configurations in both specimen types.

Six and three replicates were constructed and tested for the double pullout and the full-scale wall splice specimens, respectively. Dimensions and general parameters used for this experimental design were selected based on the existing literature and previous research performed at the University of Saskatchewan (Ahmed and Feldman, 2012).

1.4 Thesis Outline

This thesis consists of five chapters, a references section, and appendices. The contents of each chapter are briefly described below:

Chapter 1 – This chapter presents the background, general and specific objectives, methodology, and scope of the research program.

Chapter 2 – Provides a synthesis of previous and relevant research projects related to the study of the bond mechanisms in masonry and reinforced concrete construction, the behaviour of

continuous and spliced reinforcement, and contact and non-contact lap splices in concrete block specimens.

Chapter 3 – Provides a detailed description of the experimental design, specimen construction, and testing methods.

Chapter 4 – Presents the results obtained from the testing of companion specimens to establish the material properties, the results of the tensile resistance of the lap spliced bars versus splice displacement for the double pullout specimens, and the load versus midspan deflection and splice resistance for the wall splice specimens. The tensile resistance, failure modes, and crack propagation patterns are compared for the different splice configurations tested in both specimen types. The results of a regression analysis, which modelled the relationship between splice length and lateral bar spacing in the wall splice specimens, and the comparison of the experimental results of the wall splice specimens with the current U.S. and Canadian code provisions are additionally presented and discussed.

Chapter 5 – Provides a summary of the findings and relevant conclusions. A brief section of suggestions for future research is also included.

CHAPTER 2

LITERATURE REVIEW

2.1 Introduction

Embedded steel reinforcing bars are used in concrete block masonry to enhance the tensile and shear capacity of a structure while providing increased ductility (Drysdale and Hamid, 2005). Primarily for ease of construction, such reinforcement is frequently spliced to provide continuity in cases when a structure is taller or longer that the length of typically produced reinforcing bars. Although alternatives exist for reinforcing bar splicing (i.e. mechanical connectors or welded splices), lap splicing, defined as the overlapping of the ends of two parallel bars, represents the most common and cost-effective solution used in reinforced masonry construction (NCMA, 1999).

Typical construction practice generally does not include using tie wire to ensure contact between lap spliced bars. As a result, a transverse spacing up to approximately 50 mm between the lap spliced bars tends to result, which means that these bars are not in a direct contact. A sufficient splice length must be provided to ensure the adequate performance of a structure. A potential bond failure at the location of the splice may result if the resistance is less than in cases when continuous reinforcement is provided. In such cases, the bars cannot develop their full yield capacity.

The force in a lap splice is transferred from one bar to the other through the surrounding grout. The effectiveness of a lap splice therefore relies not only on the reinforcing bars but also

on the composite action between the reinforcement, the grout, and the masonry units. At present, the mechanisms of bond and stress transfer in masonry are not fully understood and therefore have become areas of increased research interest.

This chapter provides a summary of relevant literature related to the bond mechanisms in masonry. An overview of previous investigations of contact and non-contact lap splices in pullout and wall splice concrete block specimens under different loading schemes is also presented.

2.2 Bond Mechanisms in Masonry

A fundamental assumption used as the basis in the flexural analysis of reinforced concrete and masonry members is that the strain in the cementitious materials surrounding the reinforcement is equal to the strain in the reinforcement. In other words, perfect bond is assumed between the cementitious materials and the reinforcement. An adequate development length, l_d, defined as the bonded length of a reinforcing bar required to develop its nominal yield stress at a given critical location (ACI Committee 408, 2003), is therefore required (Drysdale and Hamid, 2005).

Figure 2.1-a) shows a concrete beam reinforced with continuous plain steel bars and subjected to four point bending. Figure 2.1-b) shows the free body diagram of a small segment of one reinforcing bar adjacent to the right hand support. This bar will be in tension as a result of the applied load. The bond stress, u, assumed to be distributed uniformly on the surface of the reinforcement as shown in Figure 2.2-b), is the mechanism that will prevent slippage between the

reinforcement and the surrounding concrete. If the development length is insufficient to fully develop the design stress in the reinforcement, the bond stress resistance will be exceeded and slip of the reinforcing bars will occur, therefore leading to a possible failure of the member (MacGregor and Bartlett, 2000).

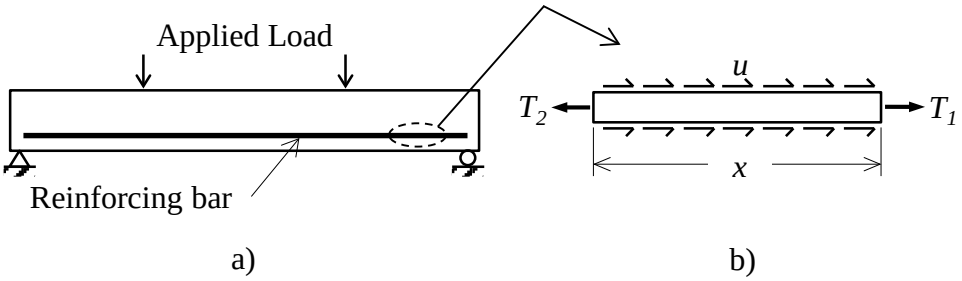

Figure 2.1 Bond stress and development length in plain reinforcement – Modified from Drysdale and Hamid (2005): a) beam under flexure, and b) bond stress on the surface of the reinforcing bar as a result of the applied load.

Neglecting the self-weight of the member in Figure 2.1, the general equation for the required development length, l_d, is derived from horizontal equilibrium of forces from the free body diagram of the reinforcing bar as:

$$T_2\text{-}T_1 = A_s f_y = \pi\, d_b\, u\, l_d \qquad \text{[Eq. 2.1]}$$

where A_s is the cross-sectional area of the reinforcing bar, f_y is the nominal yield strength of the reinforcement, d_b is the nominal bar diameter, and u is the average bond stress. Knowing that $A_s = \pi d_b^{\,2}/4$, the following equation for the development length therefore results:

$$l_d = \frac{f_y d_b}{4u} \qquad \text{[Eq. 2.2]}$$

Equation 2.2 allows for the calculation of the development length required to develop the yield capacity of the reinforcement considering the bond stress as uniformly distributed along the reinforcing bar. However, as several studies have verified (Uniat, 1985; Cheema and Klingner, 1985; Soric and Tulin, 1989), the actual bond stress in the reinforcement is not uniform, but depends upon the type of reinforcement, the development length, the magnitude of the applied load, the masonry or concrete characteristics, the amount of cracking, and bar slip (Soric and Tulin, 1989). Equation 2.2, therefore, does not entirely account for the actual bond forces developed at specific locations along the length of the bars (at the interface between the reinforcement and the cementitious materials), and factors such as the stress concentrations at the bar ribs in the case of deformed reinforcement as will be further discussed in the next section.

Current provisions in CAN/CSA Standard S304.1–04 (R2010): Design of Masonry Structures (CAN/CSA, 2004a) (hereafter referred to as CSA S304.1-04), and TMS402-11/ACI530-11/ASCE5-11: Building Code Requirements for Masonry Structures (MSJC, 2011) (hereafter referred to as TMS402-11), provide modified empirically derived equations to account for the factors influencing bond strength. The required development length of deformed reinforcing bars in tension in CSA S304.1-04 is defined in Clause 12.4.2 (CAN/CSA, 2004a). Provided that the clear cover to the reinforcement is equal to or greater than d_b, the development length for walls having a clear spacing between reinforcing bars greater than $2d_b$, or members with a clear bar spacing of at least $1.4d_b$ containing minimum stirrups or ties within l_d is equal to:

$$l_d = 0.45 k_1 k_2 k_3 \frac{f_y}{\sqrt{f'_{gr}}} d_b \qquad \text{[Eq. 2.3]}$$

For other cases, the development length is given by:

$$l_d = 0.6 k_1 k_2 k_3 \frac{f_y}{\sqrt{f'_{gr}}} d_b \qquad \text{[Eq. 2.4]}$$

In these two equations, k_1 is a bar location factor equal to 1.3 for horizontal reinforcement and 1.0 for other cases, k_2 is a coating factor equal 1.0 for uncoated reinforcement and 1.2 or 1.5 for different epoxy-coated reinforcement types, k_3 is a bar size factor equal to 0.8 for No. 20 and smaller bars, and 1.2 for No. 25 and No. 30 bars, f_y is in MPa and is equal to the yield strength of the reinforcement, f'_{gr} is equal to the in-situ compressive strength of the grout in MPa, and d_b is the nominal bar diameter in mm.

TMS402-11 (MSJC, 2011) defines the required development length for reinforcing bars in tension or compression in Clause 2.1.7.3, as follows:

$$l_d = \frac{1.5 d_b^2 f_y \gamma}{K \sqrt{f'_m}} \qquad \text{[Eq. 2.5]}$$

where, d_b is the bar diameter in mm; f_y is the yield strength of the reinforcement in MPa; γ is equal to 1.0 for No. 3 (I) though No. 5 (I) bars, 1.3 for No. 6 (I) through No. 7 (I) bars, and 1.5 for No. 8 (I) through No. 11 (I) bars; K is the smallest of the minimum masonry cover, the clear spacing between adjacent reinforcement splices, and $9d_b$ in mm; and f'_m is equal to the specified compressive strength of the masonry in MPa.

The concepts of development length and splice length are closely related, as the development length is the basis for the calculation of the length of lap for splices in tension as stated in Clause 12.5.4.2 in CSA S304.1-04 (CAN/CSA, 2004a), and for splices in tension or compression in Clause 2.1.7.7.1 in TMS402-11 (MSJC, 2011). Two types of lap splices are

defined in CSA S304.1-04: Class A splices, in which the maximum percentage of spliced reinforcement is less than 50 and the ratio of the provided to required area of reinforcement is equal to or greater than two, and Class B splices in which any other splice configuration is used. The lap splice length in accordance with CSA S304.1-04 is calculated as $1.0l_d$ for Class A splices and $1.3l_d$ for Class B splices, where l_d is calculated with Equations 2.3 or 2.4 and shall be no less than 300 mm. The lap splice length, l_d, as calculated using Equation 2.5 shall not be less than 305 mm in accordance with TMS402-11.

2.3 Behaviour of Continuous and Spliced Tension Reinforcement

Figure 2.2 illustrates the bond interaction forces occurring in continuous and spliced deformed reinforcement in a flexural member when the steel bars are in tension. As shown in Figure 2.2-a) for $T_1 = 0$ and $T_2 \neq 0$, the bearing action of the bar ribs against the surrounding material for a continuous deformed bar creates an inclined compressive force whose longitudinal and radial components cause shearing between the bar deformations and the grout, and circumferential tensile forces, respectively. Pullout of the reinforcement occurs by shearing if the shear resistance of the grout is exceeded, whereas splitting cracks occur if the circumferential tensile forces exceed the tensile resistance of the surrounding grout (Schuller et al., 1993).

In lapped reinforcing bars, an increased splice length will reduce the nominal bond stress of the reinforcement thus allowing the bars to fail by pullout or yielding before the grout tensile capacity is exceeded. However, as shown in Figure 2.2-b), an additional lateral force is created as a result of the relative movement of the bars in contact riding over each other with increasing slip. Such additional stresses often result in longitudinal splitting failure of the masonry

specimen. The reduced clear cover to the exterior masonry surface that results when using spliced reinforcement also increases the probability of splitting cracks developing parallel to the reinforcing bars (Schuller et al., 1993).

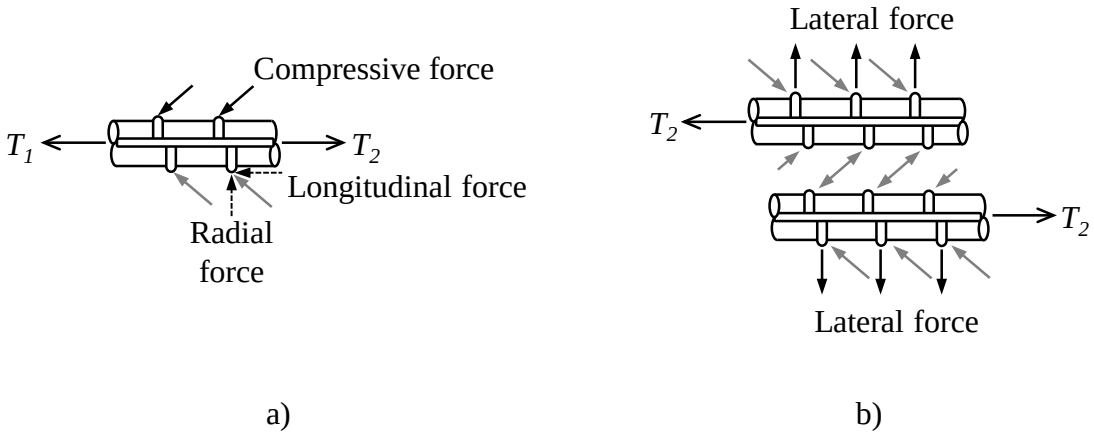

Figure 2.2 Bond interaction forces in deformed reinforcement – Modified from Schuller et al. (1993): a) bond, shear, and radial forces exerted by a continuous bar, and b) additional lateral force occurring in spliced reinforcement due to the bar ribs riding over each other.

Non-contact lap splices have been studied in reinforced concrete (Sagan et al., 1991; Hamad and Mansour, 1996); however, very little research has been identified related to non-contact lap splices in reinforced masonry. Figure 2.3 illustrates the behaviour of a non-contact lap splice, which has been represented in reinforced concrete using a truss analogy in which the transfer of forces between the spliced reinforcing bars occurs as a result of the development of diagonal compressive struts between the bars. Figure 2.3 shows that the effective splice length of a non-contact lap splice is equal to the transfer length determined based upon the angle of the inclined struts. The overall splice length is therefore equal to the effective splice length plus an additional distance which is a function of the inclination of the struts and the transverse spacing between the bars (McLean and Smith, 1997). The diagonal compressive struts have been

commonly observed at a 45 degree angle, however research conducted by Sagan et al. (1991) suggest that they may range from 20 to 70 degrees.

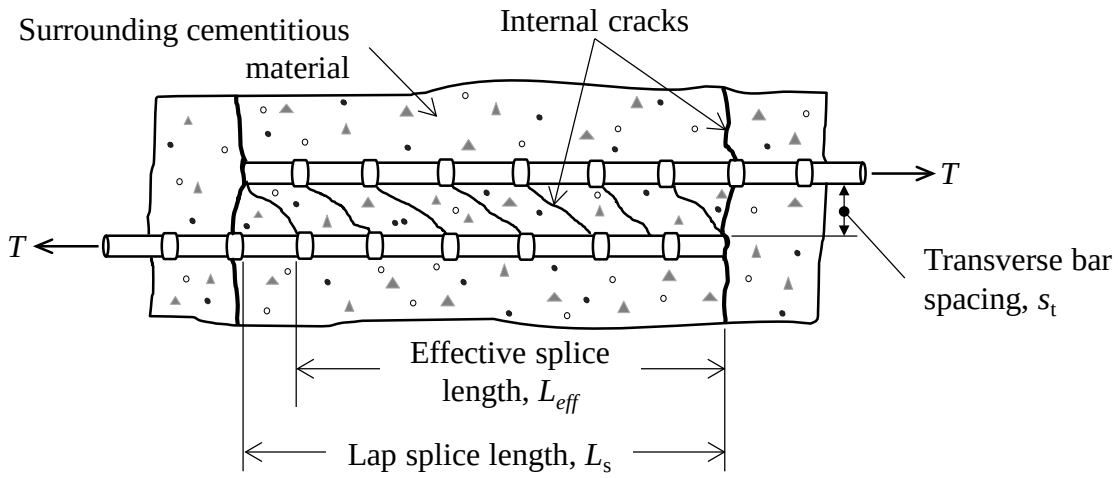

Figure 2.3 Behaviour of non-contact lapped splices – Modified from MacGregor (1997).

2.4 Previous Research Related to Contact and Non-Contact Lap Splices in Masonry

Different test specimens and configurations have been used in the past to study the behaviour of spliced reinforcement in masonry. However, two specimen types were of particular interest for the present experimental investigation: pullout and wall splice specimens. Reasons for this are discussed in the paragraphs that follow.

Pullout specimens have been widely used for research as they represent a simple and economical way to test lap splices. Their ease of construction also allows for a larger number of specimens to be cast and tested within a single project. Although the design and test methods for pullout specimens have improved over time, this type of specimen is unable to create a realistic stress state at the interface between the reinforcement and the surrounding grout. Recent research

performed at the University of Saskatchewan statistically confirms that they do not represent the behaviour of masonry walls subjected to out-of-plane bending (Ahmed and Feldman, 2012), though they may still effectively model the splice capacity in walls subjected to in-plane bending (Mjelde, 2008).

Although the construction, instrumentation, and analysis of wall splice specimens is more complex than for pullout specimens, wall splice specimens have proven to represent the behaviour of full-sized structures subject to in-plane bending, as a more realistic stress state at the interface between the reinforcement and the surrounding material is created (ACI Committee 408, 2003). Unlike pullout specimens, in which the tensile load is applied directly to the reinforcing bars, wall splice specimens under flexure induce tensile stresses in the reinforcing bars and compressive stresses in portions of the surrounding grout (Ahmed, 2011).

The following subsections present a brief summary of relevant experimental investigations related to the study of contact and non-contact lap splices in double pullout and wall splice concrete block masonry specimens. The research studies corresponding to each specimen type are presented separately in chronological order.

2.4.1 Stack pullout specimens with contact lap splices as tested by Schuller et al. (1993)

The effects of bar diameter, masonry unit width, and splice length, as related to the behaviour and strength of contact lap splices in concrete block pullout specimens, were investigated by Schuller et al. (1993). All specimens were constructed in stack bond using half concrete blocks of varying sizes: 4, 6, 8, 10, and 12 in. (102, 152, 203, 254, and 305 mm), and

reinforced with contact lap splices using either No. 4 (I), No. 6 (I), No. 8 (I), or No. 11 (I) deformed steel bars centered within the common grouting cell space. The specimen height was varied according to the different splice length configurations and ranged from 12 to 72 in (305 to 1830 mm). All specimens were fully grouted.

Figures 2.4-a) and b) show the loading arrangement for a stack pullout specimen as tested by Shuller et al., and its cross-section, respectively. Monotonic tensile loading was applied at the ends of the bars extending beyond the top and bottom of the specimens. Electronic displacement transducers, located at the specimen ends, were used to measure the load versus slip behaviour, bar slip, and the relative slip between bars. This testing setup had the advantage of eliminating the confining forces on the grout observed in previous tests with continuous bar stack pullout specimens (Baynit, 1980; Soric, and Tulin, 1989). The detailed description of these works is not relevant to the current investigation and so is not included. The eccentricity between the loads applied to the lapped reinforcing bars extending from each end of the specimens produced an in-plane bending in addition to the axial force in the specimens and complicated the interpretation of the results. Nonetheless, the results of this research program were used as the basis for the splice length provisions in TMS 402-11 (MSJC, 2011).

Three failure mechanisms were identified and described: brittle failure, observed in specimens with short lap lengths at loads below that causing yielding of the reinforcement; bar yielding and/or bar pullout followed by specimen splitting observed in specimens experiencing limited yielding of the reinforcing bars likely as a result of the additional lateral stresses in the surrounding grout; and, yielding of the reinforcement followed by bar fracture or bar pullout,

observed in specimens with the longest lap splice lengths which, in combination with a sufficient clear cover to the reinforcement, allowed for highly ductile splices.

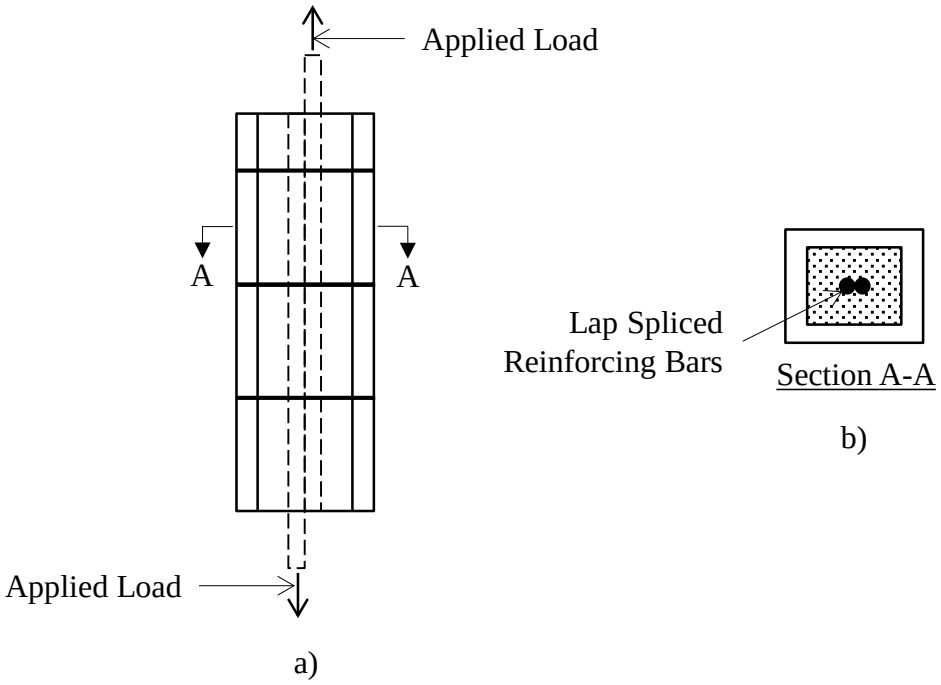

Figure 2.4 Stack pullout specimen with contact lap splices as tested by Schuller et al. – Modified from Schuller et al. (1993): a) elevation, and b) cross-section.

Sculler et al. (1993) concluded that wider block units allow for a higher tensile resistance of the splices as they provide increased cover distance to the reinforcement. In general, the tensile resistance of the lap splice was inversely proportional to the bar diameter, as larger diameter bars increase the tensile stresses that must be resisted by the surrounding grout therefore leading to a possible failure of the specimens at loads below that causing yielding of the reinforcement. Specimens constructed with 8 in. (203 mm) wide masonry units and reinforced with No. 4 (I) bars attained yielding with a minimum splice length of 12 in. (305 mm),

while those constructed with the largest bar size (i.e. No 11 (I) bars) did not allow for full development of the reinforcement in any configuration.

2.4.2 NCMA's double pullout specimen test program (1999)

An experimental program to evaluate the current splice length provisions in TMS 402-11 (MSJC, 2011), and the Uniform Building Code (ICBO, 1997), was carried out by the National Concrete Masonry Association (NCMA) in 1999 (NCMA, 1999). Figure 2.5 shows the details of the testing setup and the specimens as designed for this investigation. Double pullout specimens, constructed in a running bond pattern with all cells fully grouted, and reinforced with two pairs of lap spliced deformed bars in the second and fourth cells from the left top of the cross-section as shown in figure 2.5-b) were tested under direct tension. A testing frame consisting of four steel sections bolted together was adjusted to the height of each specimen and varied for the different splice lengths tested. High strength rods were attached to the reinforcing bars extending beyond each end of the specimens by mechanical couplers. The high strength bars were, in turn, bolted to the steel frame at one side and connected to a pair of hydraulic rams bearing against the steel frame at the other side (NCMA, 1999).

Specimens were subjected to monotonically increasing loading. Failure was defined by bar pullout, rupture of the reinforcement, or longitudinal splitting. Similar to Schuller et al. (1993), the NCMA pullout test setup eliminated the confining pressures on the grout as a symmetrical load at both ends of the reinforcement was applied. The symmetry due to the use of two spliced bars in a single specimen also minimized the in-plane bending observed in Schuller et al. (1993) specimens and thus simplified the analysis of the resulting test data.

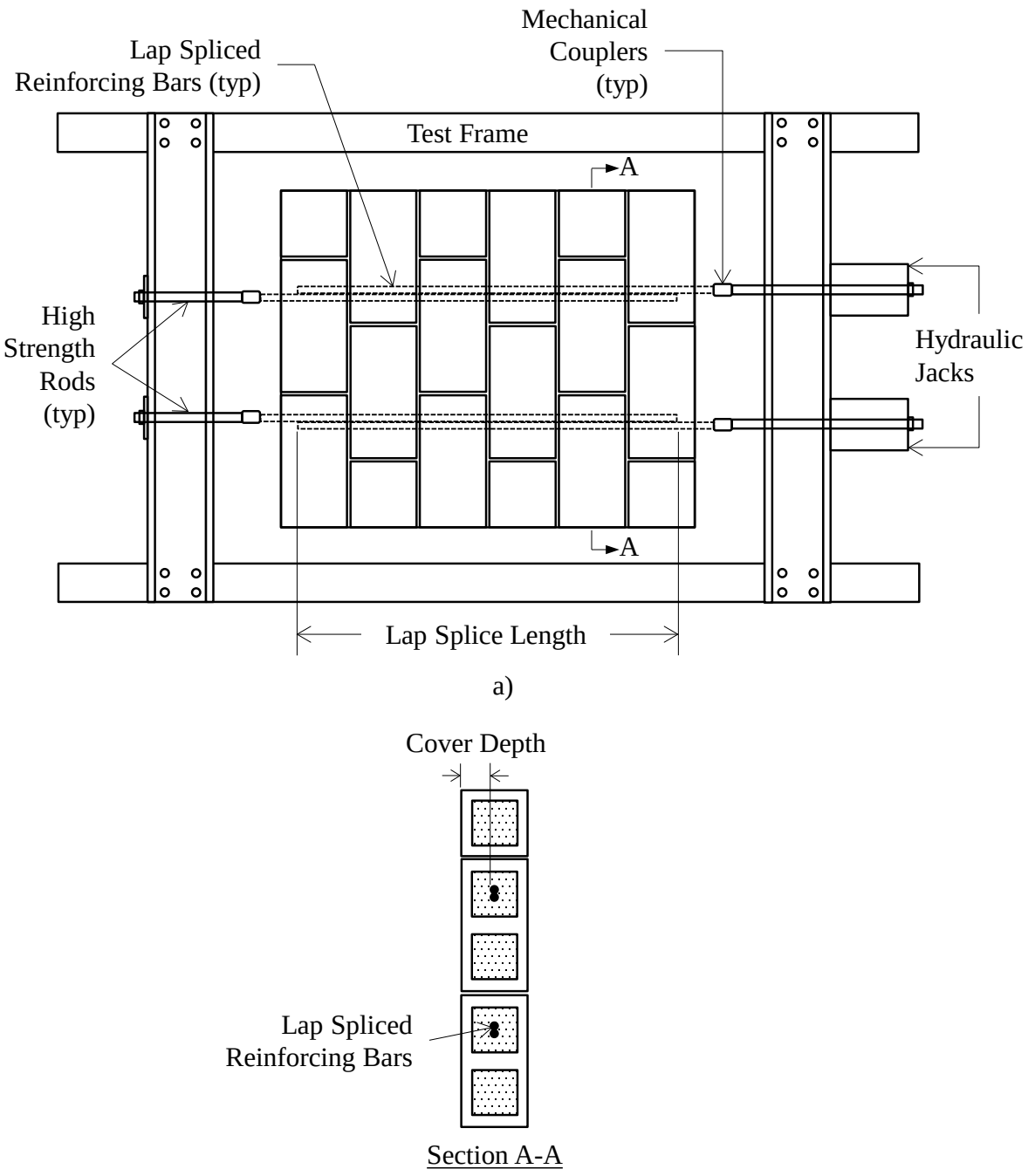

Figure 2.5 NCMA's double pullout specimens – Modified from NCMA (1999): a) test setup, and b) specimen cross-section.

The investigated parameters included splice length, compressive strength of the grout and the masonry, clear cover of the reinforcement, bar diameter, and block size. No. 4 (I) to No. 9 (I)

steel bars, splice lengths of 32 to 113d_b, cover depths of 2 and 3 in. (51, and 76 mm), and 8 and 12 in. wide concrete blocks (203 and 305 mm) were combined in 36 different configurations. The splice length parameters were chosen in an attempt to ensure that the reinforcement attained 125% of its yield capacity. Three replicates were tested per geometric configuration.

In general, yielding of the reinforcement occurred in all configurations, and the predominant observed failure mode was longitudinal splitting of the specimens. An increase in the compressive strength of the masonry from 1700 psi (11.72 MPa) to 4070 psi (28.06 MPa) (i.e. a 140% increase) improved the splice capacity of the reinforcement by approximately 27% in specimens reinforced with No. 4 (I) to No. 7 (I) bars. The cover depth of the reinforcement also showed to have influence on the splice tensile capacity: specimens with a cover depth of 3 in. (76 mm) achieved 8.5 and 18% higher tensile loads for No. 6 (I) and No. 7 (I) bars, respectively, as compared to those with the same bar sizes with 2 in. (51 mm) cover depth. In general, longer splice lengths allowed for higher tensile resistances in all configurations; however, a slight decrease in the tensile resistance was noted for lap splice lengths exceeding 115 in. (2921 mm) in specimens reinforced with No. 9 bars.

2.4.3 Double pullout specimens with spliced bars in contact as tested by De Vial (2009)

The effect of bar size, splice length, transverse reinforcement, and the distribution and positioning of the reinforcing bars in influencing the tensile resistance of contact lap spliced reinforcing bars in double pullout specimens was investigated by De Vial (2009). Figure 2.6 shows a typical pullout specimen as tested. Twelve pullout specimens were constructed with standard 8 in. wide blocks in a running bond pattern and with all cells fully grouted. Specimens

were reinforced with either No. 8 (I) or No. 6 (I) deformed bars with splice lengths of 36 and 48 in. (914 and 1219 mm), and 27 and 36 in. (686 and 914 mm), respectively. The height of each pullout specimen was selected to accommodate the lap splice length and the transverse reinforcement which consisted of two No. 4 (I) bars with a 90 degree hook at both ends. The transverse reinforcement was located outside the splice region in half of the specimens and inside the splice region in the other half.

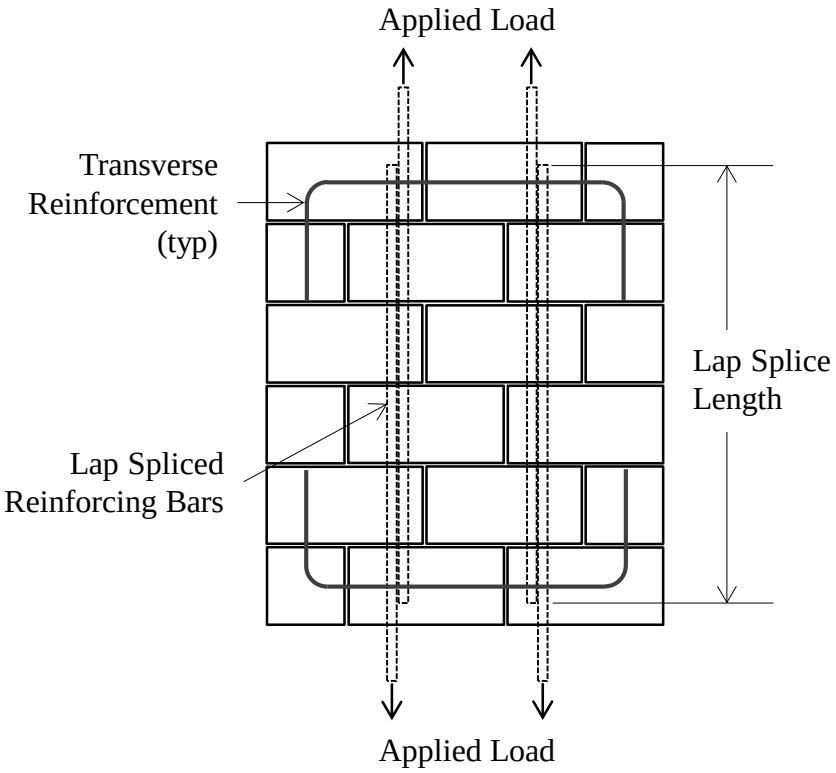

Figure 2.6 De Vial's test setup and transverse reinforcement design within the lap splice region – Modified from De Vial (2009).

All specimens were subjected to direct tension using a similar testing frame and loading arrangement as that used by the NCMA (NCMA, 1999). Figures 2.7-a) through 2.7-c) show the different vertical reinforcement distributions as tested: centered No. 6 (I) or No. 8 (I) bars, pairs

of No. 6 (I) spliced bars within a same cell, and staggered contact lap splices of No. 6 (I) bars, respectively. All specimens achieved yielding of the reinforcing bars.

Regardless of the splice length or the location of the transverse reinforcement, specimens in which two pairs of splices were provided within a single cell showed the most critical damage in the form of splitting and transverse cracking likely as a result of the reduced cover distance and the number of bars within the cell. Significant splitting was also observed for specimens reinforced with staggered lap splices; however, it was less severe than for specimens with two lap splices located within the same block cell. No. 6 (I) single centered lap spliced bars with 27 and 36 in. splice lengths (686 and 914 mm), typically failed by longitudinal splitting.

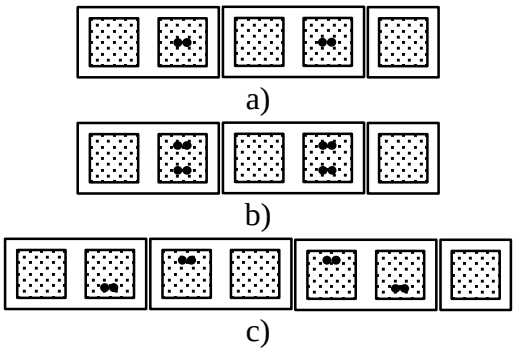

Figure 2.7 Reinforcement distributions as tested by De Vial – Modified from De Vial (2009): a) centered No. 6 or No. 8 bars, b) pairs of No. 6 spliced bars within the same cell, and d) staggered No. 6 bars.

In general, the tensile resistance of the reinforcing bars was higher for specimens reinforced with offset lap splices located in adjacent cells (as shown in Figure 2.7-c)) than for those with two pairs of splices within a single cell (as shown in Figure 2.7-b)). Transverse reinforcement located inside of the splice region allowed for a 7% increase in the splice capacity;

however, the lack of replicate specimens did not allow for a statistical evaluation of the results in this experimental program.

2.4.4 Wall splice specimens tested by Uniat (1983)

The load capacity of reinforced masonry walls and the bond and development length criteria for continuous and spliced deformed reinforcement were investigated by Uniat (1983). Figures 2.8-a) and b) show an elevation and the loading arrangement, respectively, for the wall splice specimens used in this investigation. Nineteen wall splice specimens, one-and-a-half blocks wide and eighteen courses tall, were constructed with standard 200 mm blocks in a running bond pattern, and tested vertically under lateral loading applied at the third points. Different reinforcement arrangements were provided in seventeen out of the nineteen walls constructed, with the reinforcement located in the middle cell. Only the reinforced cell was grouted. Two wall specimens were unreinforced. Strain gauges were attached to the reinforcing bars outside of the lap splice length to allow for the force in the reinforcement to be calculated. One-quarter inch by 3 in. (6.4 mm x 76 mm) square steel plates were welded to the ends of all of the reinforcing bars to prevent bar slippage and to ensure that failure occurred within the lap splice length.

The parameters investigated included No. 10, No. 15, and No. 20 bars spliced with a minimum length of 200, 350, and 500 mm, respectively, and were selected based on previous research by Baynit (1980) in an attempt to ensure the specimens to fail in bond rather than in flexure. Figures 2.9-a) through d) show the different reinforcement arrangements tested in the wall splice specimens: continuous reinforcing bars (Figure 2.9-a)), contact lap splices (Figure

2.9-b)), non-contact lap splices with the bars located at each face of the wall (Figure 2.9-c)), and two pairs of contact lap splices within the same cell (Figure 2.9-d)). The behavior and failure modes for the different reinforcement configurations were evaluated and compared.

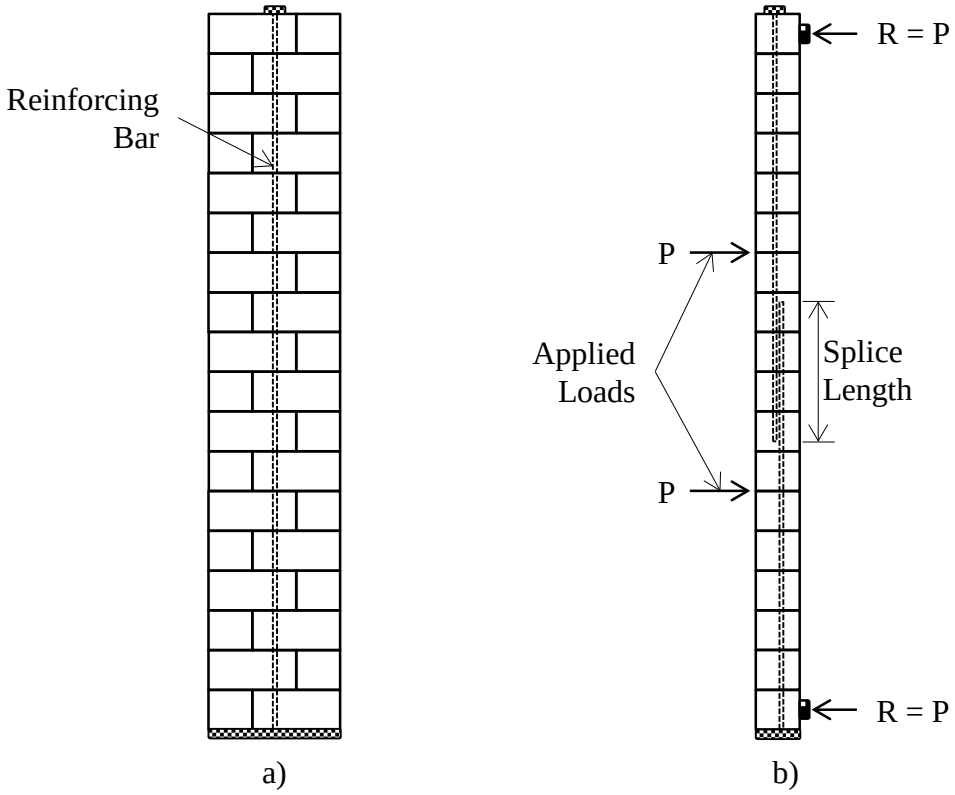

Figure 2.8 Contact lap splices in wall specimens as tested by Uniat – Modified from Uniat (1985): a) elevation, and b) side view and loading setup.

Results showed that all specimens attained yielding of the reinforcement with no indication of bond failure. The calculated moment and measured deflection at midspan varied linearly until yielding of the reinforcement initiated. The deflection at midspan then increased rapidly following yielding of the reinforcement until failure. In general, specimens reinforced with continuous longitudinal bars behaved similarly to those in which spliced bars were

provided. Specimens reinforced with two pairs of lap spliced bars within the same cell showed higher moment capacities and lower deflections at midspan than specimens reinforced with single lapped bars, though their moment-deflection curves had a similar form. The specimen in which non-contact lap splices were provided within the same cell showed a lower moment capacity and larger deflection at midspan at failure as compared to the specimens reinforced with contact lap splices.

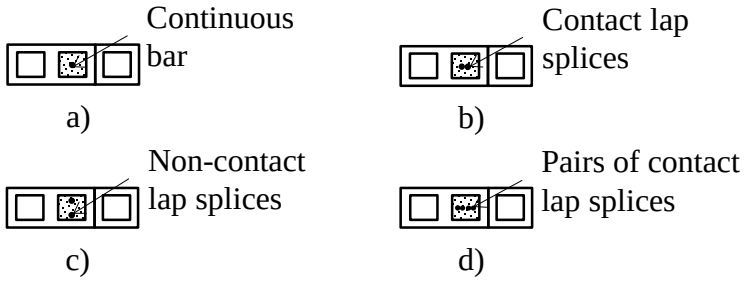

Figure 2.9 Reinforcement arrangements as tested by Uniat (1983): a) continuous reinforcing bar, b) contact lap splices, c) non-contact lap splices, and d) pairs of contact lap splices within the same cell.

The self-weight of the specimens in this test setup likely affected the lateral load carrying capacity of the walls as the resulting axial stress created a compression force and reduced the tension within the splice length (Ahmed, 2012). Furthermore, the use of internal instrumentation modified the bond at the reinforcing bar/grout interface, likely influencing the splice capacity.

2.4.5 Wall splice specimens tested by Ahmadi (2001)

The effects of bond loss in flexural walls reinforced with deformed 12 and 16 mm-diameter lap spliced reinforcing bars were investigated by Ahmadi (2001). Figures 2.10-a) and b)

show the elevation and cross-section of a typical wall splice specimen, respectively. A total of twenty wall splice specimens, one-and-a-half blocks wide and seven blocks high, were constructed in a running bond pattern and were reinforced with the splices located at mid-height in the outermost block cells. Only cells containing reinforcement were grouted. The lap splice length was 600 mm for the 12 mm-diameter bars and 700 mm for the 16 mm-diameter bars. A smooth wrap tape was used within the lap splice length to debond the spliced bars from the surrounding grout. Lap splices were debonded 0 (i.e. no wrap tape), 25, 50, 75, or 100% (i.e. splice length completely debonded). Figure 2.10-c) shows the four-point loading test setup used to test the specimens in their horizontal position.

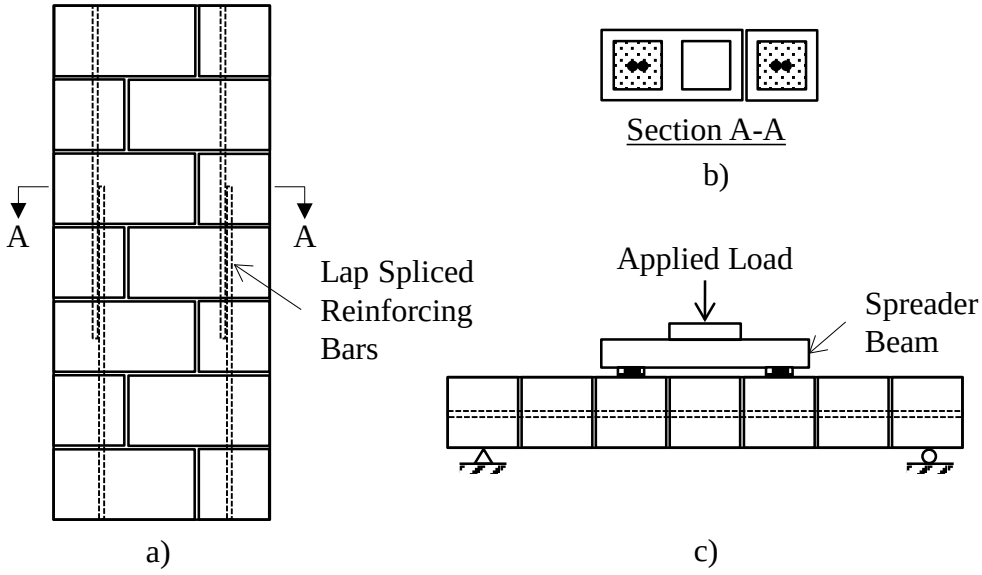

Figure 2.10 Lap splices in wall specimens as tested by Ahmadi – Modified from Ahmadi (2001): a) elevation, b) cross section, and c) test setup.

Results showed that specimens in which the lap splice length was debonded up to 25%, typically failed by shear with diagonal cracks starting at the supports, while all specimens in which the lap splice length was 50, 75, or 100% debonded, failed by bar pullout with the cracks

starting at midspan. In general, the flexural strength of the wall splice specimens decreased with an increased percentage of debonded lap splice length. The load carrying capacity was higher for specimens reinforced with 16mm-diameter lap spliced bars than for specimens with 12 mm-diameter bars at the same percentage of debonded splice length.

2.4.6 Pullout and wall splice specimens tested by Mjelde (2008)

An experimental investigation to evaluate the performance of lap splices in double pullout and wall splice specimens was performed at Washington State University (Mjelde, 2008). Nine wall splice specimens that were three-blocks wide and thirteen courses tall, and nine double pullout specimens with the same cross-section but with varying height to accommodate the different lap splice lengths tested were constructed in running bond, and subjected to in-plane bending and direct tension, respectively. The longitudinal deformed reinforcement in all specimens was spliced at mid-height and transverse reinforcement was provided every other course. Pullout specimens were tested in the horizontal position with a similar testing frame and loading arrangement as that used by NCMA (NCMA, 1999) as described in section 2.3.2 in this chapter.

Figure 2.11 shows the construction details and testing setup of a typical wall splice specimen. Each wall splice specimen was constructed on a reinforced concrete footing which was anchored to the laboratory strong floor and provided vertical and rotational restraint at the base of the wall. Ninety-degree hooks were used to cast the bottom vertical reinforcement into the concrete footing. A steel frame was bolted at the 11^{th} course of the wall and connected to a hydraulic actuator to apply the in-plane loading. String potentiometers attached to the concrete

block were used to measure the lateral displacement of the wall at the level of the applied load (i.e. at the 11th course), and strain gauges were used to measure the strain of the reinforcing bars at the interface between the wall and the concrete footing.

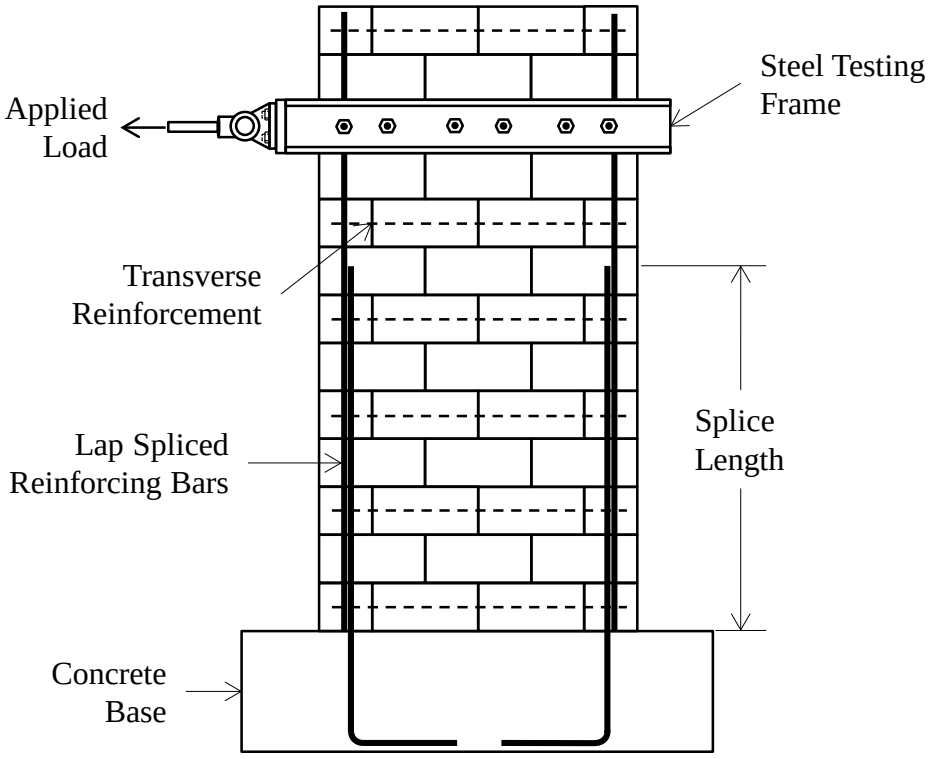

Figure 2.11 Testing setup and reinforcement arrangement of the wall splice specimens tested by Mjelde – Modified from Mjelde (2008).

Figures 2.12-a), b), c), and d) show the different reinforcement configurations that were tested in both the double pullout and wall splice specimens. Three specimens were longitudinally reinforced with No. 8 (I) bars in both exterior cells and were transversely reinforced with a No. 4 (I) bar in every other course (Figure 2.12-a)); one specimen was longitudinally reinforced with No. 8 (I) bars placed in the outer cells and horizontally reinforced in alternate courses with a pair of No. 3 (I) bars (Figure 2.12-b)); two specimens were reinforced with No. 6 (I) spliced bars in

the two exterior-most cells on both sides and horizontally reinforced every other course with a single No. 4 (I) bar (Figure 2.12-c)); and, three wall splice specimens were transversely reinforced every other course with a single No. 4 (I) straight bar placed between two pairs of No. 6 (I) lap splices located in the same cell (Figure 2.12-d)). Splice lengths of 36, 48, and 60 times the nominal bar diameter, d_b, for both the No. 6 (I) and No. 8 (I) bars were tested.

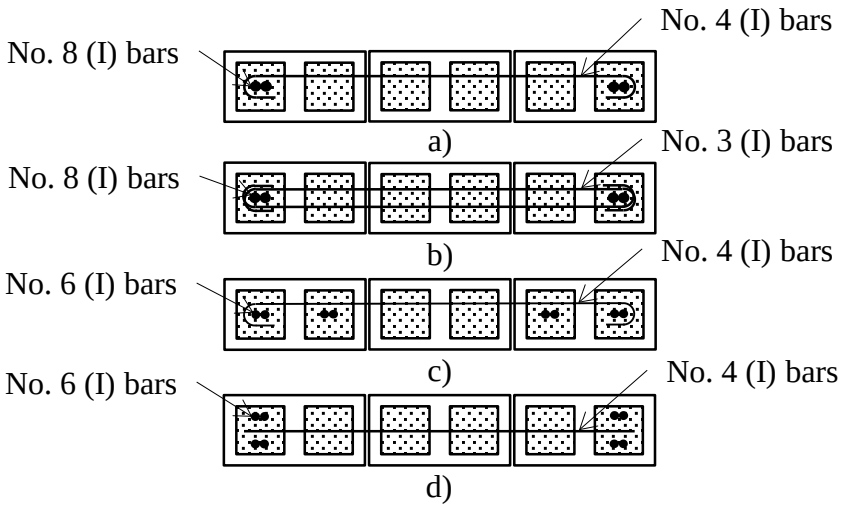

Figure 2.12 Reinforcement arrangement in pullout and wall splice specimens as tested by Mjelde – Modified from Mjelde (2008): a) centered No. 8 bars with single transverse reinforcement, b) centered No. 8 bars with double transverse reinforcement, c) centered No. 6 bars in the two outer cells with single transverse reinforcement, and d) two pairs of spliced No. 6 bars with single transverse reinforcement.

The lap splice length requirements in ACI 530-05: Building Code Requirements for Masonry Structures (MSJC, 2005), and the International Building Code 2006 (IBC, 2006) were compared to the experimental results, and a comparison of the lap splice resistance and failure modes for both specimen types (i.e. the double pullout and the wall splice specimens) was also evaluated. Yielding of the reinforcement was attained for all reinforcement configurations in

both the double pullout and the wall specimens, and all specimens failed by splitting of the masonry assemblage. Increased lap splice lengths allowed for an increased load resisting capacity and lateral displacements in the wall specimens. Longer lap splice lengths also allowed for higher stresses to develop in the longitudinal reinforcement in both specimen types.

Results indicated that the clear cover distance to the reinforcement has a significant influence in the lap splice performance, as specimens reinforced with offset spliced bars failed at lower stresses as compared to those with the splices centered within a block cell. Specimens reinforced with two pairs of splices within a single cell attained lower stresses in the reinforcing bars than those with single splices. A significant difference in the lap splice resistance was not found between the two specimen types.

MSJC (2005) provisions appeared to be accurate for No. 6 (I) bars but overly conservative for No. 8 (I) bars. The simplified equation for lap splice length provided in the International Building Code (IBC, 2006), proved accurate for the walls with No. 6 (I) and No. 8 (I) bars with No. 4 (I) transverse reinforcement, but overly conservative for double pullout specimens with offset reinforcement. Replicate specimens were not tested in this investigation.

2.4.7 Contact and non-contact lap splices tested by Ahmed and Feldman (2012)

An evaluation of contact and non-contact lap splices in double pullout and wall splice specimens was recently completed at the University of Saskatchewan (Ahmed and Feldman, 2012). A total of 32 specimens were constructed and tested to evaluate the splice resistance of No. 15 deformed reinforcing bars, and to determine whether a statistically significant difference

between the splice arrangements and specimen types existed. Eight replicates per specimen type were constructed for contact and non-contact lap splices with all cells fully grouted. A 300 mm splice length was used for all specimens. Figures 2.13 and 2.14 show the details of the splice configurations used in the double pullout and the wall splice specimens. Figures 2.13-a) and 2.14-a) show the geometry of the double pullout and the wall splice specimens with contact lap splices, respectively, while Figures 2.13-b) and 2.14-b) show the geometry of the same specimen types containing non-contact lap splices.

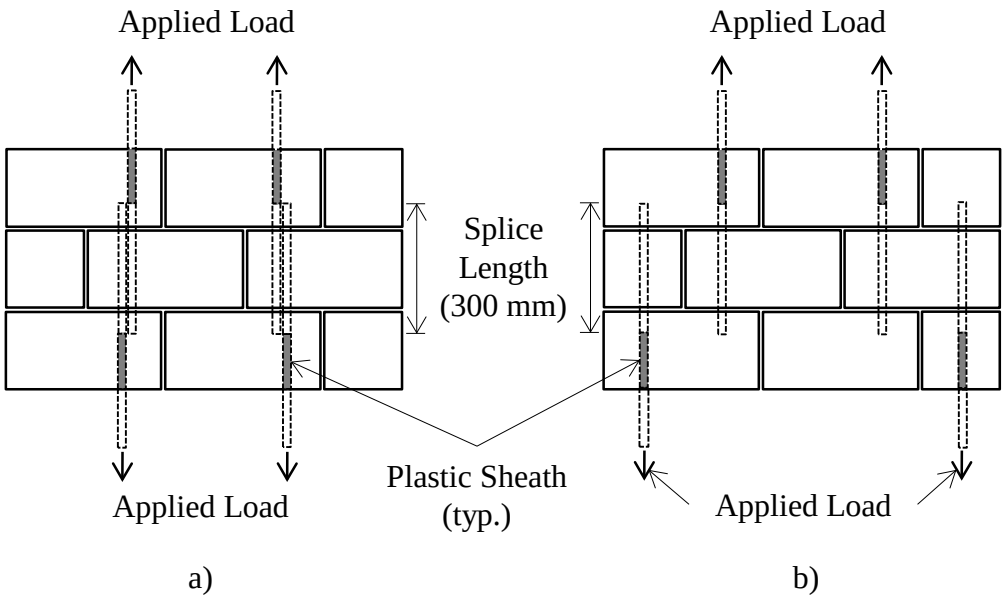

Figure 2.13 Double pullout specimens as tested by Ahmed and Feldman (2012) – Modified from Ahmed and Feldman (2012): a) with contact lap splices, and b) with non-contact lap splices.

Both specimen types were two-and-a-half blocks wide and constructed in running bond, with the splices located at mid-height. Contact lap splices were tied with wire and centered in the second and fourth specimen cells from the left end of the specimen as shown (Figures 2.13-a) and 2.14-a)), while the bars for the non-contact lap splices were located in alternate cells with the

bottom bars positioned in the exterior cells of the specimen and the top bars located in the first interior cells (Figures 2.13-b) and 2.14-b)). Double pullout and wall splice specimens were three and thirteen blocks high, respectively. Plastic sheaths were used to de-bond the reinforcing bars outside of the splice region from the surrounding grout in the double pullout specimens to ensure failure occurred within the splice region.

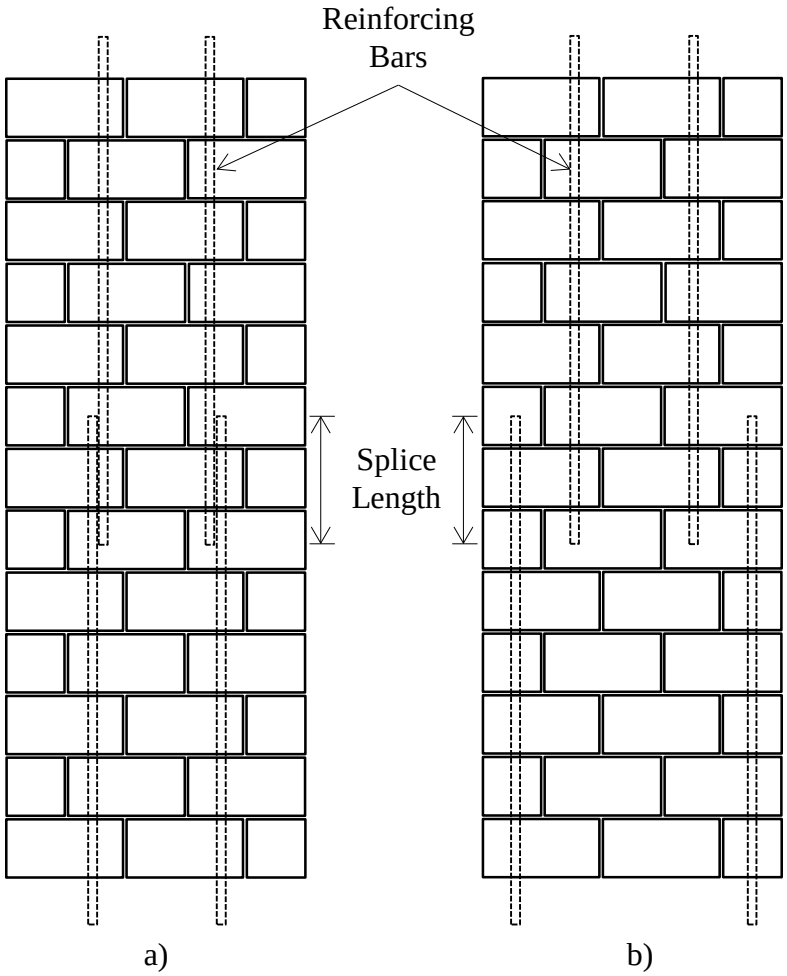

Figure 2.14 Wall splice specimens as tested by Ahmed and Feldman (2012) – Modified from Ahmed and Feldman (2012): a) with contact lap splices, b) with non-contact lap splices.

Double pullout specimens were subjected to direct tension, while wall splice specimens were tested horizontally in four point loading. At least one of the lapped bars in both the pullout and the wall splice specimens with contact lap splices attained yield before failure. In contrast, double pullout specimens and wall specimens with non-contact lap splices failed at 46.1% and 78% of their predicted yield load capacity, respectively. The specimens with contact lap splices typically failed due to bond loss between the reinforcing bars and the grout, whereas the specimens with non-contact lap splices failed due to bond loss between the grout and the masonry block web.

A statistical analysis of the results showed that the tensile resistance of the lap spliced reinforcing bars in contact, and the non-contact lap splices with the bars located in alternate cells, was statistically significantly different at the 95 % confidence level in both specimen types. Such a statistical comparison, however, was deemed not meaningful for the double pullout specimens due to the several failure modes observed in those specimens. Contrary to the findings reported by Mjelde for wall splice specimens subjected to in-plane loading and double pullout specimens subjected to direct tension (Mjelde, 2008), Ahmed and Feldman (2012) concluded that the tensile resistance of the lap spliced bars in the double pullout and wall splice specimens was significantly different at the 95% confidence level for the same splice configuration. In general, higher lap splice tensile resistances were obtained for the wall splice specimens as compared to the double pullout specimens for the same reinforcement arrangement. Despite the statistically significant difference in the splice resistance between both specimen types, the authors concluded that the similar failure modes observed for each reinforcement arrangement supported the validity of pullout testing when contact lap splices are used.

2.5 Summary

This chapter provided an overview of previous research related to the bond mechanisms occurring in reinforced masonry and the study of lap spliced reinforcement using pullout and wall splice specimens. A review of the preceding literature shows that very little research has been conducted to evaluate the performance of non-contact lap splices in masonry or the effect of transverse bar spacing and splice length on the bond performance of spliced reinforcement.

The present experimental investigation was therefore designed to evaluate the mean splice resistance given varying lap splice lengths and transverse bar spacings of No. 15 lapped reinforcing bars located within a same cell using double pullout and full-scale concrete block wall splice specimens. The following chapter provides the details of the experimental program, including the description of the double pullout and the wall splice specimens used in this investigation, the evaluated variables, and the construction and testing methods for all specimens.

CHAPTER 3

EXPERIMENTAL PROGRAM

3.1 Introduction

An experimental investigation was conducted to evaluate the mean splice resistance given varying lap splice lengths and transverse bar spacings for No. 15 lapped reinforcing bars located within the same cell in full-scale concrete block wall splice specimens subjected to out-of-plane loading with the lap splices provided at mid-height. The project was carried out in two stages. In the first stage, double pullout specimens reinforced with contact lap splices were used to determine an adequate range of values of splice length that ensured the specimens would fail in bond rather than by yielding of the reinforcement. The three values of lap splice length, as established experimentally from the testing of the pullout specimens, were then tested in full-scale wall splice specimens using three different transverse spacings between the spliced bars, including bars in contact. The double pullout specimens were tested in direct tension while the wall splice specimens were subjected to a four point loading arrangement. This chapter provides a detailed description of the test specimens, their specified material properties, and the construction and testing processes followed in this investigation.

3.2 Experimental Plan

A total of 18 double pullout and 27 wall splice specimens were constructed for this experimental program. Table 3.1 shows the different combinations of splice length and transverse bar spacing as tested in the double pullout and the full-scale wall splice specimens in each of the two construction phases of the project.

Table 3.1 Experimental plan.

Construction phase	Specimen type	Lateral bar spacing (mm)	Splice length (mm)	Number of replicate tests
I	Pullout specimens	0	150	6
			200	6
			250	6
	Wall splice specimens	25	150	3
			200	3
II	Wall splice specimens	0	150	3
			200	3
			250	3
		25	250	3
		50	150	3
			200	3
			250	3

Three values of splice length (150, 200, and 250 mm) were tested based upon the results of previous research which had demonstrated that a 300 mm lap splice length is capable of developing the nominal yield capacity of Grade 400, No. 15 reinforcing bars in double pullout and wall splice specimens with the splices located at mid-height (Ahmed and Feldman, 2012). The selected splice lengths were tested using double pullout specimens with 0 mm transverse spacing between the lap spliced bars (i.e. contact lap splices). Six replicate specimens per arrangement were used, given that this was the minimum number of replicates required to perform a statistical assessment of the results and successfully detect outliers (Ahmed, 2011; Bartlett, 1999). Additionally, as shown in Table 3.1, six full-scale wall splice specimens, 3 replicate specimens reinforced with 150 and 200 mm lap spliced bars with a transverse spacing of 25 mm between the lap spliced bars were constructed and tested in the first construction phase.

As will be further discussed in the following chapter, the three splice lengths tested in the double pullout specimens from Phase I allowed for a bond failure of the reinforcement and were therefore selected to be tested in the full-scale wall splice specimens as part of the second construction Phase. The designated lap splice lengths were tested in combination with three values of clear transverse spacings: 0, 25, and 50 mm. Each such configuration was based on typical construction practices and accounts for the CSA Standard A371-04 (CSA, 2004b) provisions for the minimum continuous unobstructed cell space of 50 mm x 74 mm that must be provided in all masonry structures.

Due to the increased project size and construction costs that come with the construction and testing of full-scale specimens, only three replicates of wall splice specimens were constructed for each reinforcement configuration to validate the results. Details of the test specimens, material properties, and experimental setup are provided as follows.

3.3 Description of the Test Specimens

Two specimen types were used in this experimental investigation: double pullout specimens reinforced with contact lap splices, and full-scale wall splice specimens reinforced with contact and non-contact lap splices. Both specimen types were reinforced with No. 15 bars and constructed in a running bond pattern with all cells fully grouted. The following subsections describe the specific geometry and general characteristics of the two specimen types.

3.3.1 Double pullout specimens with contact lap splices

Figures 3.1-a) and 3.1-b) show the cross-section and elevation of the double pullout specimens, respectively. The pullout specimens were two-and-a-half blocks wide and three courses tall and were constructed in a running bond pattern. All specimens were reinforced with No. 15 lap spliced bars centered in the second and fourth specimen cells from the left end of the specimen as shown, with the contact lap splices provided at mid-height (Figure 3.1-b)).

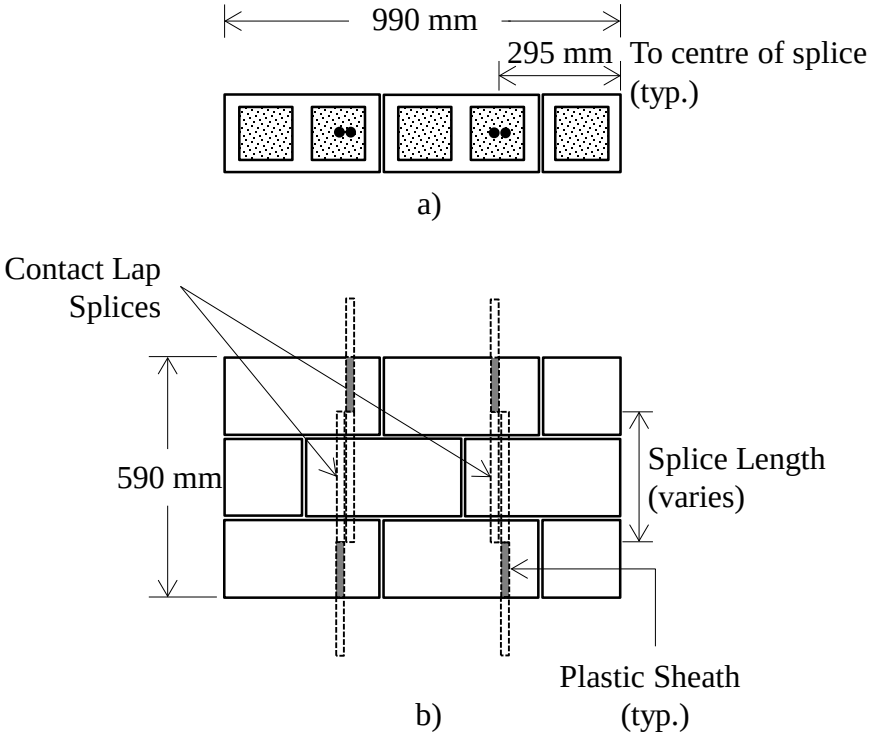

Figure 3.1 Double pullout specimens with contact lap splices – Modified from Ahmed and Feldman (2012): a) top view, and b) elevation.

The spliced reinforcing bars extended about 190 mm above and below the top and bottom of the specimens to allow the bars to be connected to the testing frame. Plastic sheaths were used

to cover the reinforcing bars outside the splice region to debond the reinforcement from the surrounding grout, as shown in Figure 3.1-b), to ensure failure occurred within the lap splice region.

3.3.2 Wall splice specimens with contact and non-contact lap splices

Figures 3.2-a) and b) show the overall dimensions of the full-scale wall splice specimens. Wall splice specimens had the same cross-section as the double pullout specimens (i.e. two-and-a-half blocks wide). All of the wall splice specimens were also constructed in running bond with all cells fully grouted.

Figure 3.2-a) shows the elevation of the wall splice specimens. All specimens were reinforced with deformed No. 15 reinforcing bars in the cells as shown with the splices provided at mid-height. Figure 3.2-b) shows a cross-section of the specimen within the mid-height splice region and shows that a template made of commercial welded wire mesh was placed in the bed joints immediately above and below the seventh block course to maintain the proper transverse spacing of the reinforcement in the specimens containing non-contact lap splices. As will be further discussed in the subsequent sections, contact lap splices were tied with wire prior to their installation; therefore, no wire mesh was required for the specimens with such reinforcement configurations.

As per the double pullout specimens, the spliced reinforcing bars were centered within the common grouting cell space in the second and fourth specimen cells from the left end of the specimen. Bars extended approximately 190 mm above and below the top and bottom of the wall

specimens, respectively, in order to provide proper anchoring at the reinforcement ends throughout testing, and ensure failure occurred within the lap splice length. No transverse reinforcement was provided in the specimens as the calculated shear resistance of the walls assuming full fielding of the reinforcing bars was considered sufficient (Ahmed and Feldman, 2012).

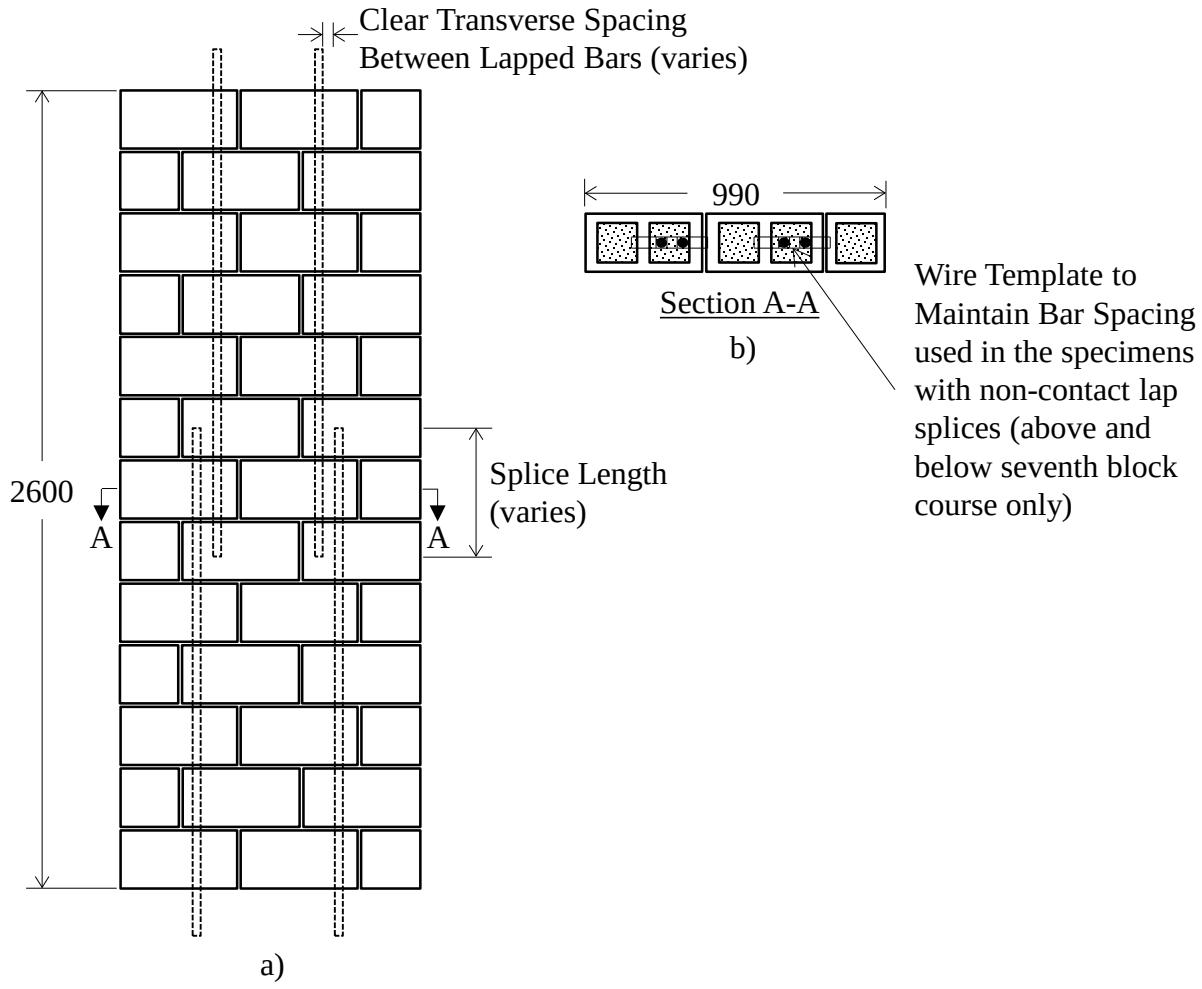

Figure 3.2 Wall splice specimens: a) elevation, and b) cross-section within the lap splice length.

3.4 Materials

All materials were provided by local suppliers and were procured from a single batch for each construction phase. Materials were stored in the laboratory for at least one week prior to the beginning of construction. The preparation of the required materials, as well as the construction and testing of the specimens were carried out in the Structures Laboratory at in the University of Saskatchewan.

3.4.1 Concrete masonry units

Figures 3.3-a) and b) show the overall dimensions of the masonry block units that were used in all specimens. Standard flat and frogged ended hollow concrete masonry blocks (390 mm long x 190 mm wide x 190 mm tall), meeting the specifications provided in CSA Standard A165-04 (CSA, 2004c), were provided by Cindercrete Products Ltd. of Saskatoon in two stages. The blocks required in each phase of this experimental project came from the same batch and half blocks were cut in the laboratory using a masonry brick/block saw rather than ordering half blocks, in order to ensure all blocks within each specimen had the same material properties.

3.4.2 Mortar

Laboratory prepared Type S mortar, a blend of Type S mortar cement, masonry sand, and water, with a minimum 28-day nominal compressive strength of 12.5 MPa in accordance with CSA Standard A179-04 (CSA, 2004d) was used for laying the masonry blocks. Type S Lafarge mortar cement and masonry sand were provided by a local supplier and stored in the laboratory. Table 3.2 shows the gradation of the masonry sand from the sieve analysis performed in

accordance with CSA Standard A23.2-2A (CSA, 2009). As shown, the masonry sand used in the mortar preparation met the gradation requirements as defined in CSA Standard A179-04 (CSA, 2004d).

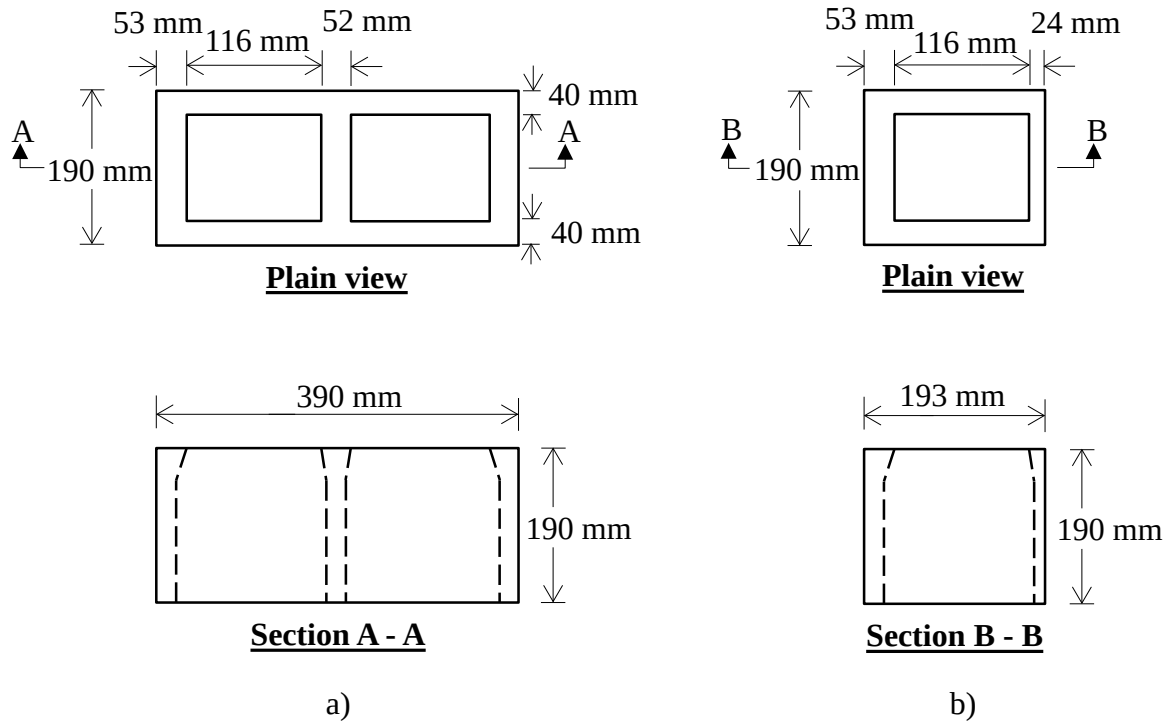

Figure 3.3 Concrete block units dimensions – modified from Ahmed (2011): a) standard full block, and b) half-block as cut from full blocks.

3.4.3 Grout

High slump grout with a high water/cement ratio resulting in a measured slump of about 250 mm was used throughout. A target minimum 28-day compressive strength of 12.5 MPa in accordance with CSA Standard A179-04 (CSA, 2004d) was intended. The grout was mixed in the laboratory and hand placed in the cells of all specimens. Type GU Lafarge Portland cement and pre-mixed gravel with a 2:3 fine to coarse aggregate proportion and a maximum aggregate

size of 10 mm, in accordance with CSA A179-04 (CSA, 2004d), were provided by a local supplier for grout preparation.

Table 3.2 Aggregate gradation of the fine aggregate (sand) used in the mortar mix.

ISO sieve size	Fine aggregate (sand), % passing			CSA A179-04 requirements
	Sample 1	Sample 2	Sample 3	
14 mm	--	--	--	--
10 mm	--	--	--	--
5 mm	100	100	100	100
2.5 mm	98.7	98.7	98.6	90-100
1.25 mm	95.7	95.4	95.6	85-100
630 µm	78.9	86.0	87.1	65-95
315 µm	37.3	31.6	30.1	15-80
160 µm	8.91	6.2	6.0	0-35

Tables 3.3 and 3.4 shows the fine and coarse aggregate gradation from the sieve analyses, respectively, as performed in accordance with CSA Standard A23.2-2A (CSA, 2009). In general, Table 3.3 shows that the masonry sand used in the grout preparation met the gradation requirements as defined in CSA Standard A179-04 (CSA, 2004d). Table 3.4, however, shows that the coarse aggregate did not completely meet the CSA Standard A179-04 requirements for the 5 and 10 mm sieve sizes. Nonetheless, as will be discussed in the following chapter, the resulting grout mix met the requirements for the minimum 28-day compressive strength as defined in Clause 9 in CSA Standard A179-04 (CSA, 2004d). The use of the coarse aggregate as provided by the supplier for grout preparation was therefore permitted as specified in Clause 5.3.2.5 in CSA Standard A179-04 (CSA, 2004d).

Table 3.3 Aggregate gradation of the fine aggregate (sand) used in the grout mix.

ISO sieve size	Fine aggregate (sand), % passing				CSA A179-04 requirements
	Sample 1	Sample 2	Sample 3	Sample 4	
14 mm	--	--	--	--	--
10 mm	--	--	--	--	--
5 mm	100	100	100	100	100
2.5 mm	93.3	92.4	93.8	94.4	90-100
1.25 mm	86.1	85.5	87.9	87.8	85-100
630 µm	64.8	68.4	71.8	64.8	65-95
315 µm	12.7	15.9	18.3	11.5	15-80
160 µm	1.6	2.1	2.6	1.7	0-35

Table 3.4 Aggregate gradation of the coarse aggregate used in the grout mix.

ISO sieve size	Coarse aggregate, % passing				CSA A179-04 requirements
	Sample 1	Sample 2	Sample 3	Sample 4	
14 mm	100	100	100	100	100
10 mm	62.0	57.9	61.3	58.8	85-100
5 mm	2.6	1.8	1.9	1.8	10-30
2.5 mm	0.6	0.4	0.7	0.5	0-10
1.25 mm	0	0	0	0	0-5
630 µm	--	--	--	--	--
315 µm	--	--	--	--	--
160 µm	--	--	--	--	--

3.4.4 Steel reinforcing bars

Grade 400 hot-rolled deformed steel reinforcement with a nominal diameter of 15 mm was used in all specimens. Bar samples were obtained from each of the two heat batches used during construction, and were tested in accordance with ASTM Standard A370-11 (ASTM, 2011a) to establish the actual material properties for the two construction phases. The following mechanical properties of the reinforcement were evaluated: yield stress, modulus of elasticity, strain at the initiation of strain hardening, and ultimate stress.

3.5 Specimen Construction

All specimens were constructed by a journeyman mason and the construction process was completed in two phases. Eighteen double pullout specimens and six full-scale wall splice specimens were constructed in Phase I, while twenty-one wall splice specimens were constructed during Phase II. Phase I was completed between September 6th and 12th, 2011, and Phase II was completed between April 11th and 24th, 2012. The following subsections provide the details of the construction process including the reinforcement and concrete blocks preparation, mortar and grout mixing, cast of the corresponding companion specimens, and block laying for the test specimens.

3.5.1 Concrete block preparation

Figure 3.4 shows the electric table-mounted masonry brick/block saw used for cutting the blocks. As previously discussed in Section 3.4.1, half-blocks were cut from standard full blocks in the laboratory in order to ensure all blocks within each specimen had the same material properties. The dimensions of the resulting half-blocks are shown in Figure 3.3-b). After cutting, half-blocks were stored in the laboratory for at least three days prior to construction to allow drying. Figure 3.5 shows a typical half block as used.

3.5.2 Reinforcement preparation

The 6 m long No. 15 steel reinforcing bars, as provided by the supplier, were cut to the required lengths using an abrasive electric saw. Figure 3.6-a) shows the cutting process of a steel bar. The length of the required reinforcing bars for the double pullout and the wall splice

specimens was calculated considering the corresponding splice length plus the 190 mm that the bars extended above and below the top and bottom of the specimens as discussed in Sections 3.3.1 and 3.3.2. The contact lap splices for both the double pullout and the wall splice specimens were tied with wire prior to their installation. Figure 3.6-b) shows the contact lap splices as prepared, and the reinforcing bar lengths as cut for the specimens with non-contact lap splices.

Figure 3.4 Masonry brick/block saw used for cutting the blocks.

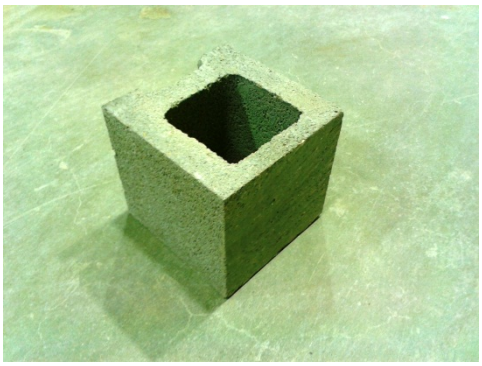

Figure 3.5 Typical half block as cut in the laboratory.

As discussed in Section 3.3.2, templates made of commercial welded wire mesh were used in the bed joints above and below the center course of the wall splice specimens reinforced with non-contact lap splices in order to maintain the proper alignment of the bars. As part of the reinforcement preparation, 1 x 11 in. (25 x 280 mm) strips of Ben-Mor wire mesh were cut from 1 in. x 36 in. x 6 ft. (25 x 914 x 1829 mm) rolls using wire cutting pliers. Figure 3.7 shows a strip of the wire template as cut prior to construction.

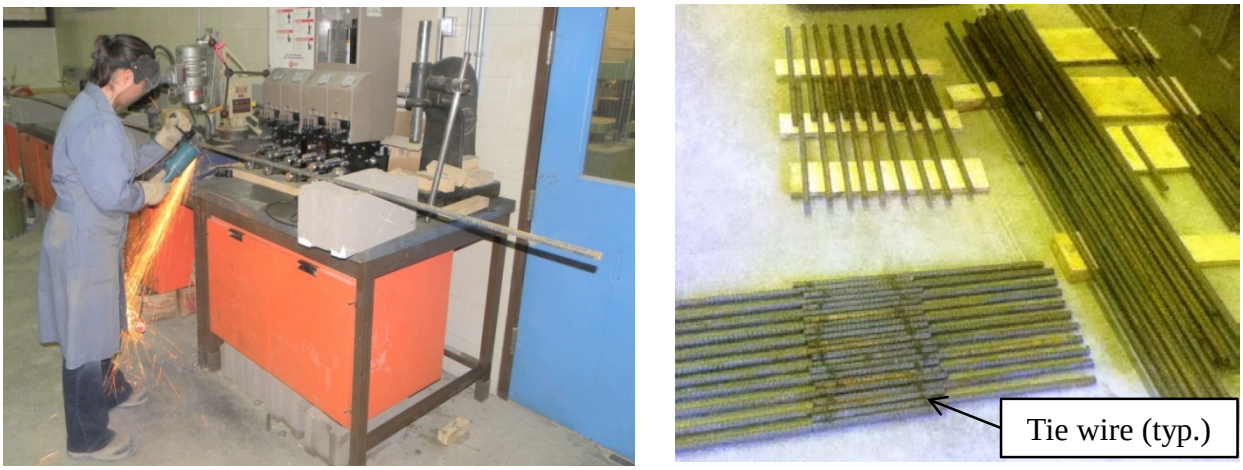

a) b)

Figure 3.6 Reinforcing bars preparation: a) rebar cutting, and b) spliced bars tied with wire prior to their installation.

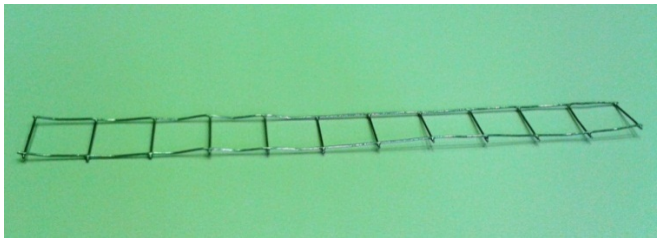

Figure 3.7 Wire mesh templates used to maintain proper spacing of the bars in the wall splice specimens reinforced with non-contact lap splices.

3.5.3 Mortar preparation

Laboratory prepared Type S mortar, a mixture of water, mortar cement, and sand in the ratio of 0.7:1:3 by volume, was used throughout. Figure 3.8 shows the electric mixer used to prepare the mortar. Rotating blades inside of the machine's revolving container were designed to mix fine aggregate mixes such as mortar. Half of the water was first placed into the mixer followed by the masonry sand and mortar cement. The rest of the water was added gradually until a uniform consistency was achieved. The mortar preparation was supervised by the

journeyman mason who continued to temper the mortar during block laying to maintain its workability.

A total of eighteen and twenty-one 50 mm mortar cubes were prepared in accordance with CSA A3004-C2 (CSA, 2008) as part of construction phases I and II, respectively, to establish the compressive strength of the mortar. Figure 3.9 shows the mortar cubes as cast in the 50 x 50 mm brass moulds. The mortar cubes were then covered with plastic sheeting and allowed to set for a minimum of 24 hours prior to demoulding.

Figure 3.8 Mortar mixing.

Figure 3.9 Mortar cube preparation.

3.5.4 Grout preparation

Figure 3.10-a) shows the power barrel mixer that was used to mix the grout in the laboratory. Grout was mixed with water, cement, and gravel in the ratio of 2:1:3 by volume, a mix that resulted in a measured slump of about 250 mm. Half of the water and half of the aggregate were first added to the mixer. The cement and the remaining aggregate were loaded

subsequently and the rest of the water was gradually added until the mix was of uniform consistency. After 3 to 5 minutes of mixing, the grout was placed into wheelbarrows to be transported and hand placed in the cells of the masonry specimens. Figure 3.10-b) shows a picture of the slump test that was conducted for each grout batch.

a) b)

Figure 3.10 Grout preparation: a) grout mixer, and b) grout slump test.

Material properties for the grout were established from the non-absorptive cylinders and absorptive prisms prepared in accordance with CSA Standard A179-04 (CSA, 2004d) and ASTM C1019 (ASTM, 2011b), respectively. These specimens were tested along with the double pullout and the wall splice specimens. Figure 3.11 shows that the absorptive grout prisms were 100 mm wide x 100 mm long x 190 mm high, and were formed by four concrete blocks lined with paper to facilitate demoulding. The absorptive grout prisms were cast in two layers with each layer rodded 25 times, and were covered with plastic for a minimum of 24 hours prior to their removal. A total of twenty-two absorptive grout prisms were cast as part of construction Phase I, and twenty-one more were cast as part of Phase II.

Figure 3.12 shows that the non-absorbent grout cylinders were cast in 75 mm diameter x 150 mm high plastic moulds. Grout cylinders were cast in two layers with each each rodded 20 times. The cylinders were covered with plastic sheets for a minimum of 24 hours prior to removal. A total of twenty-two and twenty-one non-absorptive cylinders were cast during the first and second construction phases, respectively.

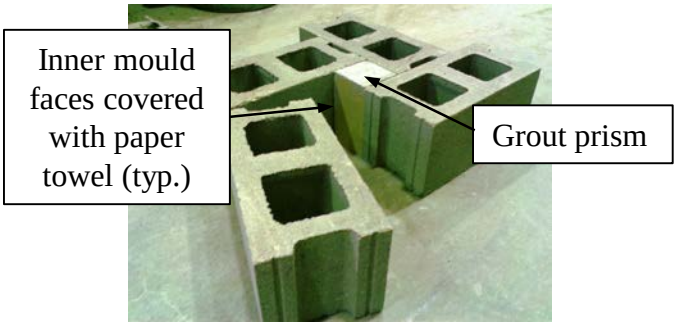

Figure 3.11 Absorptive grout prisms.

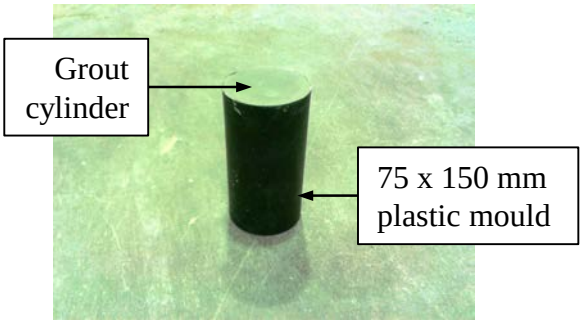

Figure 3.12 Non-absorptive grout cylinders.

3.5.5 Masonry prisms

Three-block high by one-block wide masonry prisms were constructed to establish the mechanical properties of the masonry assemblage. A total of 18 and 21 masonry prisms were constructed as part of the construction Phases I and II, respectively (i.e. one masonry prism per specimen), in accordance with CSA Standard S304-04 Annex D (CSA, 2004a). Figure 3.13 shows a masonry prism as constructed. The block laying and grouting of the masonry prisms were carried out in parallel to the construction of the double pullout or wall splice specimen corresponding to each prism.

Figure 3.13 Masonry prisms constructed along with the double pullout and the wall splice specimens.

3.5.6 Pullout specimens construction

Figure 3.14-a) shows that the double pullout specimens were constructed on a base formed by 3 blocks beneath a 200 x 990 x 12 mm drilled plywood sheet used as a template to accurately position the reinforcing bars within each specimen. As previously discussed in Section 3.3.2, the reinforcing bars outside of the splice region were debonded from the surrounding grout to ensure that failure occurred within the lap splice region. Eighteen millimeter diameter PVC pipe sections cut to the required lengths were glued to the plywood bases to debond the reinforcement below the splice region. Lengths of PVC pipe, as shown, were also glued to drilled plywood strips that were placed at the top of the specimens to debond the reinforcement above the splice region, and to maintain the proper alignment of the bars (Figure 3.14-a)). Figure 3.14-b) shows block laying of the pullout specimens by the mason. All specimens were allowed to set for a minimum of 12 hours before grouting. The lap spliced bars in contact were placed in the specimens, and plywood strips were used to secure the bars at the top. Figure 3.15-a) shows that the grout was hand placed in the cells of the double pullout

specimens. A mechanical vibrator was used to ensure grout compaction in all specimen cells. The completed double pullout specimens are shown Figure 3.15-b).

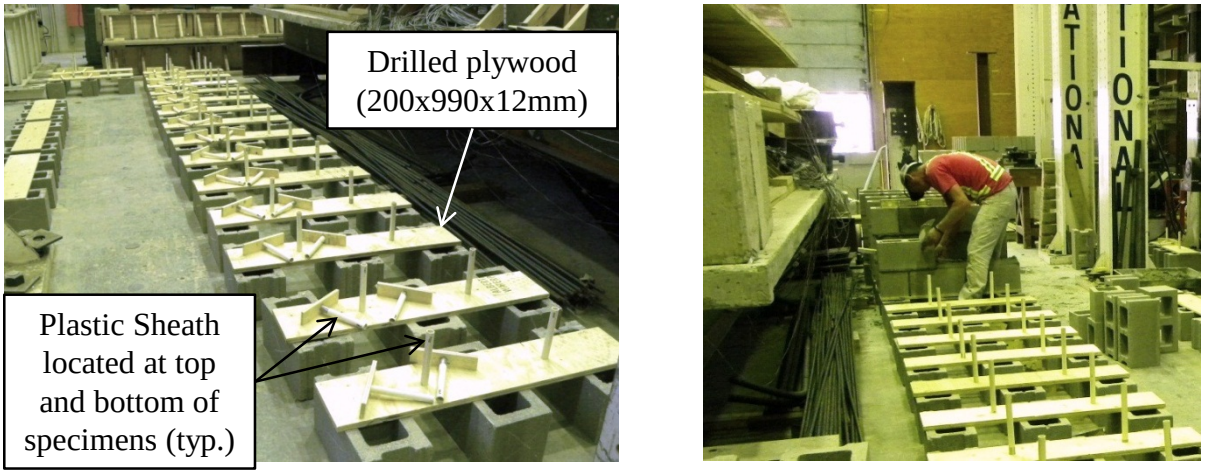

a) b)

Figure 3.14 Pullout specimens construction: a) drilled plywood bases and plastic sheaths, and b) block laying.

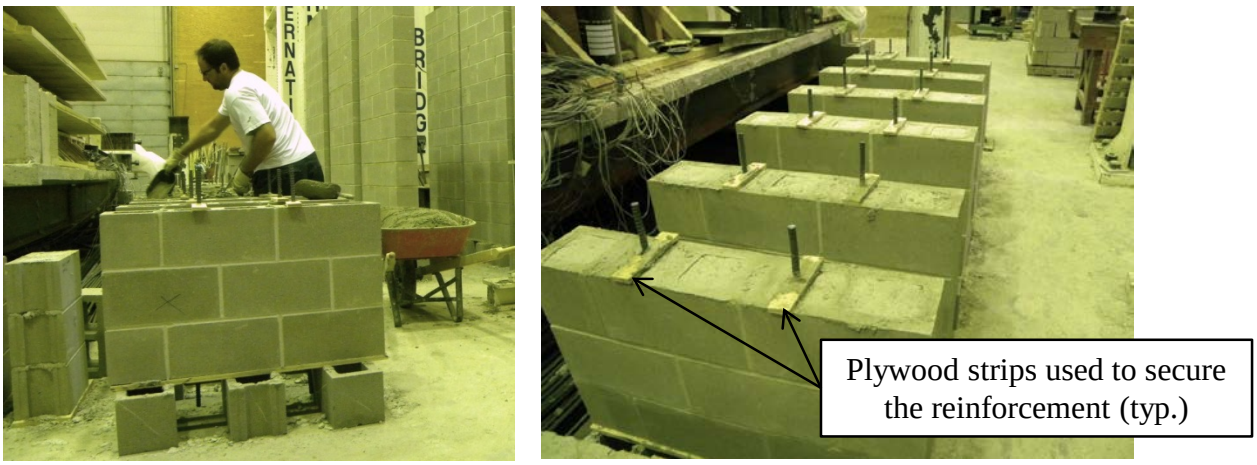

a) b)

Figure 3.15 Grouting of the pullout specimens: a) grout placement, and b) completed pullout specimens.

3.5.7 Wall splice specimens construction

Wall splice specimens were constructed on a base similar to that used for the double pullout specimens. The full-scale wall splice specimens were thirteen courses tall and were constructed in two lifts. Figure 3.16-a) shows the block laying of the first lift of the wall splice specimens by the mason. A first lift of 8 courses was constructed to provide full embedment of the bottom reinforcement and all reinforcement within the lap splice length. Figure 3.16-b) shows the positioning of the wire mesh templates used to maintain the proper transverse spacing of the bars in the specimens reinforced with non-contact lap splices as discussed in Section 3.5.2. The templates were positioned above and below the seventh wall course during block laying.

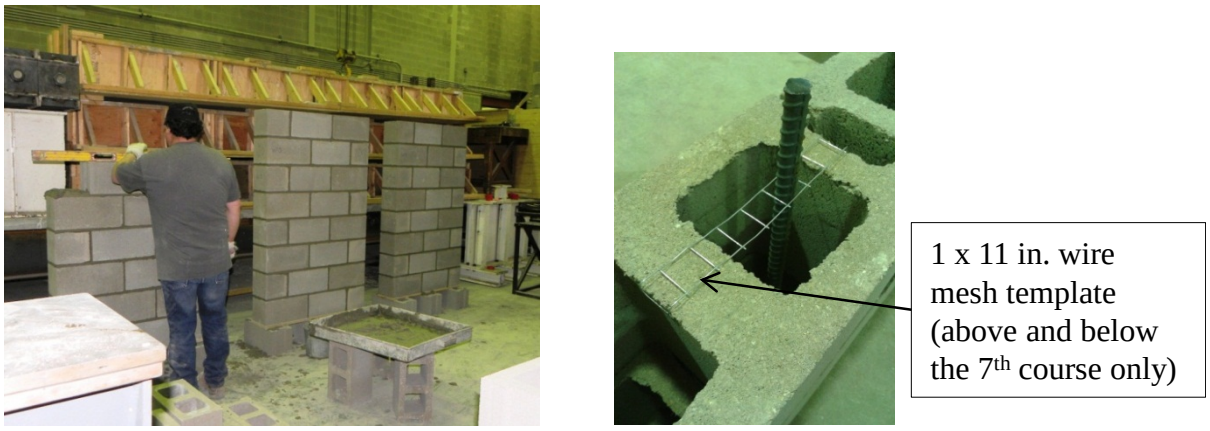

a) b)

Figure 3.16 Construction of the first lift of the wall splice specimens: a) block laying by the mason, and b) positioning of the wire mesh templates used to maintain the proper transverse spacing of the bars in the specimens with non-contact lap splices.

The first lift of the wall splice specimens was allowed to set for a minimum of 12 hours prior to grouting. The reinforcing bars were then placed in the wall splice specimens and grout was hand poured into the block cells. Figure 3.17 shows that a mechanical vibrator was used for

compacting the grout in all specimen cells. The grout was allowed to set for a minimum of 12 hours before the construction of the second five-course lift. Figure 3.18-a) shows the second lift of block laying by the mason. The grout was hand placed in the remaining cells after a 12 hour set period as shown in Figure 3.18-b), and a mechanical vibrator was used to ensure proper compaction.

Figure 3.17 Compaction of the grout using a mechanical vibrator.

3.5.8 Specimen curing

After construction, all specimens were cured for a minimum of 28 days in the laboratory environment prior to testing. Figure 3.19 shows the curing of the double pullout and the wall splice specimens, while Figures 3.20-a) and b) show the curing of the masonry prisms and the curing of the mortar cubes, grout cylinders, and absorptive grout prisms, respectively. Measures of the temperature and humidity conditions in the laboratory during the curing period of the specimens for both construction phases showed that the temperature ranged between 20 and 22˚C, while the humidity ranged from 40 to 55%.

a) b)

Figure 3.18 Construction of the second lift of the wall splice specimens: a) block laying by the mason, and b) grout placement.

Figure 3.19 Double pullout and wall splice specimen curing.

3.6 Testing Procedures

The testing of the specimens started following the 28-day curing period. The following subsections provide a comprehensive description of the testing procedures used throughout this

investigation. Details of the instrumentation and testing setup used for the double pullout and the wall splice specimens, as well as for the construction materials (i.e. steel reinforcing bars and concrete masonry blocks), and companion specimens are included. Table 3.5 shows the testing dates for the specimens within each construction phase and the range of ages of the specimens at the time of testing. Details of the construction and testing dates for each particular specimen are reported in Appendix 3A.

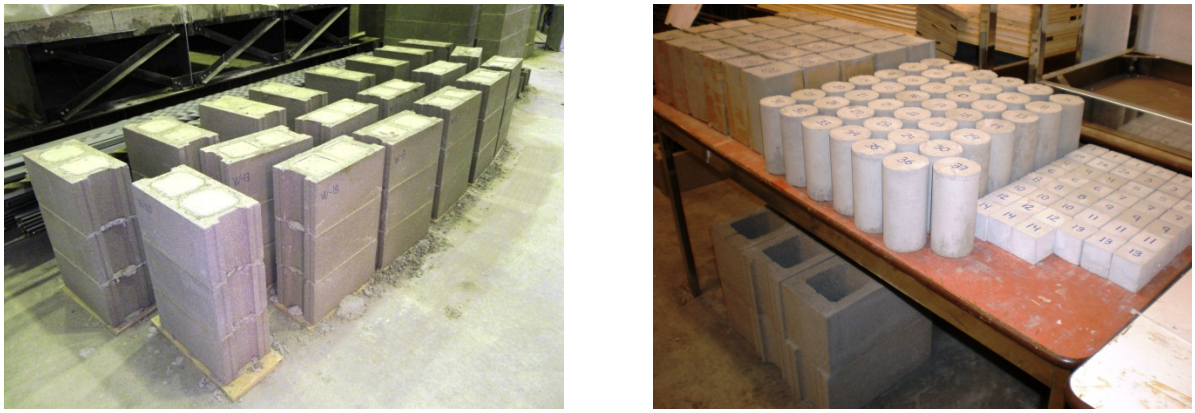

a) b)

Figure 3.20 Companion specimen curing: a) masonry prisms, and b) mortar cubes, grout cylinders and absorptive prisms.

Table 3.5 Testing dates and range of age of the specimens at the time of testing.

Construction phase	Specimen type	Testing dates	Range of age of the specimens (days)
I	Pullout specimens	Oct 24th – Dec 2nd, 2011	43 – 102
	Wall splice specimens	Jan 12th – Jan 19th, 2012	123 – 130
II	Wall splice specimens	June 7th – July 25th, 2012	45 – 93

3.6.1 Concrete block masonry units

Compressive strength testing of the concrete blocks was performed in accordance with ASTM Standard C140-10 (ASTM, 2010). A total of 8 and 10 full-size masonry blocks were tested in compression as part of construction Phases I and II, respectively. Figure 3.21 shows the test setup for the concrete block compressive test. The concrete blocks were tested in a 2000 kN-capacity Amsler Beam Bender, and a data acquisition system connected to the testing machine collected the applied load data for the specimens until such time as failure occurred. Figure 3.21 shows that fibre board sheets were placed at the top and bottom of the blocks to ensure uniform loading of the specimens over their top and bottom surfaces.

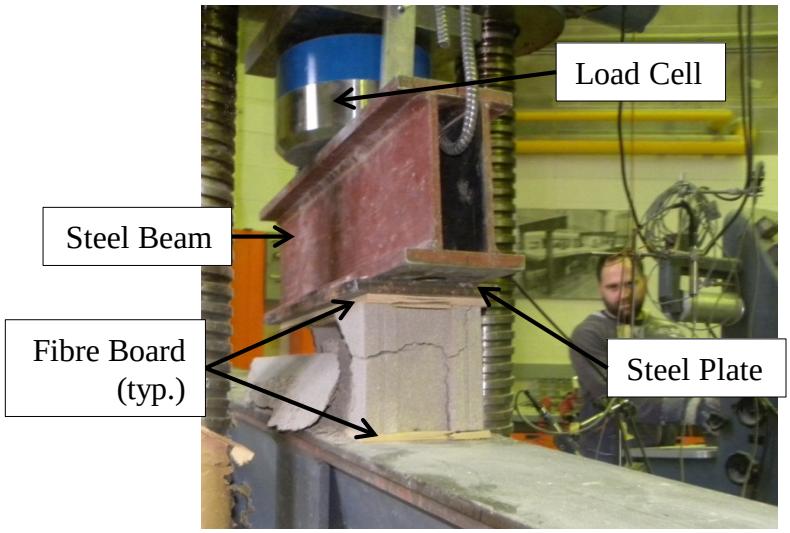

Figure 3.21 Concrete masonry blocks compression test.

The mean compressive strength of the masonry units was calculated based on the resulting load test data, as obtained from the compression test, and the average net cross-sectional area of the blocks as obtained from an absorption test conducted in accordance with

ASTM C140-10 (ASTM, 2010). Figures 3.22-a) and b) show the submersion and weighing of the oven-dry units, respectively, performed as part of the absorption test. A total of 6 full-sized masonry units were tested for water absorption as part of the first construction phase, while a total of 12 blocks were tested during the second phase.

a)

b)

Figure 3.22 Absorption test: a) submerged masonry units, and b) weighing of the oven dry blocks.

3.6.2 Mortar cubes

The compressive strength of the mortar was established from the 50 x 50 mm mortar cubes tested in accordance with CSA A3004-C2 (CSA, 2008). A total of 18 and 21 mortar cubes were tested as part of the first and second construction phases, respectively. Figure 3.23 shows the testing of a mortar cube. A 600 kN-capacity Instron 600DX Universal Testing Machine was used to test the cubes at a constant loading rate of 10 kN/min. The load was applied uniformly on one of the smooth lateral faces of the cubes; a data acquisition system connected to the testing

machine collected the applied load and vertical deformation data until such time as failure occurred.

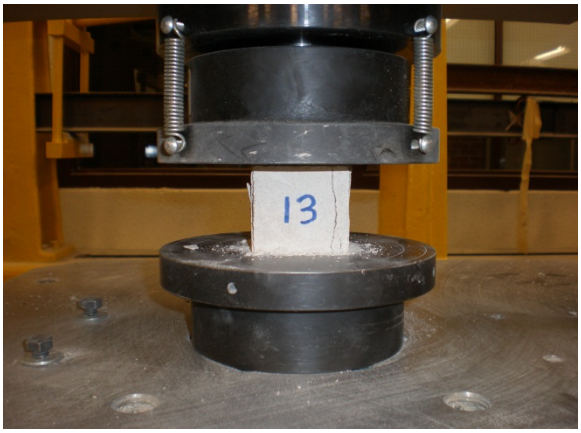

Figure 3.23 Mortar cubes test.

3.6.3 Non-absorbent grout cylinders and absorptive grout prisms

Material properties for the grout were established from the non-absorptive cylinders and absorptive grout prisms tested along with the double pullout and the wall splice specimens. The non-absorptive grout cylinders and absorptive prisms were tested using the Instron 600DX Universal Testing Machine.

Non-absorptive cylinders were tested in accordance with CSA A179-04 (CSA, 2004d). Figure 3.24-a) shows the compressive strength test of the grout cylinders. Prior to testing, the ends of the non-absorptive cylinders were capped with sulfur to ensure a uniform and smooth surface perpendicular to the applied load throughout testing. Load was applied at a constant loading rate of 10 kN/min until failure; the data acquisition system recorded the applied load and

vertical deformation data for the specimens throughout the test. A total of 22 and 21 non-absorptive grout cylinders were tested as part of construction phases I and II, respectively.

Figure 3.24-b) shows the 100 mm wide x 100 mm long x 190 mm high absorptive grout specimens that were tested in accordance with ASTM C1019-11 (ASTM, 2011b). Fibre board sheets were placed at the top and bottom of the grout prisms, as shown, to ensure uniform loading of the specimens over their entire surface. Load was applied at a constant rate of 12 kN/min until failure. The applied load and vertical deformation of the specimens were recorded by the data acquisition system. Twenty-two specimens were tested during the first construction phase, while twenty-one more were tested as part of the second construction phase.

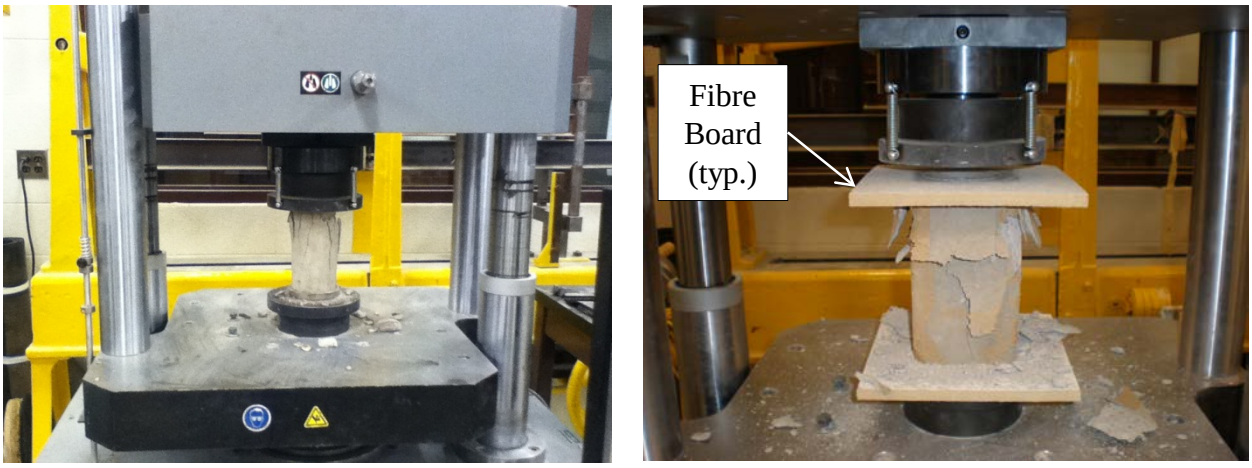

a) b)

Figure 3.24 Grout companion specimens testing: a) non-absorptive grout cylinders, and b) absorptive grout prisms.

3.6.4 Masonry prisms

Three-block high by one-block wide masonry prisms were used to establish the mechanical properties of the masonry assemblage. Masonry prisms were tested in the 2000 kN-

capacity Amsler Beam Bender in accordance with CSA Standard S304-04 Annex D (CSA, 2004a) at constant loading rate of 1 kN/s. Uniform loading over the entire surface of the specimens was ensured by using fiberboard sheets at the top and bottom of the specimens. Figure 3.25-a) shows the dimensions and details of the instrumentation used in the masonry prisms test, while Figure 3.25-b) shows a photograph of the test setup.

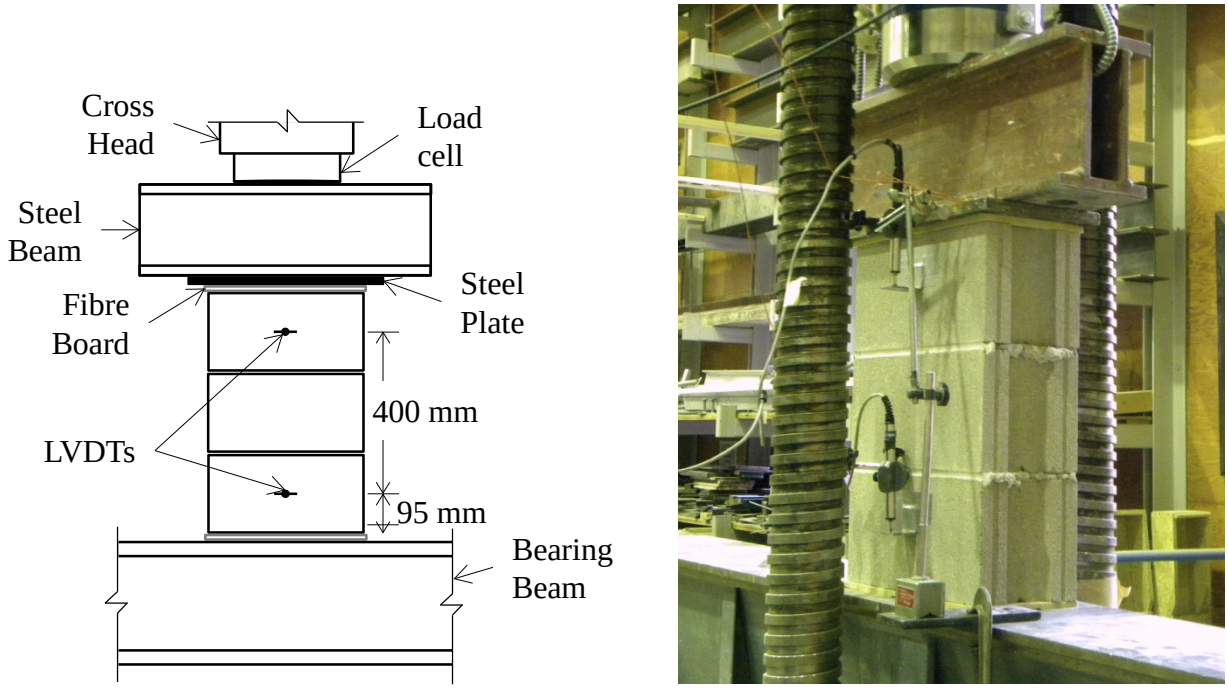

a) b)

Figure 3.25 Masonry prism test – Modified from Ahmed (2012): a) dimensions and instrumentation, and b) test setup.

Two linear variable differential transducers (LVDTs) were attached to the face shell at the mid-height of the top and bottom blocks to measure the vertical deformation of the specimens as testing progressed. Readings from the load cell and the LVDTs were recorded at a rate of 1 Hz by a National Instruments data acquisition device with LabVIEW software that was

connected to the testing machine. A total of 18 and 21 masonry prisms were tested as part of the first and second construction phases, respectively.

3.6.5 Reinforcing steel

A total of 6 steel bar samples were obtained from each of the two heat batches used in the construction of the double pullout and the wall splice specimens and were tested in accordance with ASTM Standard A370-11 (ASTM, 2011a) to establish the actual material properties of the reinforcement. Figure 3.26 shows the test setup and instrumentation used to test the deformed reinforcing bars. The bars were tested in tension at a constant loading rate of 200 N/s using the Instron 600DX Universal Testing Machine. An 8 in. gauge length extensometer was attached to the reinforcing bar to measure the strain in the reinforcement; the data acquisition system connected to the testing machine collected the stress and corresponding displacement data until such time as failure of the reinforcing bars occurred.

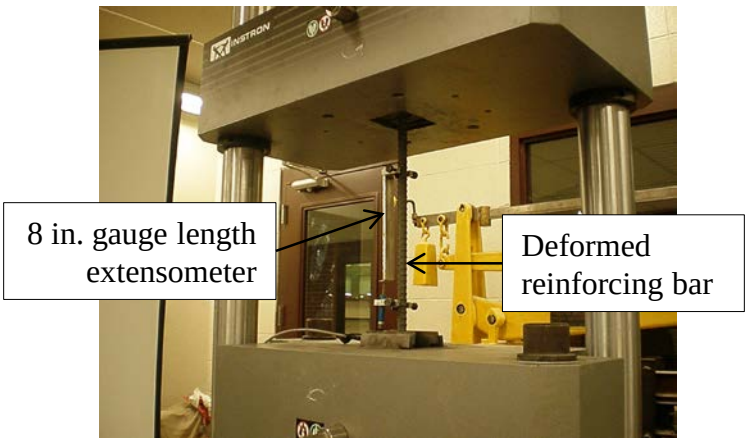

Figure 3.26 Reinforcing steel bars test.

3.6.6 Double pullout specimens

Double pullout specimens were tested in direct tension using a similar test setup as that used by Ahmed and Feldman (2012). Figure 3.27 shows the details of the test setup. Prior to the frame assemblage, each pullout specimen was moved from its construction position using the laboratory overhead crane and placed horizontally on two steel pipes to reduce friction between the specimen and the laboratory strong floor. The steel testing frame consisted of two pairs of 2400 mm long C250x23 channel sections welded back-to-back with five 12 mm thick steel plates each, resulting in a 64 mm gap between the sections, that were bolted together using two 50 mm diameter threaded bars at both ends. The 50 mm threaded bars were bolted to the channel sections using two steel plates welded 200 mm from each end of the sections.

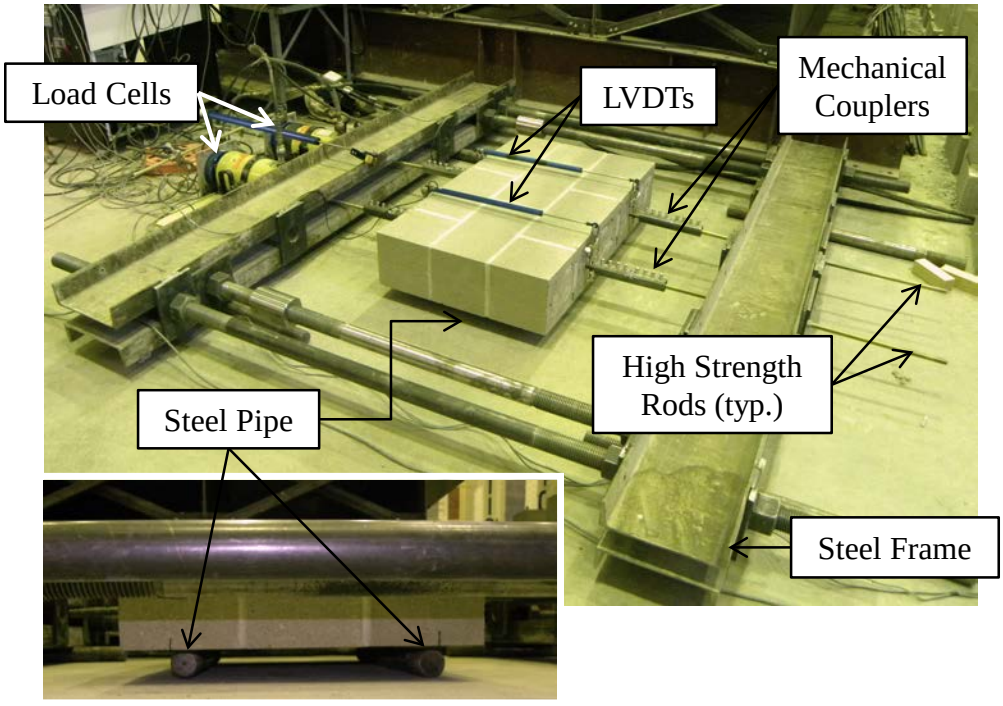

Figure 3.27 Double pullout specimens test setup.

The reinforcing bars extending beyond each end of the double pullout specimens were sprayed with white paint to more easily identify bar displacement. Type 2 Zap Screwlok mechanical couplers were then used to attach the reinforcing bars to 16 mm diameter high strength threaded steel rods. Details of the Zap Screwlok mechanical couplers are provided in Appendix 3B. The high strength rods, extending about 800 mm above and below the top and bottom of the testing frame, were then connected to a pair of hydraulic rams bearing against the steel frame at one end, and bolted to the steel frame at the other end using nuts and 200 mm square x 8 mm thick steel plates with a drilled hole in their centre. The hydraulic rams had a 220 kN capacity and a stroke of 300 mm.

Two 300 mm-range linear variable differential transducers (LVDTs) were attached to both ends of each splice with clamps to measure the deformation of the lap spliced reinforcing bars. The LVDTs and load cells were connected to a National Instruments data acquisition device controlled by LabVIEW software which recorded the bar deformation and applied load as testing progressed.

The tensile load was applied by the hydraulic rams at a constant rate of 0.025 mm/s. The hydraulic pressure in the fluid for the two rams was controlled by a valve, which alternately allowed the incremental displacement of each hydraulic cylinder such that the displacement was first applied to one set of lap spliced bars and then to the other, once the valve of the ram connected to the first loaded splice had closed. The load and displacement of the lap splices, therefore, was not uniform but increased one after the other. Unequal deformation of the two lap splices at the same displacement level of the hydraulic cylinders, and consequently a load

differential between the splices, may result due to factors such as a bolt shear failure in the mechanical couplers or bar slippage (Ahmed, 2011).

3.6.7 Wall splice specimens

Wall splice specimens were tested horizontally in four point loading. Figure 3.28 shows the details of the horizontal steel beams and end bearing plates that were used to assemble the rigging frame used to safely secure the walls while transporting and rotating them to the testing position. Figures 3.29-a) through d) show the positioning of the wall splice specimens using the laboratory overhead crane. Figure 3.29-a) shows that one of the two horizontal steel beams, consisting of two C 250 × 23 channel sections welded back-to-back 250 mm apart using two 10 mm thick plates at both ends (Figure 3.28), was first positioned at the bottom of the wall specimens and bolted to two 10 mm end bearing plates as shown. Figure 3.29-b) shows that the second horizontal steel beam was positioned at the top of the wall and connected to the bottom section using 16 mm high strength threaded bars.

Figure 3.29-c) shows that two 50 mm threaded bars bolted on each side of the horizontal sections through a centre hole in the end plates were used as a pivot to rotate the wall splice specimens to the horizontal position. Figure 3.29-d) shows that the steel sections were then removed and the wall splice specimen was accommodated in the testing frame on two supports: one pin and one roller. Figures 3.30-a) and b) show the pin and roller support assemblies, respectively. The supports consisted of a steel roller on top of a steel base. The screws were purposely loose to achieve a roller support, or snug such that a pin support resulted.

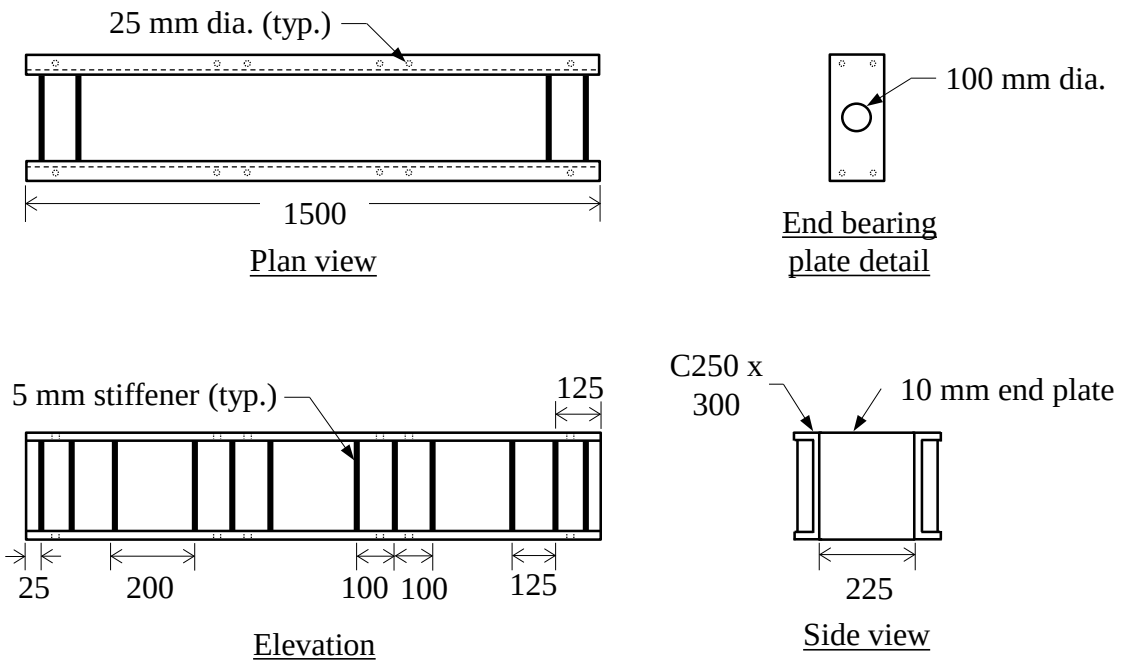

Figure 3.28 Details of the horizontal steel beam of the frame and end bearing plate used to rotate and translate the wall splice specimens – Modified from Ahmed (2011).

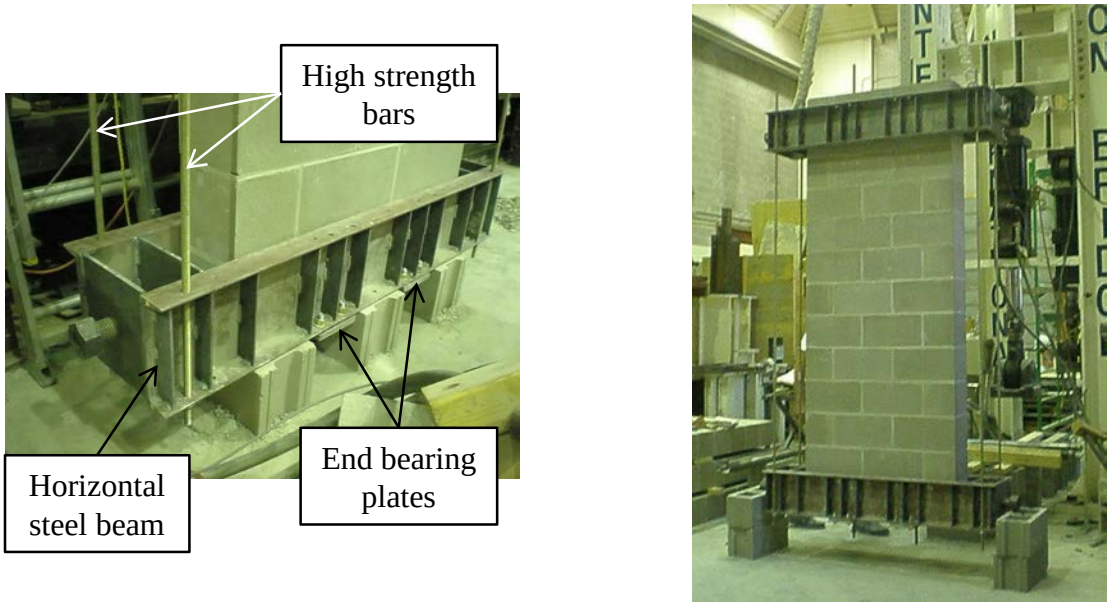

a) b)

c) d)

Figure 3.29 Wall splice specimens positioning: a) components of the steel frame, b) vertical lifting of a wall, c) specimen rotation, and d) wall positioned in the testing frame.

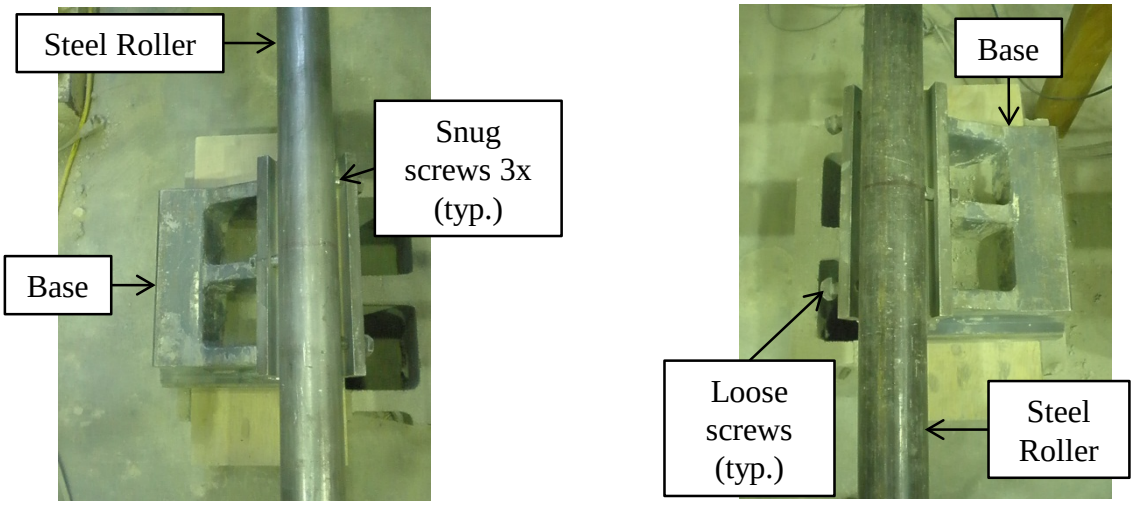

a) b)

Figure 3.30 Support conditions for the wall splice specimens: a) pin support, and b) roller support.

Figures 3.31-a) and b) show the four-point loading setup and instrumentation used in the testing of the wall splice specimens, and a photograph of the test setup, respectively. Prior to testing, end anchorages were provided for the reinforcement at each of the wall ends to prevent bar slippage and ensure failure would occur within the lap splice region. The anchorages consisted of 200 mm square x 8 mm thick steel plates, with a drilled hole in their centre, and were secured against the specimen ends with Zap Screwlok mechanical couplers tightened onto the excess bar lengths that extended beyond both ends of the wall splice specimens. A layer of mortar was used as a leveling compound to ensure full contact between the specimen and the steel plates.

Six LVDTs were used to measure the vertical displacement at different locations along the specimen length. Two LVDTs were located on each side of the wall at the specimen centreline, while the remaining four LVDTs, were located at 200 and 600 mm on either side of the specimen centerline (i.e. one specimen side only was instrumented at these four locations).

The load was applied by an MTS hydraulic actuator at the centerline of a spreader beam. The contact points between the spreader beam and the wall splice specimen were such that the four-point loading arrangement shown in Figure 3.31-a) was achieved. Load was applied at a constant displacement of 0.5 mm/min until failure, defined as a 60% load reduction from that recorded at the maximum carrying capacity. A National Instruments data acquisition device with LabVIEW software recorded the values of the applied load as the test progressed.

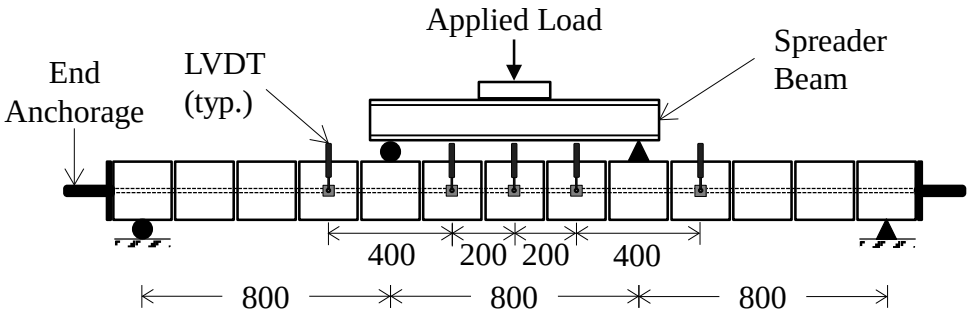

a)

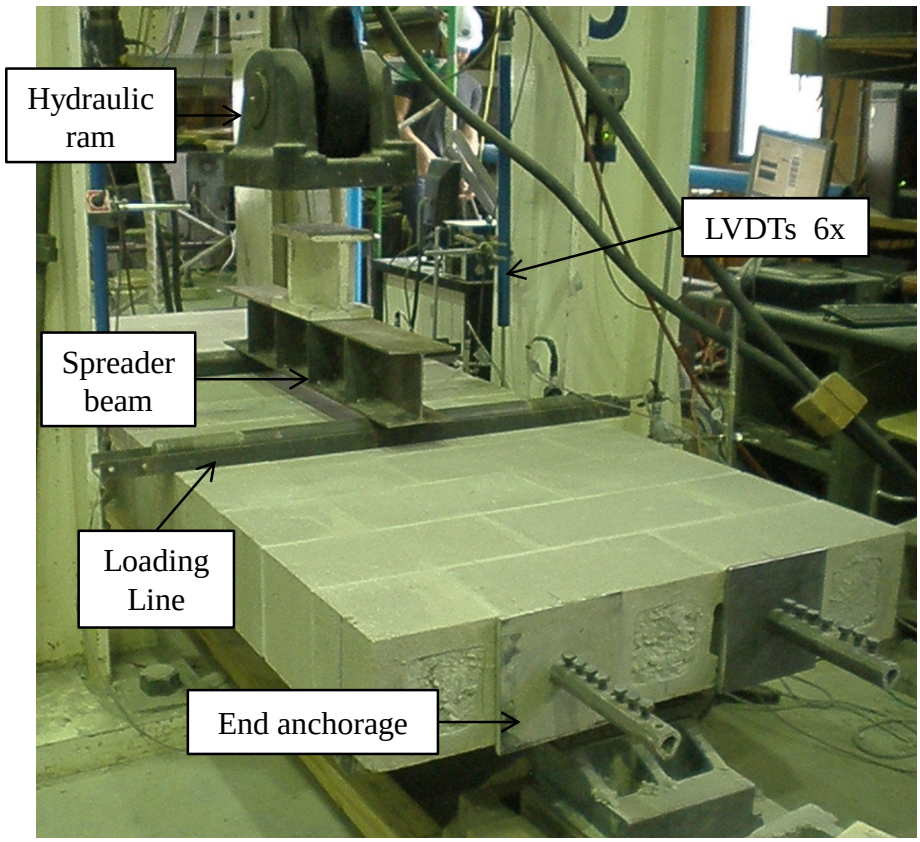

b)

Figure 3.31 Wall splice specimens testing: a) dimensions and instrumentation (Modified from Ahmed and Feldman (2012)), and b) test setup.

3.7 Summary

This chapter provided a detailed description of the experimental program designed to evaluate the effect of the lap splice length and transverse bar spacing in the tensile resistance of lapped No. 15 reinforcement in full-scale wall concrete block specimens. Details of the double pullout and wall splice specimens used in this investigation, their specified material properties, and the construction and testing methods followed throughout the two construction Phases of this project were presented.

The following chapter presents the results obtained from testing the companion specimens to determine the mechanical properties of the different materials used, the lap splice resistance versus splice displacement as obtained for the double pullout specimens reinforced with contact lap splices, and the load versus midspan deflection and calculated splice resistance of the wall splice specimens for the different reinforcement configurations tested. A comprehensive analysis of the splice resistance, failure modes, and crack propagation patterns for the different splice configurations tested in both specimen types is included. The results of a regression analysis performed to model the relationship between splice length and lateral bar spacing are also presented and discussed.

CHAPTER 4

TEST RESULTS AND ANALYSIS

4.1 Introduction

This chapter presents the test and analysis results for the double pullout and wall splice specimens included as part of this investigation. As discussed in the previous chapters, the objective of this experimental project was to evaluate the tensile resistance of No. 15 lap spliced reinforcing bars as a function of the lap splice length and the transverse spacing between the bars when the spliced bars are located within a single block cell.

Eighteen double pullout specimens reinforced with bars in contact and lap splice lengths of either 150, 200, or 250 mm were first tested to ensure that the selected lap splice lengths allowed for bond failure of the specimens prior to yielding of the steel reinforcement. Three lap splice length values that proved to result in a bond failure of the reinforcement in the double pullout specimens were then tested in a total of 27 wall splice specimens in combination with three values of transverse bar spacing: 0, 25, and 50 mm. The double pullout specimens were tested in direct tension while the wall splice specimens were tested under a four point loading arrangement. Details of the specimens included in the experimental program, their construction, and testing procedures are provided in Chapter 3.

The tensile resistance of the lap spliced reinforcing bars was obtained directly from the load versus bar displacement relationship for the double pullout specimens, while a numerical analysis, incorporating the as-tested material properties of the construction materials, was

performed to obtain the tensile resistance of the lap spliced reinforcing bars in the wall splice specimens from the load versus midspan deflection relationship. Crack patterns and failure modes were compared for the different reinforcement configurations in both specimen types and internal damage was investigated by randomly cutting open some of the test specimens.

The analysis of the wall splice specimens further includes a regression model to describe the relationship between the tensile resistance of the lap spliced reinforcing bars in the wall splice specimens as a function of the splice length and the transverse bar spacing. The experimental results are also compared to the development and splice length provisions in CSA S304.1-04 (CAN/CSA, 2004a) and TMS 402-11 (MSJC, 2011).

4.2 Material Properties Results

Table 4.1 provides a summary of the average compressive strength for the different companion specimens tested along with the double pullout and the wall splice specimens; showing results for: masonry units, mortar cubes, non-absorptive grout cylinders, absorptive grout prisms, and masonry prisms. Resulting values of the coefficient of variation are also shown. The preparation and testing procedures for these companion specimens were previously presented in Sections 3.5.3 to 3.5.5 and 3.6.1 to 3.6.4, respectively. Table 4.2 shows a summary of the average mechanical properties for the reinforcing steel that are applicable to both the double pullout and wall splice specimens included in each construction phase. Mechanical properties include: yield stress, modulus of elasticity, strain at the initiation of strain hardening, slope at the initiation of strain hardening, and ultimate stress. The testing method for the reinforcing steel samples is outlined in Section 3.6.5. The following subsections provide a

detailed description of the information presented in both tables, while the individual test results for all the companion specimens are presented in Appendix 4A.

Table 4.1 Material properties for the companion specimens tested in conjunction with the double pullout and wall splice specimens.

Companion specimen type	Tested in conjunction with	Construction Phase	No. of specimens tested	Mean compressive strength (MPa)	COV[(1)] (%)
Masonry block	Pullout and wall splice specimens	I	8	25.4	6.42
	Wall splice specimens	II	10	23.4	8.13
Mortar cubes	Pullout specimens	I	11*	16.6	11.0
	Wall splice specimens	I	6	18.9	12.8
		II	21	13.5	11.5
Grout cylinders	Pullout specimens	I	10	20.5	10.6
	Wall splice specimens	I	12	18.7	10.8
		II	20*	14.1	8.26
Absorptive grout prisms	Pullout specimens	I	10	22.1	10.4
	Wall splice specimens	I	12	18.4	12.3
		II	21	16.2	11.0
Masonry prisms	Pullout specimens	I	17*	11.0	10.6
	Wall splice specimens	I	5*	12.7	2.83
		II	21	12.5	12.5

[(1)]Coefficient of Variation
**One outlier was identified that is not included in the subsequent calculations of the material properties.*

4.2.1 Concrete block masonry units

A total of 8 and 10 concrete masonry blocks were tested in compression as part of the first and second construction phases, respectively. The mean compressive strength of the

masonry units was calculated based upon the resulting load test data and the average net cross-sectional area of the blocks as obtained from an absorption test as described in Section 3.6.1. Table 4.3 shows a summary of the absorption test results for the 6 and 12 blocks that were tested as part of Phases I and II, respectively. Details of the compression and absorption test results for the individual samples are provided in Tables 4A-1 and 4A-2 in Appendix 4A, respectively.

Table 4.2 Mechanical properties for the reinforcing steel used during the two construction phases.

Constr. Phase	No. of specimens tested	Mean yield stress, f_y (MPa)	Mean modulus of elasticity, E_s (GPa)	Mean strain at initiation of strain hardening, ε_{sh}	Mean slope at initiation of strain hardening (MPa)	Mean ultimate stress, f_{ult} (MPa)
I	6	434	174	0.014	5596	611
II	6	434	180	0.013	4360	615

Table 4.3 Absorption test results for the concrete masonry blocks.

Constr. Phase	No. of Specimens tested	Mean absorption (%)	Mean density, D (Kg/m^3)	Mean net volume, V_n (mm^3)	Mean average net area, A_n (mm^2)
I	6	9.15	1890	7.34×10^6	3.86×10^4
II	12	6.49	1920	8.072×10^6	4.25×10^4

A review of the data presented in Table 4.1, showed that the masonry units tested as part of the two construction phases met the requirements for the minimum compressive strength as specified in CSA Standard A165.1 (CSA, 2004c). The mean compressive strength of the masonry units used to construct both the double pullout and the wall splice specimens in Phase I was 25.4 MPa with a coefficient of variation of 6.42%. The mean compressive strength of the blocks tested as part of the second construction phase was 23.4 MPa with a coefficient of

variation of 8.13%. No outliers were identified at the 95% confidence level for either of the two phases. The difference between the two mean values was found to be statistically significant as determined from the student “t” test. The material properties for the individual masonry units, however, were not directly required for the analysis of the test specimens. The possible impact that a higher compressive strength of the masonry units may have had on the masonry assemblage was later incorporated into the analysis by means of the masonry prisms tested in conjunction with each of the test specimens.

4.2.2 Mortar cubes

Fifty-millimetre cubes were tested to establish the compressive strength of the mortar as described in Section 3.6.2. A total of 12 mortar cubes were tested along with the double pullout specimens during the first construction phase, while 6 and 21 cubes were tested alongside of the wall splice specimens constructed as part of the first and second construction phases, respectively. Individual specimen results are presented in Tables 4A-3 and 4A-4 in Appendix 4A.

Table 4.1 shows that the mean compressive strength of the mortar cubes satisfied the minimum required compressive strength of 12.5 MPa as prescribed in CSA Standard A179-04 (CSA, 2004d) for both construction phases. The mean compressive strength for the Phase I double pullout specimens was 16.6 MPa, with one outlier identified at the 95% confidence level. The average compressive strength of the mortar cubes for the Phase I wall splice specimens was 18.9 MPa with no identified outliers. The difference in the mean compressive strength of the

mortar for both specimen types was not statistically significant and thereby indicating that the samples were from a single normal distribution.

The mean compressive strength for the mortar cubes tested as part of the second construction phase was equal to 13.5 MPa, with no outliers identified at the 95% confidence level. The average compressive strengths for the mortar cubes tested as part of the first and second construction phases were found to be statistically significantly different at the 95% confidence level. Although the coefficient of variation was similar for the two phases, the difference in the compressive strength of the mortar may have been the result of a variation in the water content of the mortar batch mixes as different masons participated in the two construction phases with each adding water to the mortar mix based upon their own appraisal and preference for workability during block laying. The difference between the mean compressive strength of the mortar between both construction phases was not considered to be significant based on the results of previous investigations which demonstrated that a 100% increase in the compressive strength of the mortar can increase the strength of the masonry assemblage by only 10 % (Drysdale and Hamid, 2005).

4.2.3 Non-absorbent grout cylinders and absorptive grout prisms

Non-absorptive cylinders and absorptive prisms were cast and tested alongside the double pullout and the wall splice specimens following the procedures discussed in Section 3.6.3 to determine the compressive strength of the grout. Individual test results are provided in Tables 4A-5 to 4A-8 in Appendix 4A.

A review of the data presented in Table 4.1 for the non-absorptive grout cylinders and absorptive grout prisms showed that the compressive strength for both companion specimen types tested as part of both construction phases met the minimum requirements as specified in CSA Standard A179-04 (CSA, 2004d). Mean compressive strengths of 20.5 and 18.7 MPa resulted based on the ten and twelve non-absorptive grout cylinders tested in conjunction with the double pullout and the wall splice specimens constructed during Phase I, respectively. No outliers were identified in the two data sets at the 95% confidence level and the difference between the mean values of the compressive strength was not statistically significant. The twenty-one Phase II non-absorptive grout cylinders had a mean compressive strength of 14.1 MPa, with one outlier identified from the data at the 95% confidence level. The difference between the mean compressive strengths for the non-absorptive grout cylinders tested in conjunction with the wall splice specimens during the two construction phases was statistically significant as determined from the statistical “t” test.

Similar to the non-absorptive grout cylinders, a total of 10 and 12 absorptive grout prisms were tested in conjunction with the double pullout and the wall splice specimens constructed in Phase I, respectively. Twenty-one specimens were tested during the second construction phase. The mean compressive strength of the grout prisms tested along with the double pullout specimens was 22.1 MPa, while that for the prisms tested in conjunction with the wall splice specimens during Phases I and II was 18.4 and 16.2 MPa, respectively. No outliers were identified for any of the data sets at the 95% confidence level.

The mean compressive strength of the Phase II non-absorptive grout cylinders and absorptive grout prisms was approximately 25 and 10% lower than that of the Phase I cylinders, respectively. Tables 3.3 and 3.4 show that the gradation of the aggregate used in both construction phases was reasonably uniform. The difference in the mean compressive strength of the grout was therefore likely the result of a variation in the material or water proportions in the mix, or a variation of the moisture content of the sand or the coarse aggregate between the two construction phases. This difference was not considered to be significant given that a previous investigation showed that an increase in the compressive strength of the grout from 20 to 30 MPa increased the compressive strength of the masonry assemblage by only 5% (Hamid and Drysdale, 1979). Furthermore, previous research by the NCMA (1999) (see Section 2.4.2) showed that a 140% increase in the compressive strength of the masonry improved the splice capacity of reinforcing bars in tension by only 27% (Ahmed, 2011).

Table 4.1 shows that the compressive strength of the Phase I absorptive and non-absorptive grout companion specimens tested in conjunction with the wall splice specimens were roughly equal. In contrast, the compressive strength of the absorptive grout prisms tested in conjunction with the double pullout specimens and the Phase II wall splice specimens was about 8 to 15% higher than that for the corresponding non-absorptive cylinders. This is consistent with previous research results that show that the reduction of the water-cement ratio, occurring as a result of the water absorbed by the masonry blocks, will typically increase the compressive strength of the grout (Drysdale and Hamid, 2005).

4.2.4 Masonry prisms

Sections 3.5.5 and 3.6.4 describe that one masonry prism per test specimen (i.e. double pullout and wall splice specimen), was constructed to establish the compressive strength of the masonry assemblage. A total of 18 and 6 masonry prisms were tested along with the double pullout or the wall splice specimens during Phase I, respectively, while 21 specimens were tested in conjunction with the twenty-one Phase II wall splice specimens. Test results for all individual masonry prisms are provided in Tables 4A-9 and 4A-10 in Appendix 4A.

The mean compressive strength of the masonry prisms corresponding to the Phase I pullout specimens was 11 MPa, with one outlier identified at the 95% confidence level. The prisms tested in conjunction with the wall splice specimens during Phases I and II had average compressive strengths of 12.7 and 12.5 MPa, respectively, with one outlier identified in the data set corresponding to one of the Phase I specimens. The difference in the mean compressive strength of the masonry prisms tested in conjunction with the wall splice specimens in both construction phases was found not to be statistically significant. Overall results for the mean compressive strength of the masonry prisms for both construction phases were compared to the requirements for the specified compressive strength of the masonry assemblage in accordance with CSA S304.1-04 (CAN/CSA, 2004a). Results showed that the compressive strengths as obtained for both, Phases I and II, roughly coincided with those indicated in the design code.

As described in Section 3.6.4, two linear variable differential transducers (LVDTs) were attached to the face shell at the mid-height of the top and bottom blocks of the masonry prisms to measure the vertical deformation of the specimens as testing progressed. Figure 4.1 shows a

representative stress versus strain curve of a masonry prism as obtained experimentally. The complete strain versus strain relationship could not be recorded for all the masonry prisms as the rotation of the face shell that occurred as a result of the applied load often caused the loosening of the steel angles used as supports for the LVDTs. Nonetheless, the curves for the masonry prisms with satisfactory measurements of the vertical deformation were used in the analysis of the wall splice specimens as will be discussed in subsequent sections.

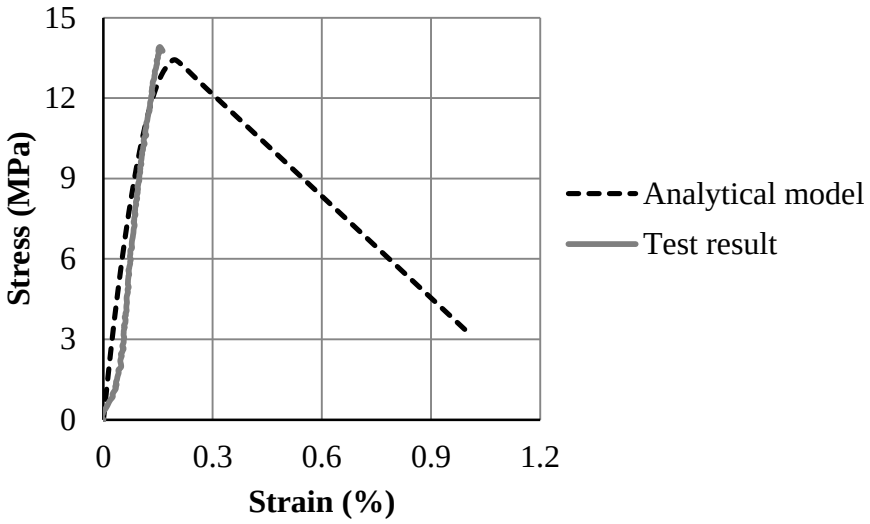

Figure 4.1 Representative stress-strain curve for a masonry prism.

4.2.5 Reinforcing steel

Table 4.2 shows a summary of the mechanical properties of the reinforcing steel as obtained from tests of bar samples obtained from the material supplied for the two construction phases. Details of the testing setup and instrumentation are provided in Section 3.6.5. Individual test results are presented in Table 4A-11 in Appendix 4A. A total of 6 samples were tested as part of each construction phase and resulted in an average yield stress of 434 MPa for both

Phases I and II. Figure 4.2 shows a representative stress-strain curve for one of the reinforcing steel bar samples.

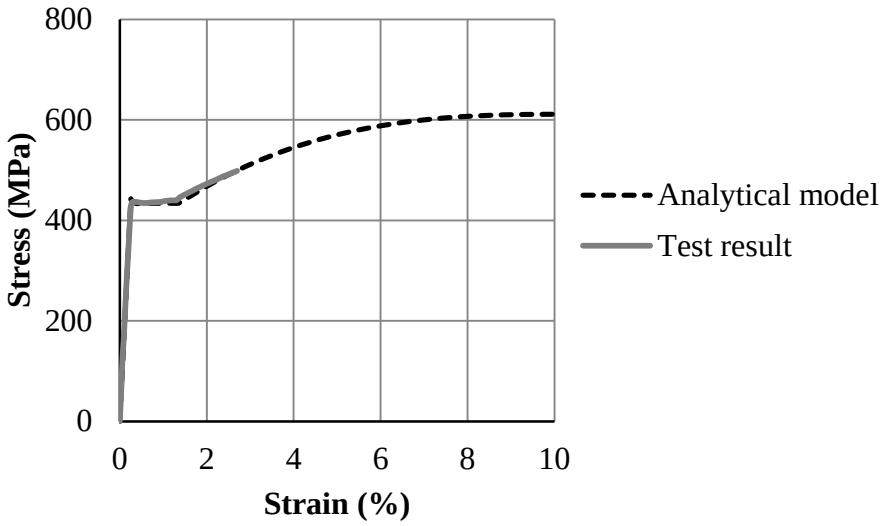

Figure 4.2 Representative stress-strain curve for the reinforcing steel.

4.3 Double Pullout Specimens with Contact Lap Splices

The following subsections present the results of the 18 double pullout specimens that were tested in tension during the first construction stage. As discussed previously, the double pullout specimens were reinforced with bars in contact with splice lengths of 250, 200, and 150 mm, to confirm that these lap lengths would all result in a bond failure of the reinforcement rather than a flexural failure initiated by yielding of the reinforcement. If the results for these splice lengths proved satisfactory, they would be tested in full-scale wall splice specimens. Otherwise, smaller lap splice lengths would be incorporated. The experimental plan is described in Section 3.2, whereas Sections 3.3.1, 3.5.6, and 3.6.6 provide the details of the test specimens, the construction process, and the test setup for the double pullout specimens, respectively. The

tensile resistance versus bar displacement relationship of the lap spliced bars, failure modes, and observed internal damage for all the reinforcement configurations tested in these specimens are presented and discussed herein.

4.3.1 Tensile resistance of the lap spliced reinforcement

The tensile resistance of the reinforcement in the double pullout specimens was obtained directly from the load versus displacement response as recorded by the data acquisition system. This section presents a summary of the experimental results for the different splice configurations tested in the double pullout specimens. The specimen ID used is of the form Paaa-b where 'P' indicates that double pullout specimens were used, aaa is the lap splice length in millimetres, and 'b' is the replicate number within each series.

Figures 4.3, 4.4, and 4.5 show the tensile resistance versus splice displacement curves for representative specimens with 150, 200, and 250 mm lap splice lengths, respectively. The curves for all the individual replicates are provided in Appendix 4B. In each figure, the horizontal dotted line indicates the theoretical yield load of the reinforcement equal to 86.8 kN as established based upon the as-tested yield strength for the first construction phase (see Section 4.2.5) multiplied by the nominal cross-sectional area of the reinforcing bars. In general, and regardless of the lap splice length provided, the splice tensile resistance versus displacement behaviour for all double pullout specimens showed that the load increased linearly with small displacements from the origin to the point that typically represented the maximum load. The load then remained constant with increasing splice displacements until failure either by bar pullout only, or by bar pullout combined with a longitudinal splitting failure.

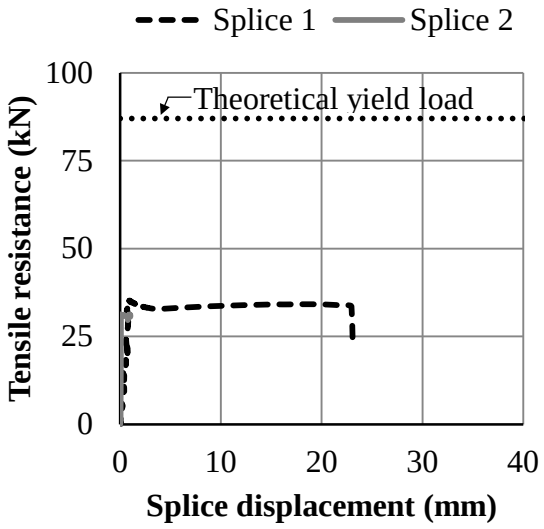

Figure 4.3 Tensile resistance of the lap spliced reinforcement versus displacement – Specimen P150-3.

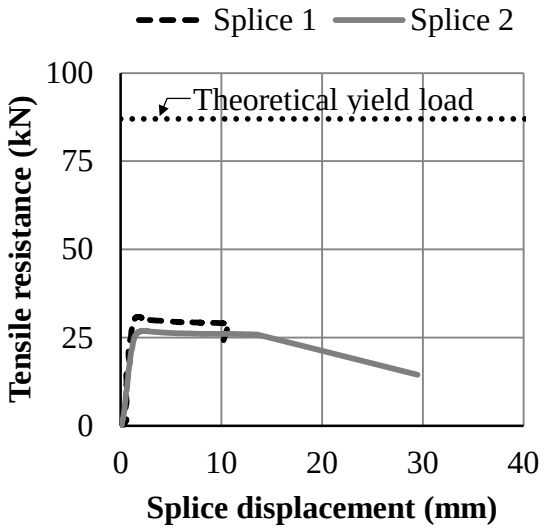

Figure 4.4 Tensile resistance of the lap spliced reinforcement versus displacement– Specimen P200-5.

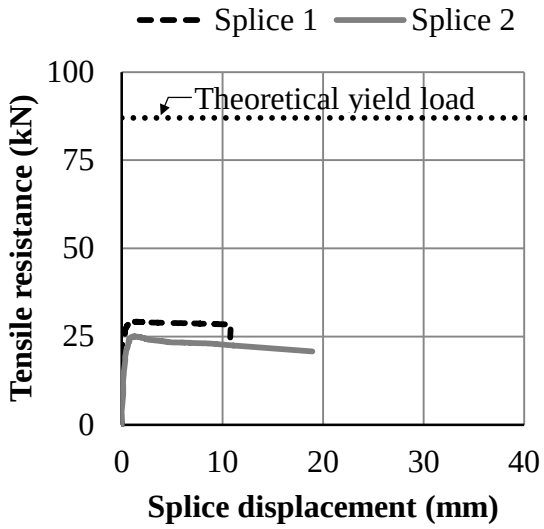

Figure 4.5 Tensile resistance of the lap spliced reinforcement versus displacement – Specimen P250-2.

All lap splices in all replicate specimens failed at loads equivalent to 26 to 41% of the theoretical yield load of the reinforcement, suggesting that a bond failure occurred in all specimens. As a result of the alternating incremental displacements of the hydraulic cylinders used in the testing of the double pullout specimens, as was previously described in Section 3.6.6, one of the lap splices (i.e. Splice 1, connected to the left load cell on the frame (see Figure 3.27)) typically attained a higher tensile resistance at failure as compared to the second splice (i.e. Splice 2, connected to the right load cell on the frame (Figure 3.27)). The mean difference in the applied load between the two splices in a given specimen was equal to approximately 12.8, 7.6, and 12.6% of the maximum recorded load for the specimens with 150, 200, and 250 mm lap splice length, respectively.

Table 4.4 shows a summary of the recorded tensile resistance for the two sets of lap spliced bars, and the failure mode identified for each of the six replicates that were reinforced with either 150, 200, or 250 mm lap spliced bars in contact. The representative maximum tensile resistance for the reinforcement in a given specimen, marked with an asterisk in the table, was defined as the maximum load recorded for the splice in which failure was first detected. In the case of specimen P150-4, which did not show evident signs of failure in any of the lap splices, the maximum tensile resistance was defined as the maximum load recorded for either of the splices.

Table 4.4 Tensile resistance and failure modes for the lap spliced reinforcement in the double pullout specimens.

Specimen	Splice no.	Tensile resistance (kN)	Failure mode	Mean tensile resistance (kN)	C.O.V. (%)
P150-1**	1	37.6	Pullout of splice No. 2	33.2	5.4
	2	33.4*			
P150-2	1	37.2	Pullout of splice No. 2		
	2	33.2*			
P150-3	1	35.3*	Pullout of splice No. 1		
	2	31.3			
P150-4	1	34.9*	Longitudinal splitting		
	2	30.0			
P150-5**	1	32.1*	Pullout of splice No. 1 and specimen splitting		
	2	39.3			
P150-6	1	29.9	Pullout of splice No. 2 and longitudinal splitting		
	2	30.4*			
P200-1**	1	31.1*	Pullout of splice No. 1 and longitudinal splitting	30.3	6.5
	2	31.1			
P200-2	1	32.0*	Pullout of splice No. 1 and longitudinal splitting		
	2	28.7			
P200-3	1	32.2*	Pullout of splice No. 1 and longitudinal splitting		
	2	28.6			
P200-4	1	30.0*	Pullout of splice No. 1		
	2	29.0			
P200-5	1	31.0	Pullout of splice No. 2 and longitudinal splitting		
	2	26.9*			
P200-6	1	29.5*	Pullout of splice No. 1 followed by coupler failure		
	2	27.3			
P250-1**	1	28.1	Pullout of splice No. 2	25.2	7.7
	2	26.2*			
P250-2	1	29.3	Pullout of splice No. 2		
	2	25.1*			
P250-3	1	28.4*	Pullout of splice No. 1 and longitudinal splitting		
	2	23.4			
P250-4	1	27.4	Pullout of splice No. 2 and longitudinal splitting		
	2	24.4*			
P250-5	1	28.2	Pullout of splice No. 2 and longitudinal splitting		
	2	24.5*			
P250-6	1	26.2	Pullout of splice No. 2 followed by coupler failure		
	2	22.7*			

** Representative maximum tensile resistance of the reinforcement in the specimen.*

*** Indicates that the test for this specimen had to be repeated due to a coupler or test frame problem prior to specimen failure.*

A double asterisk (**) as shown for specimen P150-1 in Table 4.4, was used to identify specimens in which one of the couplers used in the testing frame failed due to shearing of the bolts resulting in slip of the reinforcement. Such coupler failures generally occurred prior to any signs of cracking or bar pullout in the specimens. A review of the data for these specimens did not identify any plastic deformation of the reinforcement resulting from the coupler failure. The test in such cases was stopped and resumed after the coupler was replaced and bolted again to the reinforcing bars and the testing frame. The observed crack pattern and recorded maximum load for the specimens in which a coupler failure occurred were consistent with those obtained for the other replicates in the same group and therefore considered as part of the database of test results.

The mean tensile resistance of the reinforcement in the specimens with a 150 mm lap splice length was 33.2 kN with a coefficient of variation of 5.4%. The mean splice tensile resistance and coefficient of variation for the specimens with 200 and 250 mm lap splice lengths were 30.3 kN and 6.5%, and 25.2 kN and 7.7%, respectively. No outliers were identified at the 95% confidence level in any of the data sets. The difference between the mean tensile resistances of the reinforcement was found to be statistically significant at the 95% confidence level as established from the one-way analysis of variance (ANOVA) statistical test.

Although the load versus splice displacement behavior obtained for the double pullout specimens is comparable to that observed in similar investigations, results show that the tensile resistance of the contact lap splices in the double pullout specimens was inversely proportional to the lap splice length provided. A detailed analysis of the results did not identify any particular reason for this behaviour. A possible explanation for this phenomenon is the linear but not

proportional relationship between bond force and lap splice length known from reinforced concrete (ACI Committee 408, 2003). For short lap splice lengths such as those used in this investigation, the ratios of the bond force and lap splice length for the different reinforcement configurations are close to the origin with the possibility of a non-constant variation between them. The bond force-lap splice length relationship for the specimens with a 250 mm lap splice length may have a steeper slope but a lower y-intercept as compared to that for the specimens with 200 and 150 mm lap splice lengths and might be the result of a better grout consolidation achieved around the shorter splices. A more accurate relationship, however, would have to be established in order to confirm this phenomenon.

4.3.2 Failure modes and external crack propagation

Table 4.4 shows that three different failure modes were identified for the double pullout specimens: bar pullout, bar pullout followed longitudinal splitting cracks forming at the surface of the center block course, and sudden splitting failure of the masonry assemblage. The bar pullout and combined bar pullout with longitudinal splitting failure modes were predominant in all reinforcement configurations, whereas failure involving sudden splitting of the masonry assemblage was only identified for two replicates within the P150 specimen series. The block layout of the pullout specimens with respect to the testing frame was kept constant during testing so that failure modes and crack propagation patterns could be properly compared.

Figure 4.6 shows a photograph of a representative specimen for which a bar pullout failure was identified (Specimen P250-1). Pullout of one of the reinforcing bars at either the loaded (connected to the hydraulic rams) or the resisting (bolted to the testing frame) ends

typically occurred shortly after the lap splice attained its maximum tensile capacity. Cracking of these specimens was predominantly observed in the mortar joints adjacent to the splice that showed evidence of failure and extended in most cases to the top and bottom courses through the mortar joints.

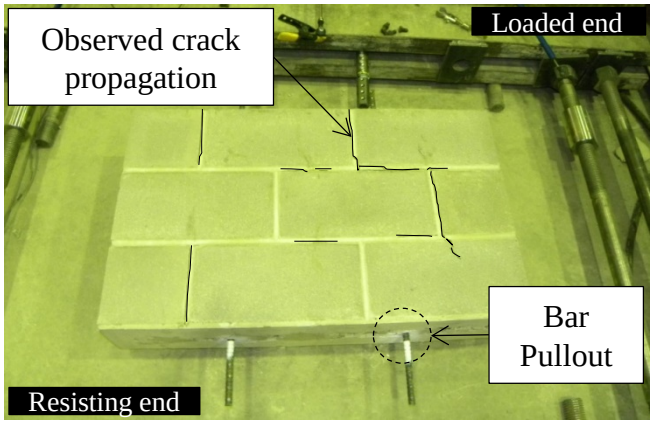

Figure 4.6 Typical bar pullout failure and crack propagation in a representative specimen – Specimen P250-1.

Figure 4.7 shows a photograph of the typical combined bar pullout and longitudinal splitting failure in a representative specimen (Specimen P200-5). Specimens exhibiting this failure mode showed the formation of longitudinal splitting cracks at the surface of the center block course, in addition to pullout of one of the reinforcing bars in either the loaded or resisting ends. The splitting cracks typically extended towards the top and bottom ends of the specimens through the mortar joints adjacent to the splice that showed evidence of failure.

Failure involving splitting of the masonry assemblage was only observed for two specimens with a 150 mm lap splice length: Specimens P150-4, and P150-5. Figure 4.8 shows a photograph of this type of failure in Specimen P150-4. Shortly after the maximum tensile

capacity of the lap splices was attained in these replicates, longitudinal splitting cracks formed on the surface of the centre block course adjacent to Splice 2 and extended towards the specimen ends through the mortar joints in the top and bottom courses. The cracks then started to widen until a sudden failure of the specimen occurred. Very little displacement was observed for the lap splices in specimen P150-5, whereas pullout of both reinforcing bars at the resisting end was observed for specimen P150-4.

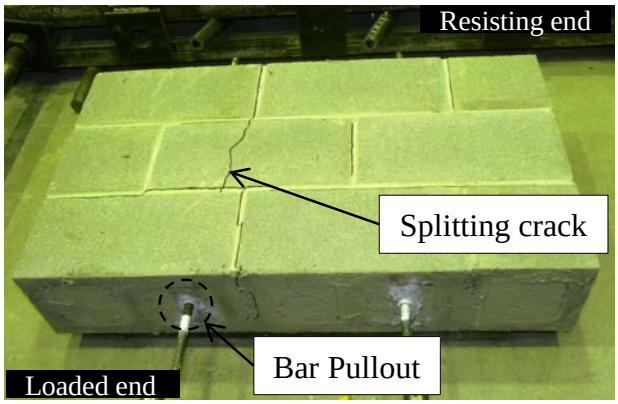

Figure 4.7 Bar pullout followed by longitudinal splitting failure mode in a representative specimen – Specimen P200-5.

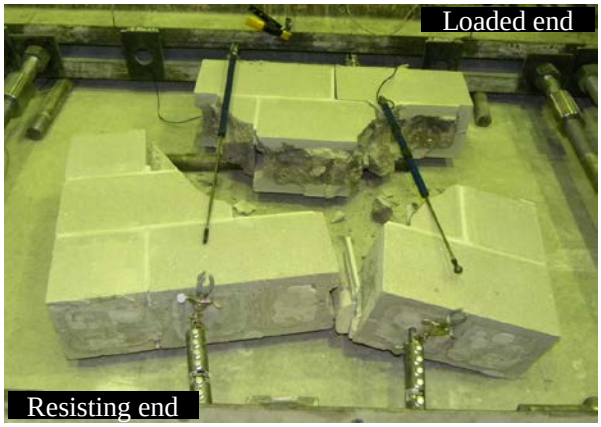

Figure 4.8 Splitting failure of the masonry assemblage observed in specimen P150-4.

As mentioned previously, several failures by shearing of the mechanical couplers that connected the test specimens to the steel frame were observed in some pullout specimens, generally prior to any signs of cracking or failure. Figure 4.9 shows a photograph of the pullout failure identified for specimens P200-6 and P250-6 that coincided with bolt shearing (i.e. coupler failure) of one of the lap splices at the resisting end. Bolt shearing in these specimens was identified for the same splice that failed by pullout of one of the reinforcing bars at the resisting end, causing a sudden drop in the applied load. The tensile resistance of the lap spliced bars versus bar displacement relationship, as well as the crack propagation pattern for these specimens were consistent to the other replicates in the P200 and P250 specimen series, respectively.

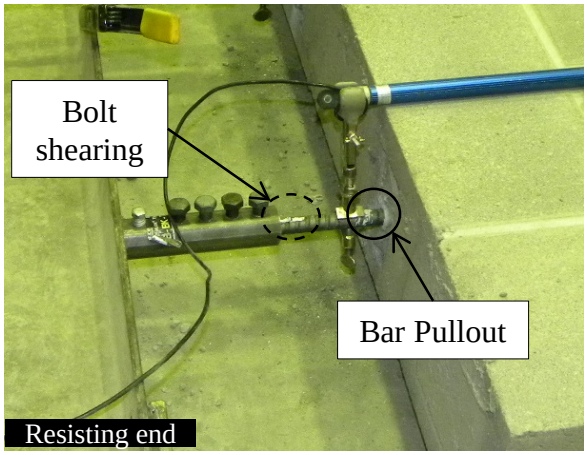

Figure 4.9 Combined bar pullout and coupler failure observed in specimen P200-6.

In an attempt to reduce the occurrence of these failures, new bolts were incorporated during the testing of the P200 specimen series, to prevent shearing of the mechanical couplers, as a visual inspection of the testing frame components showed that most of the bolt tips were

getting worn as a result of their reuse. The repeated occurrence of coupler failures in this type of test has also been reported by other authors (De Vial, 2009; Ahmed, 2011).

In addition to shearing of the mechanical couplers, some buckling of the testing frame was also typically observed with increasing applied load. The frame was adjusted several times during the testing phase in an attempt to provide more stability and prevent deformation. Possible impacts of the elastic buckling of the frame in the tensile resistance of the lap spliced reinforcing bars, the crack propagation patterns, or failure modes were not identified.

4.3.3 Observed internal damage

Following testing, the face shell and grout surrounding the reinforcement were removed for select random pullout specimens within each of the P150, P200, and P250 test series to investigate internal cracking patterns and/or bond deterioration within the lap splice length. Similar internal crack propagation patterns, after the removal of the face shell, were observed for the specimens that showed evidence of a bar pullout failure in combination with longitudinal splitting. Figure 4.10-a) shows the partial-depth saw cuts that were made in the zones adjacent to the lap splice in a representative specimen (Specimen P250-5). Figure 4.10-b) shows the observed crack propagation through the grout and towards the mortar joints that terminated in the formation of the characteristic exterior splitting cracks in the specimens that were observed once the block face shell was removed. As discussed in Section 2.3, the additional lateral forces created as a result of the relative movement of the bars in contact riding over each other with increasing slip often result in longitudinal splitting cracks when the circumferential tensile forces in the lapped reinforcing bars exceed the tensile resistance of the surrounding grout.

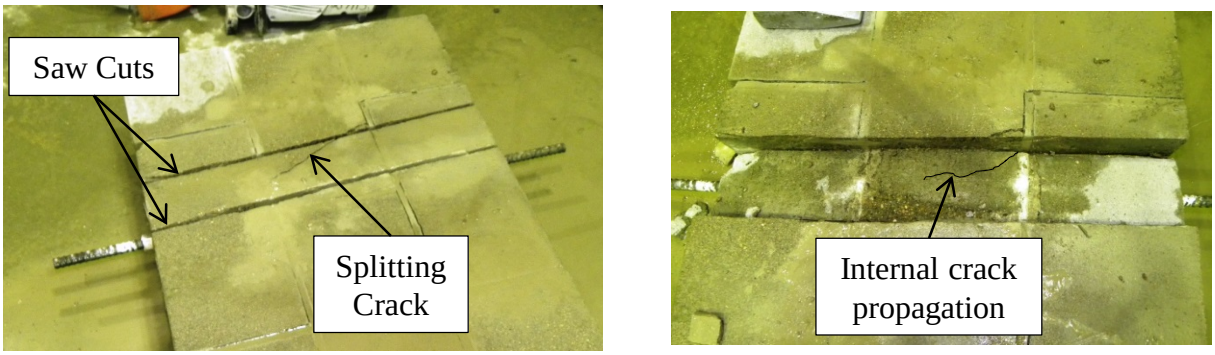

a) b)

Figure 4.10 Crack propagation observed after the removal of the face shell in specimens that failed by bar pullout followed by longitudinal splitting: a) splitting crack at the specimen surface and partial-depth saw cuts, and b) crack propagation through the grout and towards the specimen surface – Specimen P250-5.

After removing the grout surrounding the reinforcement, similar observations were noted for all specimens that failed either by bar pullout only or by bar pullout followed by longitudinal splitting. Figure 4.11 shows a photograph of the typical internal damage in a representative specimen (Specimen P250-1). Crushing of the grout between the reinforcing bar lugs and a significant bar displacement were noted, indicating that shearing between the reinforcing bars and the surrounding grout led to the pullout failure of these specimens.

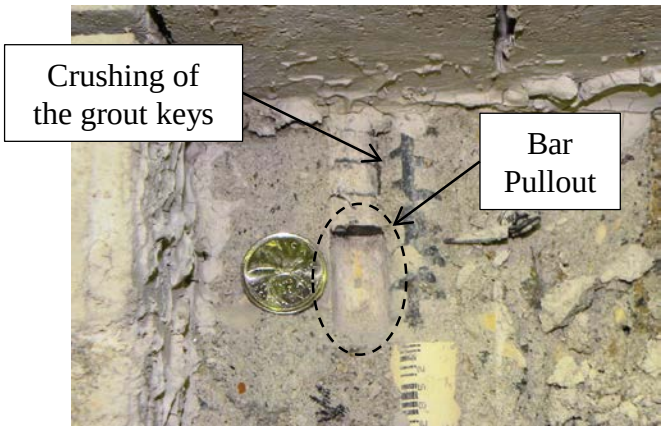

Figure 4.11 Typical internal damage observed in the specimens that failed by bar pullout only or by bar pullout followed by longitudinal splitting – Specimen P250-1.

4.3.4 Summary of double pullout specimen testing

Regardless of the lap splice length provided, all of the double pullout specimens with contact lap splices failed at loads well below the theoretical yield load of the reinforcement. The contact lap splices with a 150, 200, and 250 mm lap splice length developed approximately 38, 35, and 29% of the theoretical yield capacity of the reinforcement, respectively. These results indicate that the three values of lap splice length initially tested in the double pullout specimens allowed for a bond failure, without causing yielding of the steel reinforcement. These lap splice lengths were therefore incorporated in the full-scale wall splice specimens. Such test results are presented in the following section.

Contrary to what was expected, the results show that the tensile resistance of the contact lap splices in the double pullout specimens was inversely proportional to the lap splice length provided. A detailed analysis of the results of the companion specimens and the test specimens did not identify any particular reason for this behaviour. With the short lap splice lengths used in this investigation, the linear but not proportional relationship between bond force and lap splice length known from reinforced concrete may provide an explanation for this behaviour.

Three failure modes were identified in the double pullout specimens: bar pullout, bar pullout followed by longitudinal splitting, and splitting of the masonry assemblage with no visual evidence of bar pullout. The combined bar pullout and longitudinal splitting was identified as the predominant failure mode and occurred mainly in the specimens with a 200 and a 250 mm lap splice length. This failure mode was consistent with that observed in previous investigations of

spliced reinforcement in double pullout specimens (Ahmed and Feldman, 2012; De Vial, 2009; Mjelde, 2008; NCMA, 1999; Schuller et al., 1993; Cheema and Klingner, 1985).

Shearing of the mechanical couplers that connected the test specimens to the steel frame was observed particularly at the beginning of the tests, and prior to any signs of failure, in some of the pullout specimens. The test in such cases was stopped and repeated after adjusting or changing the couplers. Some elastic buckling of the testing frame was also frequently observed with increasing applied load. The frame had to be adjusted several times during the testing phase in an attempt to provide more stability and prevent deformation. Possible effects of the coupler failures or the observed elastic buckling in the tensile resistance of the lap spliced reinforcing bars, the crack propagation patterns, or failure modes in the double pullout specimens, were not identified.

4.4 Full-Scale Wall Splice Specimens

This section presents the results of the 27 full-scale wall splice specimens that were tested in flexure using a four-point loading arrangement. Three values of lap splice length (i.e. 150, 200, and 250 mm), as established from the results of the double pullout specimens, were tested in the wall splice specimens in combination with three values of transverse bar spacing: 0, 25, and 50 mm. The lapped reinforcing bars were located within the same block cell. A detailed description of the experimental program and the test specimens is provided in Sections 3.2 and 3.3.2, respectively, while the construction and testing procedures for the wall splice specimens are described in Sections 3.5.7 and 3.6.7, respectively.

The load versus midspan deflection response, as well as the observed failure modes, crack propagation patterns, and internal deterioration for the wall splice specimens are described in the following subsections. The results of the calculated tensile capacity for the different reinforcement configurations, and an empirical equation that describes the relationship between the evaluated parameters are then presented and discussed. Finally, a comparison of the experimental results with the development and splice length provisions in CSA S304.1-04 (CAN/CSA, 2004a) and TMS 402-11 (MSJC, 2011) is presented.

4.4.1 Load versus midspan deflection behaviour

Table 4.5 shows a summary of the load history and observed failure modes for the different splice configurations tested in the wall splice specimens. The notation system used is of the form Waaa/bb-c, where 'W' indicates that these are all wall splice specimens and "aaa" indicates the splice length in millimetres. The second number following the forward slash, "bb", corresponds to the transverse spacing provided between the lapped bars in millimetres, and the number following the hyphen, "c", indicates the replicate number within the series.

The values in Table 4.5 corresponding to the cracking load, ultimate failure load, and maximum deflection at midspan for each specimen were obtained from the load versus midspan deflection relationship as recorded by the data acquisition system connected to the MTS actuator load cell and the LVDTs. A numerical analysis, based upon the ultimate recorded load and the stress versus strain relationship for the reinforcing steel and the masonry assemblage, was performed to obtain the maximum splice tensile resistance of the wall splice specimens and will be discussed in detail in the following subsections.

Table 4.5 Load history and failure modes for the different splice configurations tested in the wall splice specimens.

Specimen ID.	Constr. Phase	Cracking load (kN)	Midspan deflection (mm)	Ultimate failure load (kN)	Failure mode	Mean cracking load (kN)	Mean ultimate failure load (kN)
W150/0-1		4.9	12.6	20.5			
W150/0-2	II	4.6	12.3	20.1		5.4	21.2
W150/0-3		4.8	11.2	23.0			
W150/25-1		4.9	10.1	17.4	Midspan flexural crack through the mortar joint		
W150/25-2	I	4.0	11.5	23.2		4.3	19.4
W150/25-3		2.5	10.4	17.5			
W150/50-1		2.8	9.3	20.3			
W150/50-2	II	6.2	8.5	17.9		4.7	19.5
W150/50-3		5.1	9.4	20.2			
W200/0-1		6.4	14.3	33.5			
W200/0-2	II	5.4	15.9	31.4		5.6	33.0
W200/0-3		5.1	15.5	34.2			
W200/25-1		5.9	13.2	19.9	Midspan flexural crack through the mortar joint[(2)]		
W200/25-2	I	5.6	10.0	21.5		4.9	22.6
W200/25-3		3.3	11.7	26.4			
W200/50-1		8.4	12.0	19.5			
W200/50-2	II	5.1	11.0	22.9		6.2	21.2
W200/50-3		5.0	12.4	21.2			
W250/0-1		2.0	16.8	34.6			
W250/0-2	II	7.1	13.2	32.7		4.0	35.1
W250/0-3[(1)]		2.8	22.6	37.9			
W250/25-1		8.7	9.6	19.6	Midspan flexural crack through the mortar joint		
W250/25-2	II	6.7	14.5	31.7		6.6	26.3
W250/25-3		4.4	14.5	27.6			
W250/50-1		6.5	14.9	28.6			
W250/50-2	II	4.6	9.9	24.0		6.4	25.1
W250/50-3		8.3	10.3	22.6			

[(1)]*The longitudinal reinforcement in this specimen yielded prior to failure at an applied load of approximately 36 kN*

[(2)]*In addition to the midspan flexural crack, a longitudinal splitting crack along one of the spliced reinforcing bars was observed in specimen W200/0-3*

Figures 4.12, 4.13 and 4.14 show the load versus midspan deflection curves for representative specimens with a 150, 200, and 250 mm lap splice length, respectively. Each of these figures shows curves corresponding to the three values of transverse bar spacing that were tested (i.e. 0, 25, and 50 mm). The individual load versus midspan deflection curves for all 27 wall splice specimens are provided in Appendix 4C. In general, the load-deflection response for all of the reinforcement configurations can be divided into two stages prior to the attainment of the maximum load. In the first stage, a linear increase from the origin to the load that represents first cracking is noted. In the second stage, the applied load continues to increase linearly with increasing deflection at a reduced slope until failure. Some visible sudden decreases in the load (i.e. noise) were associated with the formation of additional cracks. A slight reduction in slope before the ultimate load, most likely caused by a reduction in stiffness due to bond loss at the location of the splice (Ahmed and Feldman, 2012), as well as a brief gradual unloading curve after the peak load, suggests a sudden failure in bond occurred for all splice configurations.

Each of Figures 4.12 to 4.14 shows that the experimental load versus midspan deflection curves for the different reinforcement arrangements generally agreed well with the theoretical curves derived for each splice length configuration. A detailed description of the mathematical expressions used in the development of the theoretical load-deflection curve is provided in Appendix 4E. Inelastic behaviour with a well-defined plateau, indicating yielding of the reinforcement, was only observed for one of the W250/0 replicates (Specimen W250/0-3). Figure 4.15 shows the load versus midspan deflection curve for this specimen.

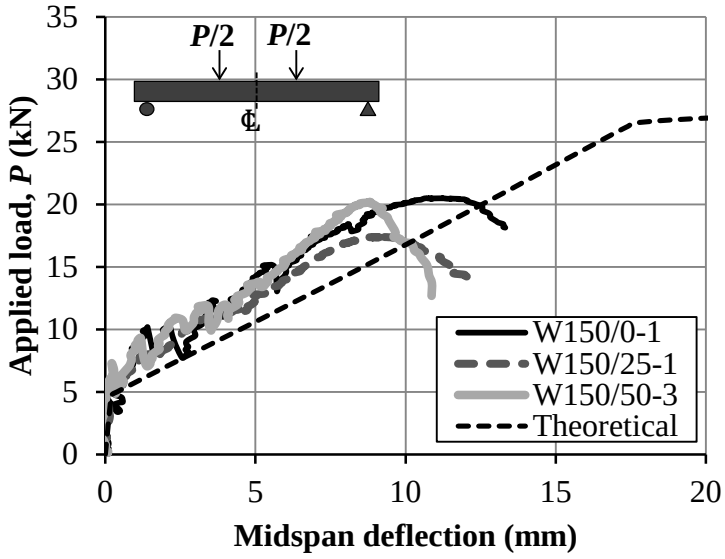

Figure 4.12 Representative applied load versus midspan deflection curves for specimens with a 150 mm lap splice length.

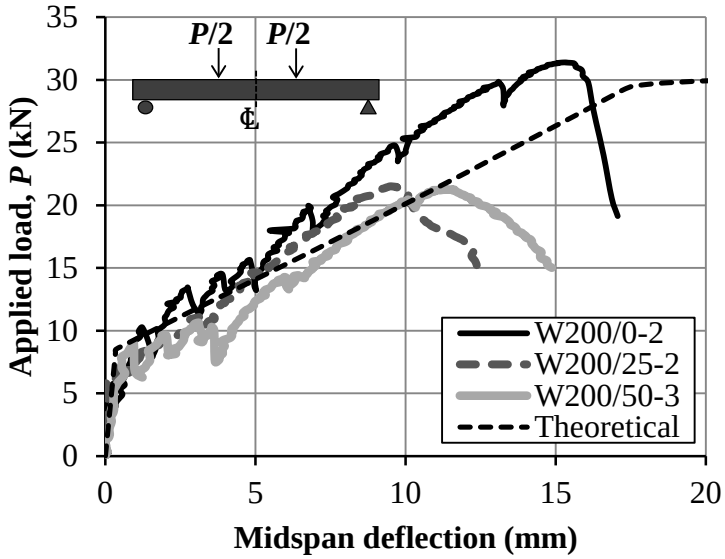

Figure 4.13 Representative applied load versus midspan deflection curves for specimens with a 200 mm lap splice length.

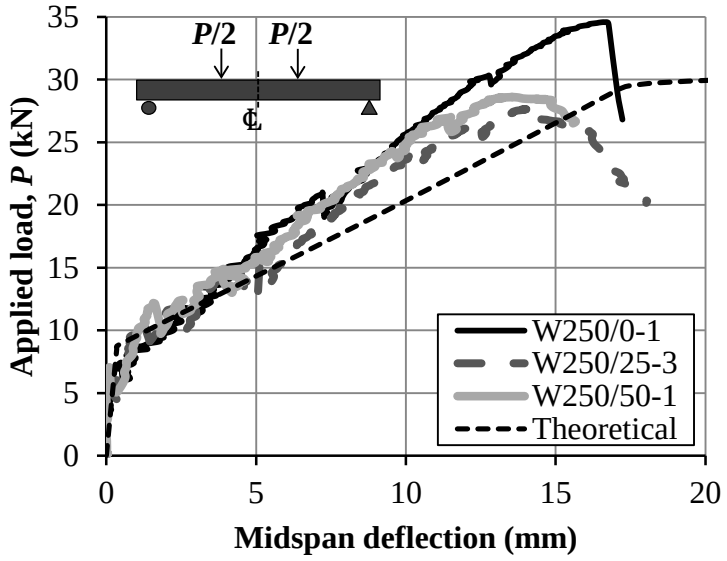

Figure 4.14 Representative applied load versus midspan deflection curves for specimens with a 250 mm lap splice length.

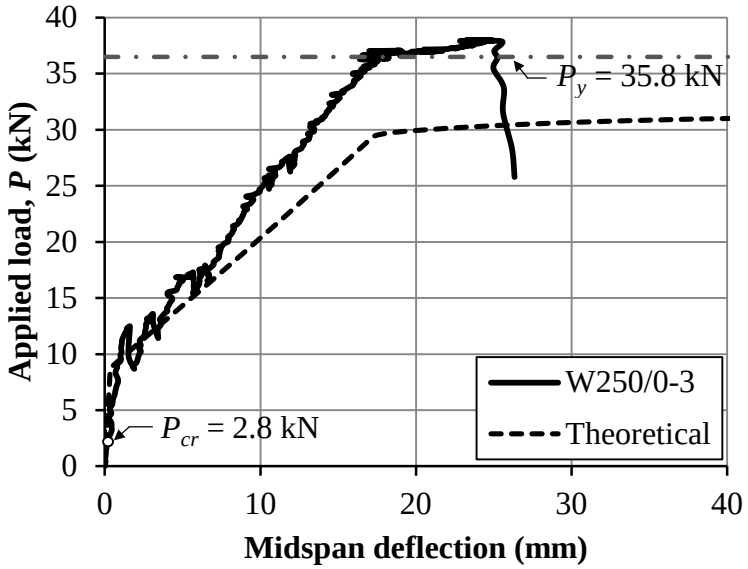

Figure 4.15 Representative applied load versus midspan deflection curve for specimen W250/0-3.

The average cracking load for the different sets of replicates ranged between 4.0 and 6.6 kN, values that are equivalent to 1.7 to 2.75 times the theoretical cracking load of 2.4 kN calculated in accordance with CSA S304.1 (CAN/CSA, 2004a) excluding the self-weight of the wall splice specimens (9.31 kN), and the weight of the spreader beam and upper supports used in the four point loading arrangement (0.94 kN). This higher cracking load as determined from testing may have been the result of an additional compressive stress possibly induced by the supports, or a higher tensile strength of the masonry assemblage as compared to that specified in the design code (Ahmed, 2011).

The load versus midspan deflection curves for all specimens with a 150 mm splice length had similar load versus midspan deflection behaviour regardless of the clear transverse spacing provided between the lap spliced bars. In contrast, specimens reinforced with 200 and 250 mm lap splices in contact generally attained about 29% and 35% higher midspan deflections respectively, as compared to those in which a non-zero clear transverse spacing was provided. In general, contact lap splices caused a slight increase in the flexural strength of the wall specimens.

The mean ultimate failure load was generally higher for the specimens with contact lap splices than for the specimens with non-contact lap splices with the same lap splice length, although this difference was minimal for the specimens with a 150 mm lap splice length, a finding that was likely due to the very short lap splice length for this set of replicates. The specimens with lapped bars in contact with 150 mm lap splice lengths failed at loads approximately 9% higher than those in which a transverse bar spacing was provided. In contrast,

specimens with 200 and 250 mm lap spliced bars in contact failed at loads 50 and 37% higher than the specimens with the same lap splice length but with non-contact lap splices, respectively.

4.4.2 External crack propagation and failure modes

The failure mode and crack propagation patterns were similar for all of the reinforcement configurations tested. Flexural cracks were only observed in the mortar joints and typically propagated from the joints adjacent to the points of applied load to the joints adjacent to the specimen centreline and up to the third or fourth joints adjacent to the supports. Figure 4.16 shows the typical crack propagation of a representative specimen (Specimen W200/0-1) at different load levels. Figures 4.16-a) through c) show the observed crack propagation at P equal to 0.3, 0.5, and 0.7 times the maximum failure load, P_{ult}, respectively, whereas Figure 4.16-d) shows the characteristic crack pattern observed at the maximum resisting load (i.e. $P = P_{ult}$).

The widest flexural cracks, usually those that caused specimen failure, were typically the cracks that developed in the joints adjacent to the centre block course. Figure 4.17 shows a photograph of the flexural cracks observed in the mortar joints adjacent to the centre course. Figure 4.18 shows a photograph of the open flexural cracks that ultimately resulted in the failure of one of the wall splice specimens.

Along with the flexural cracks extending through the mortar joints at the side and tension faces, a segmented longitudinal splitting crack at the location of one of the lap splices on the compression face was observed for specimen W200/0-3. Figures 4.19-a) and -b) show a

photograph of the splitting crack, and a diagram of the wall splice specimen indicating the location of the crack in this specimen, respectively.

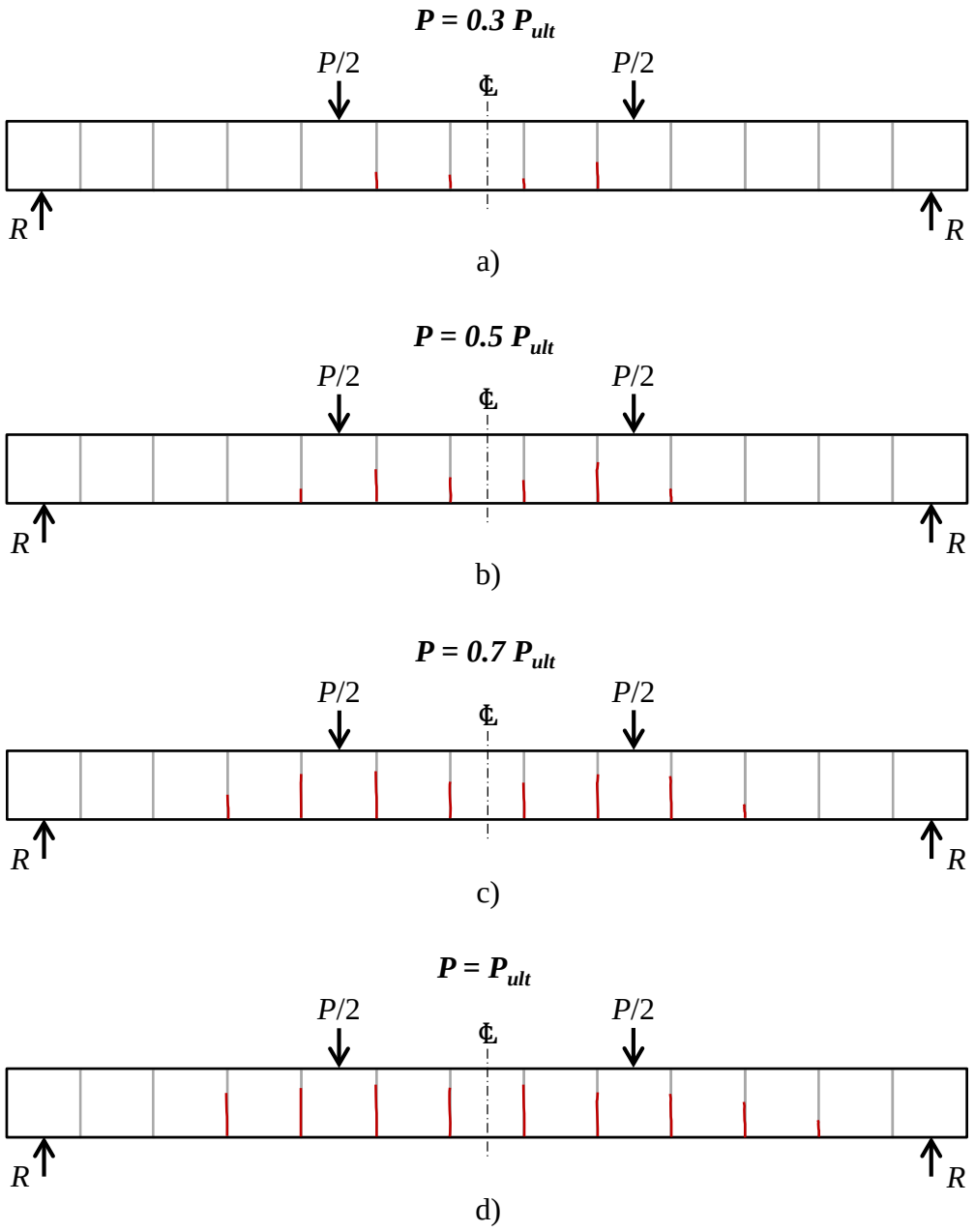

Figure 4.16 Typical crack propagation of a representative wall splice specimen at different load levels (specimen W200/0-1): a) P = 0.3 P_{ult}, b) P = 0.5 P_{ult}, c) P = 0.7 P_{ult}, and d) $P = P_{ult}$, where P_{ult} = 33.5 kN.

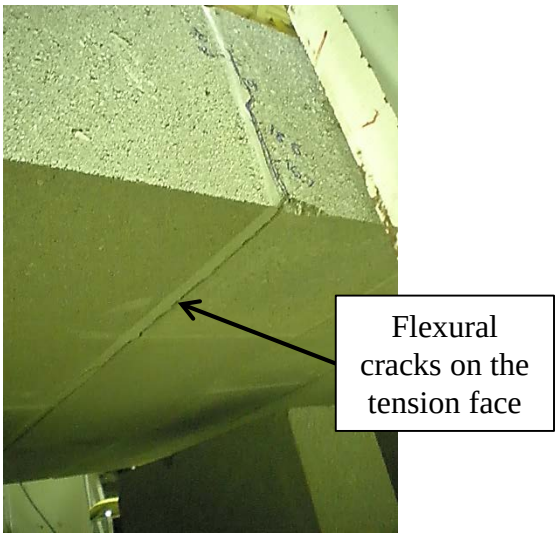

Figure 4.17 Flexural cracks observed in the mortar joints adjacent to the centre block course.

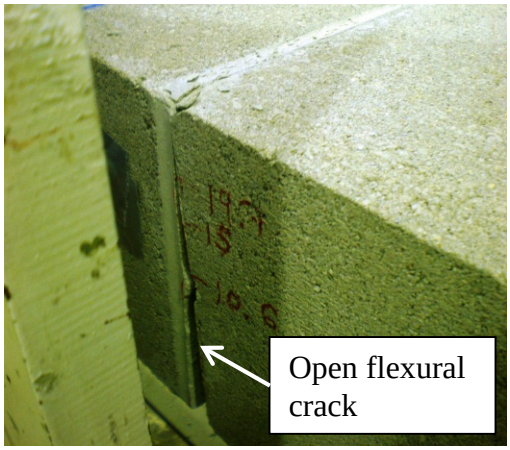

Figure 4.18 Open flexural cracks that caused specimen failure.

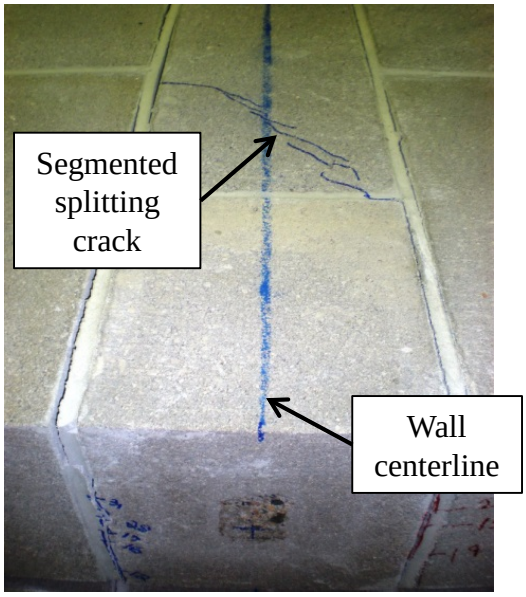

a)

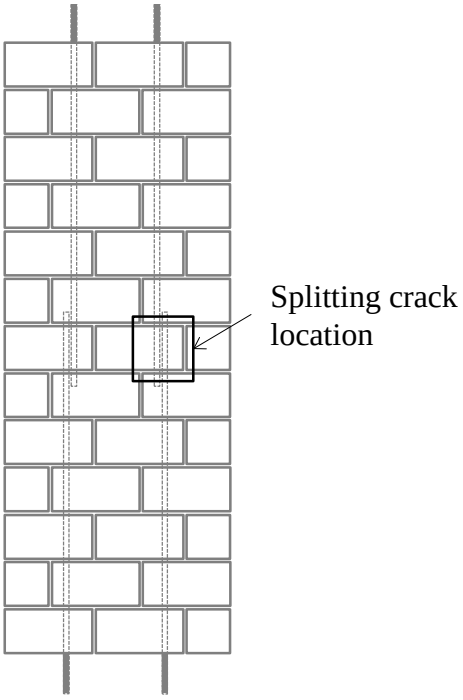

b)

Figure 4.19 Longitudinal splitting crack observed in specimen W200/0-3 – Modified from Ahmed (2011): a) splitting crack, and b) crack location.

Similar cracks were observed by Ahmed and Feldman (2012) in wall splice specimens with 300 mm long contact lap splices and No. 15 reinforcing bars. However, unlike in Specimen W200/0-1, those cracks were continuous and typically developed on the tension face (Ahmed and Feldman, 2012). The cracks observed in Specimen W200/0-1 were therefore likely the result of high compressive forces in this block course that may have caused crushing of the face shell.

4.4.3 Observed internal damage

The face shell and grout surrounding the reinforcement were removed following testing for select random specimens of each splice configuration to investigate internal cracking patterns and bond deterioration within the lap splice length. Figure 4.20 shows the typical internal damage observed in the specimens reinforced with contact lap splices (i.e. W150/0, W200/0, and W250/0 arrangements). Regardless of the lap splice length, crushing of the grout between the reinforcing bar lugs and subsequent bar pullout were observed, indicating that a bond failure between the reinforcement and the grout occurred in these specimens. Splitting cracks extending between the spliced bars through the grout and along the block-grout interface toward the mortar joints were identified, suggesting poor bond between the grout and the concrete blocks. The voids existing between block ends and areas of poor grout consolidation also facilitated the crack propagation along the mortar joints (Ahmed and Feldman, 2012).

Figure 4.21 shows the characteristic internal damage and crack propagation observed in specimens with non-contact lap splices with a 25 mm clear transverse spacing between the spliced bars (i.e. W150/25, W200/25, and W250/25 configurations). Similar to the specimens with contact lap splices, crushing of the grout keys between bar lugs and bar pullout were

observed, particularly in specimens with 200 and 250 mm lap splice lengths. Inclined struts between the lapped bars, in addition to cracks extending from the bar ends through the grout and to the mortar joints, were also identified. Bar pullout and cracking between the spliced bars were less evident for the specimens with a 150 mm lap splice length, though crack propagation from the bar ends to the mortar joints occurred and were similar to those noted in the specimens with longer lap splice lengths.

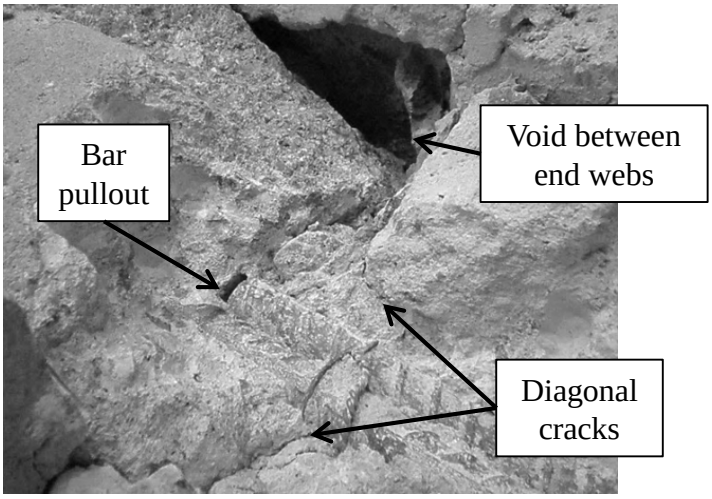

Figure 4.20 Internal damage and crack propagation observed in specimens with contact lap splices.

Figure 4.22 shows a photograph of the typical internal damage observed in specimens with a 50 mm clear transverse spacing between the spliced bars (i.e. W150/50, W200/50, and W250/50 configurations). Cracks in these specimens generally extended from the reinforcing bars to the closest grout-block interface and toward the mortar joints. Crushing of the grout between lugs, bar pullout, and cracks in the remaining grout between lapped bars were less evident as compared to specimens with lesser values of clear transverse spacing between the lap spliced bars. Cracks tended to propagate towards the nearest block-grout interface as the

transverse spacing between bars increased and was a result of the reduction in the clear cover to the reinforcement.

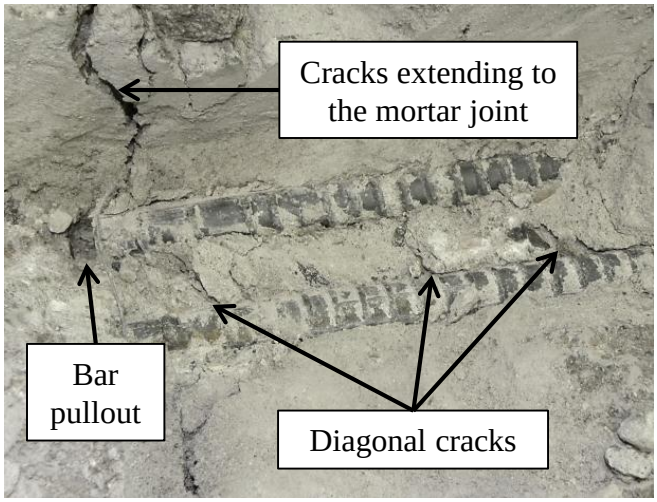

Figure 4.21 Internal damage and crack propagation observed in specimens with 25 mm splice-bar spacing.

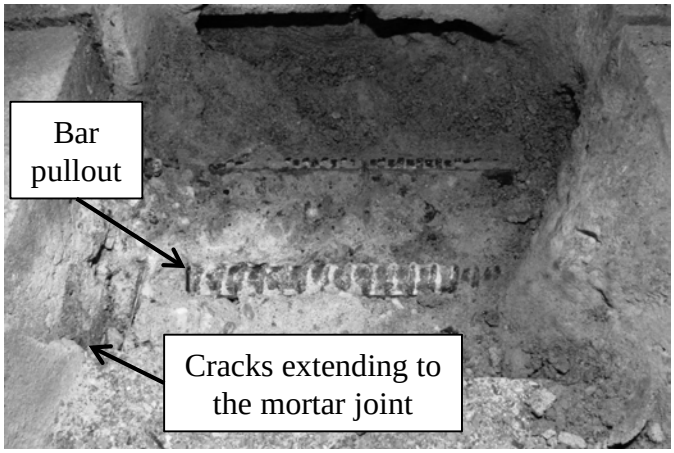

Figure 4.22 Internal damage and crack propagation observed in specimens with 50 mm splice-bar spacing.

4.4.4 Tensile capacity of the lap spliced reinforcement

Internal strain gauges were not used to instrument the reinforcing bars in the wall splice specimens and so the tension in the reinforcing bars was not directly measured. An iterative sectional analysis was therefore performed to calculate the maximum tensile resistance of the spliced reinforcing bars based upon the moment-curvature response. The analysis, similar to that adopted by Ahmed and Feldman (2012), was based upon the mechanical properties of the masonry assemblage and the reinforcing steel as obtained from the companion specimens tests, and the load history of the wall splice specimens as recorded by the data acquisition system. The following subsections describe the steps followed in the analysis of the wall splice specimens and the calculation of the tensile resistance of the lap spliced bars.

Deflection profiles for the wall splice specimens

Prior to the numerical analysis, the deflection profiles for the wall splice specimens were obtained from the vertical displacements recorded by the LVDTs. Figures 4.23-a) to -d) show the deflection profiles for a representative specimen at different levels of applied load. The figures show the vertical displacement readings at each LVDT location at the indicated applied load, as well as the second order parabolic fit that was applied to the data. The second order polynomial function is of the form $y(x)=Ax^2+Bx$, where x is the distance along the length of the specimen from the left support, y is the vertical displacement from the reference position, and A and B are the quadratic best-fit coefficients for the data set.

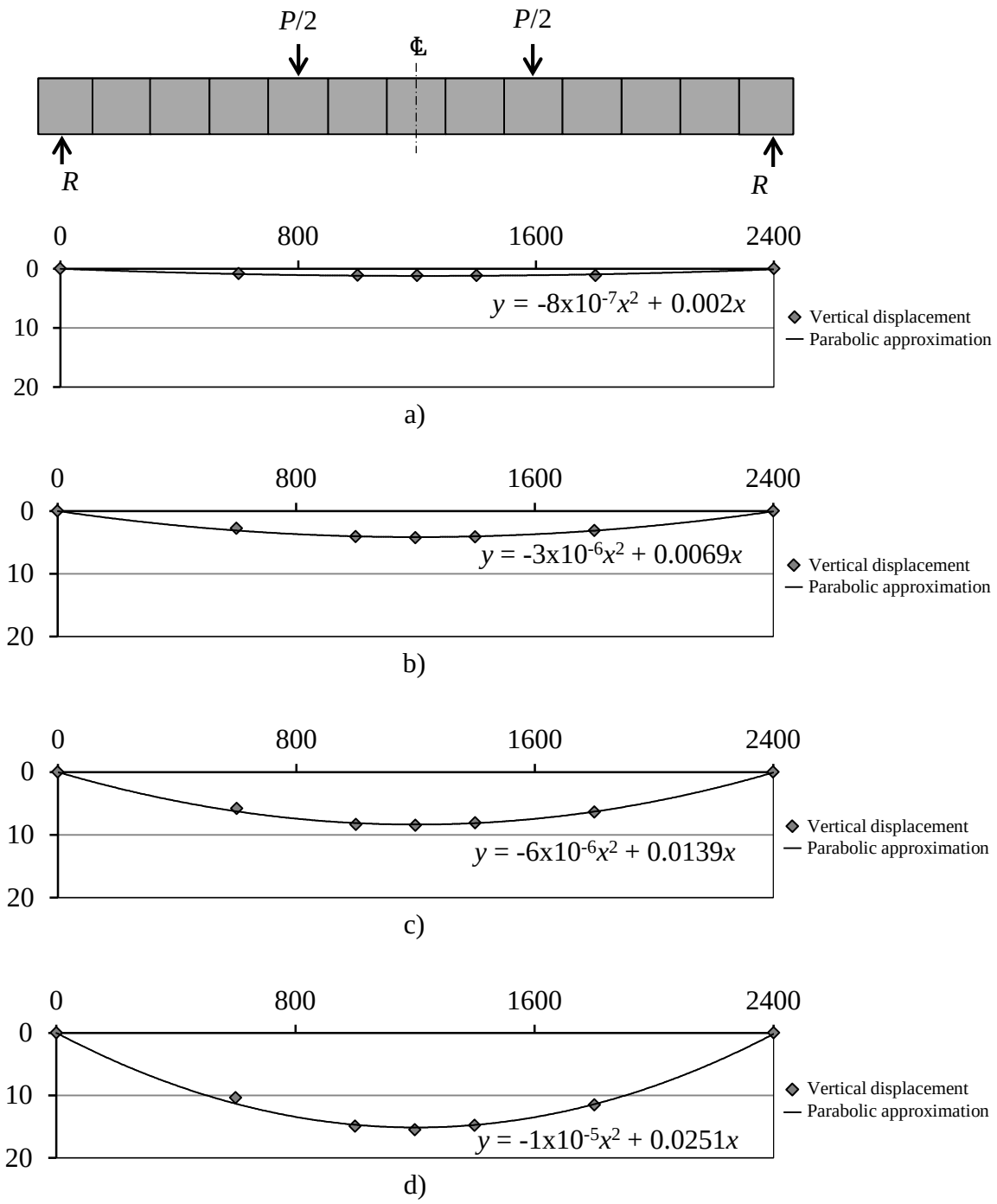

Figure 4.23 Deflection profiles for a representative specimen at different load levels (Specimen W200/0-1): a) $P = 0.3\ P_{max}$, b) $P = 0.5\ P_{max}$, c) $P = 0.7\ P_{max}$, and d) $P = P_{max}$, where P_{max} = 33.5 kN.

Moment-curvature analysis

As part of the moment-curvature analysis, the theoretical stress versus strain relationship for the masonry assemblage was first obtained by fitting the experimental data obtained for the companion masonry prisms to a modified Park-Kent curve (Park et al., 1982). Figure 4.1 in Section 4.2.4 shows that the derived strain-stress curve for the masonry prisms has two segments: a parabolic increasing segment from the origin to the point that represents the maximum stress, and a linear falling segment. The mathematical expression for this analytical model is presented in Appendix 4D. In general, the theoretical curves showed good agreement with the experimental curves measured from the companion masonry prisms.

The average mechanical properties of the reinforcing bar samples from each heat batch presented in Table 4.2 were also used to derive the theoretical stress-strain profiles for the reinforcing steel. The derived theoretical curves exhibited a linear stress-strain relationship with a slope equal to the modulus of elasticity, E_s, from the origin to the yield point. The strain then continued to increase until reaching the beginning of the strain hardening region. At this point a fourth-order parabolic curve was used to model the stress increase with strain to the ultimate strength. Figure 4.2 shows that the theoretical stress-strain curve for the reinforcing steel agreed well with the experimental curve obtained from a companion specimen tests. A detailed description of the mathematical expressions used for the analytical model is also presented in Appendix 4D.

The theoretical moment-curvature relationships for the wall splice specimens were then calculated based upon the internal moment effect resulting from the applied load level. The

curvature of the uncracked masonry section, $\varnothing_{uc}$, was obtained directly from the ratio of the internal applied moment at mid-height, M_a, divided by the flexural rigidity of the gross section, EI_{gr}. An iterative procedure, which divided the compression zone into 100 layers of equal depth, was then used to establish the neutral axis depth, c, of the cracked section at a given applied moment, M_a, based on horizontal equilibrium such that the compressive force of the masonry assemblage and the tensile force in the reinforcement were equal ($C=T$). Figures 4.24-a) to -c) show the stress diagram, the strain diagram, and the compressive and tensile forces distribution considered for the analysis.

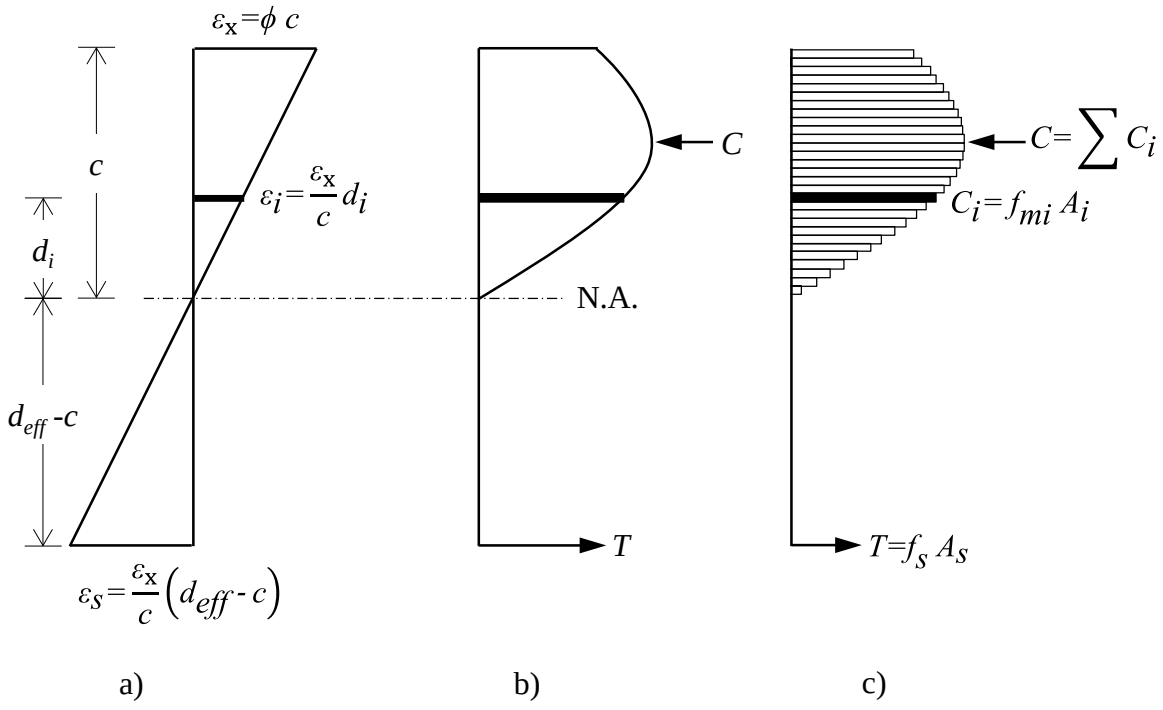

Figure 4.24 Analysis method for the wall splice specimens – Modified from Ahmed (2011): a) strain profile, b) stress profile, and c) compressive and tensile forces distribution.

The strain at the extreme compression fibre, ε_x, was first calculated using similar triangles as the product of the curvature and the neutral axis depth (ϕc). The distance between the extreme

compression fibre and the location of the neutral axis was divided into 100 equal layers and the strain at mid-height of each layer calculated considering a linear strain relationship along the specimen depth. The compressive stress, f_{mi}, corresponding to the given strain at mid-height each layer was obtained from the theoretical stress-strain curves derived for the masonry prisms. The total compressive force, *C*, was then calculated as the sum of the compressive force developed at each layer, and was set equal to the compressive stress times the cross-sectional area of each layer ($(^{c}/_{100})*b$). The strain at the effective depth of the reinforcement, ε_s, was also obtained from basic mechanics considering a linear strain profile. The tensile resistance of the reinforcement, *T*, was then calculated as the multiplication of the tensile stress, f_s, corresponding to the steel strain $(f_s(\varepsilon_s))$, as obtained from the theoretical stress-strain relationships for the reinforcing steel, and the cross-section area of the steel, A_s. The iterative program established the neutral axis depth such that a maximum difference of 0.5% existed between *T* and *C*. Finally, the resisting moment was calculated as the sum of the compressive force in each layer times the distance from the centroid of the layer to the neutral axis, and the tensile force in the reinforcement times the distance from the centroid of the reinforcing steel to the neutral axis.

An assumption used in the analysis was that plane sections remained plane until failure, and that perfect bond existed between the reinforcement and the surrounding grout. The tensile force in the concrete blocks and the grout, and the axial compressive forces that may have resulted due to friction developed at the supports were neglected.

A theoretical moment-curvature relationship was developed for each set of wall splice specimen replicates following the analytical procedure as described above. Figure 4.25 shows the

theoretical curve for a representative set of replicates (W200/25) and the experimental moment-curvature relationship of one of the specimens within the set (specimen W200/25-1). The experimental and theoretical curves for all of the specimens are presented in Appendix 4D. The theoretical moment-curvature relationship derived for each set of replicates was compared to the experimental curves as obtained from the load-deflection profiles of the wall splice specimens. The experimental curvature corresponding to an applied moment was given by the second derivative of the deflection. Therefore, the second order polynomial functions of the form $y(x)=Ax^2+Bx$, corresponding to the deflection profiles, were derived twice with respect to x to obtain the experimental curvature at a given value of applied load. All of the theoretical curves were adjusted for the self-weight of the specimens (9.31 kN) and the weight of the spreader beam and upper supports used in the four point loading arrangement (0.94 kN). In general, good agreement was obtained between the experimental and theoretically calculated moment-curvature profiles for the wall splice specimens.

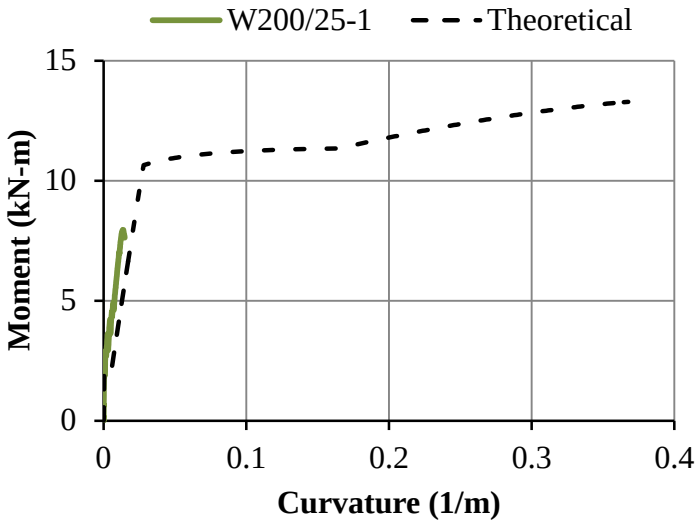

Figure 4.25 Experimental and theoretical moment-curvature curves for a representative wall splice specimen – Specimen W200/25-1.

Calculation of the tensile capacity of the lap spliced bars

The tensile resistance of the reinforcement, *T*, was computed from the theoretically calculated curvature at the maximum moment using the numerical moment-curvature analysis. The maximum moment for each replicate was calculated from the maximum failure loads reported in Table 4.5 and adjusted for the self-weight of the specimen and the weight of the spreader beam and the roller supports used in the test setup.

Table 4.6 presents the results for the maximum failure load, maximum moment, curvature at maximum moment, and calculated tensile resistance of the lap spliced bars for each of the wall splice specimen replicates. The table also shows the average tensile resistance for the different splice configurations as calculated based on tests of the three replicate specimens for each.

The maximum bending moment resulting from the maximum applied load during testing for specimens W200/0-1 and W250/0-1 slightly exceeded that corresponding to the theoretical maximum curvature of the section. The tensile resistance of the lap spliced reinforcement in these specimens could not be calculated using the numerical iterative program described in the previous subsections; therefore, these values were not included in Table 4.6. The resulting curvature at the maximum moment and the tensile resistance of the lap spliced bars for specimen W250/0-3 are also excluded from the results shown in Table 4.6 as the steel reinforcement in this specimen appeared to have yielded.

Table 4.6 Tensile resistance of the lap spliced reinforcement in the wall splice specimens.

Specimen ID.	Construction Phase	Maximum moment[(1)] (kN*m)	Curvature at maximum moment (1/m)	Lap splice tensile resistance (kN)	Mean lap splice tensile resistance (kN)
W150/0-1		12.3	0.031	72.8	
W150/0-2	II	12.1	0.030	70.5	74.3
W150/0-3		13.3	0.034	79.6	
W150/25-1		11.1	0.028	64.4	
W150/25-2	I	13.4	0.035	79.8	69.5
W150/25-3		11.1	0.028	64.4	
W150/50-1		12.2	0.031	72.8	
W150/50-2	II	11.3	0.028	65.9	70.5
W150/50-3		12.2	0.031	72.8	
W200/0-1		17.5	0.381	100	
W200/0-2	II	16.7	0.280	94.3	97.2
W200/0-3		17.8	n/a	n/a	
W200/25-1		12.1	0.032	73.3	
W200/25-2	I	12.7	0.033	75.5	78.4
W200/25-3		14.7	0.038	86.4	
W200/50-1		11.9	0.031	70.8	
W200/50-2	II	13.3	0.034	77.4	74.5
W200/50-3		12.6	0.033	75.2	
W250/0-1		17.9	n/a	n/a	
W250/0-2	II	17.2	0.334	97.7	97.7
W250/0-3		19.3	n/a	n/a	
W250/25-1		11.9	0.031	70.8	
W250/25-2	II	16.8	0.290	95.0	84.2
W250/25-3		15.1	0.067	86.8	
W250/50-1		15.5	0.185	87.1	
W250/50-2	II	13.7	0.036	81.8	82.1
W250/50-3		13.1	0.034	77.4	

[(1)]*Maximum moments corrected for the self-weight of the specimens and the weight of the spreader beam and roller supports (4.1 kN-m).*

Figure 4.26 shows a summary of the calculated mean tensile resistance, corresponding to a single lap splice in a given specimen, as obtained for each set of replicate wall splice

specimens. The error bars shown for each reinforcement configuration show the range of individual calculated tensile resistances of the reinforcement for the replicate specimens. Only one specimen provided admissible results for the W250/0 test series and so an error bar is not shown.

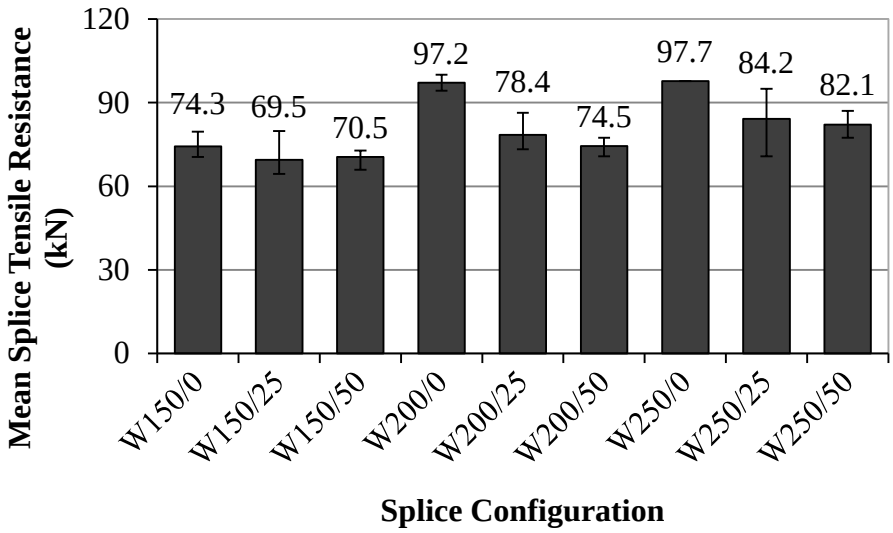

Figure 4.26 Summary of the calculated mean splice tensile resistance for each set of wall splice specimens.

In general, results show that the tensile capacity of the lap splices in contact was higher as compared to that calculated for the non-contact lap splices with the same splice length. This increased tensile capacity, however, was more evident for the two longer lap splice lengths. The fact that the lapped reinforcing bars in contact were tied with wire at both ends of the splice may also have enhanced the splice capacity of the reinforcement, as higher stresses are likely to develop between the ribs of the bars as they ride over each other with increased slip. Such practice is not common within the masonry industry.

Non-contact lap splices behaved similarly regardless of the lateral bar spacing provided. However, a slight decrease in tensile capacity with increasing transverse spacing was noted for specimens with 200 mm and 250 mm lap splice lengths. The cover distance to the adjacent block web, which is less than the cover distance to the block flanges when the bars are not in contact, may have influenced the bond capacity. The poor bond between the grout and the blocks, and the low strength of the mortar joints associated with masonry, proved to have a direct effect on the bond capacity and led to a failure of the splice in all reinforcement configurations.

4.4.5 Empirically derived equation for the lap splice tensile resistance

A regression analysis was performed to estimate the relationship between the tensile resistance of the lap spliced reinforcement as a function of the lap splice length, L_s, and the transverse bar spacing, s_t. An analysis of the 24 wall splice specimens for which the tensile resistance in the reinforcement, T, was calculated yielded the following equation for T in kN:

$$T=(0.196-0.00131s_t)L_s+47.7 \qquad \text{[Eq. 4.1]}$$

The root mean square error (RMSE) for this equation was 7.19 kN. Further refining the regression analysis such that s_t in Equation 4.1 is replaced by an indicator factor for the transverse spacing between the lapped bars, k_s, equal to 0 if the lap spliced bars are in contact and 1 if the lap spliced bars are not in contact (i.e. for s_t equal to 25 and 50 mm), decreased the RMSE to 6.71 kN and resulted in the following predictive equation for T in kN:

$$T=(0.217-0.0676k_s)L_s+46.4 \qquad \text{[Eq. 4.2]}$$

The reduction in the RMSE indicates that the tensile resistance of the lap spliced reinforcement is insensitive to the transverse spacing between the bars that are not in contact but located within the same block cell (i.e. when s_t is equal to 25 or 50 mm).

Figure 4.27 shows the fit of Equation 4.2 to the experimental data. The figure shows that the relationship between the calculated and the empirically predicted tensile resistances is linear but not proportional. This is consistent with previous findings related to reinforced concrete research which indicate that a single bar deformation within the lap splice length will develop mechanical interlock between the reinforcement and the surrounding material once slip initiates (ACI Committee 408, 2003).

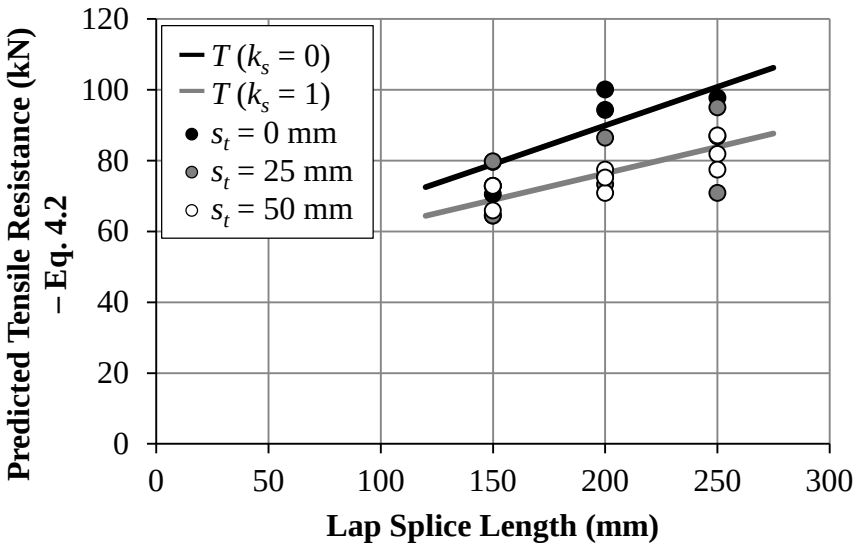

Figure 4.27 Calculated and empirically predicted tensile forces in the lap spliced bars.

Figure 4.28 shows the empirically predicted tensile resistance calculated in the lap spliced bars using Equation 4.2 versus the experimental tensile resistance calculated using the sectional

analysis discussed in the previous subsection. Also shown in the figure is the proportional line, for which the predicted tensile resistance is equal to the calculated tensile force. Specimen markers falling above the line represent the cases for which the predicted tensile resistance exceeded the calculated tensile resistance. Data points located below the proportional line indicate the cases for which the predicted tensile resistance was lower than the calculated tensile resistance of the lap spliced bars.

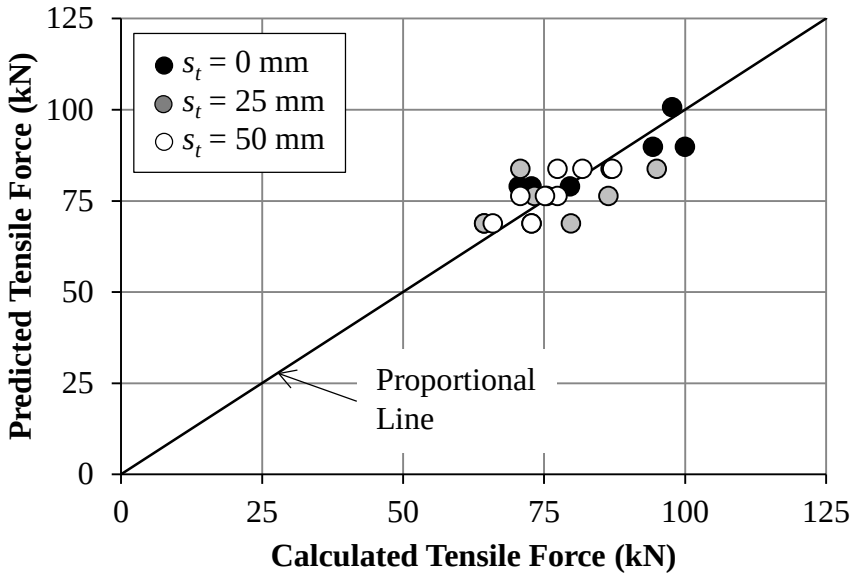

Figure 4.28 Empirically predicted-to-calculated tensile resistances in the lap spliced reinforcing bars.

The data presented in Figure 4.28 indicates that the mean and coefficient of variation of the predicted-to-calculated lap splice tensile resistances for the contact lap splices were 1.013 and 8.16%, respectively. Similarly, the mean and coefficient of variation of the predicted-to-calculated lap splice tensile resistances were 0.0996 and 10.8%, and 1.009 and 5.25% for the non-contact lap splices with 25 and 50 mm transverse bar spacing, respectively.

4.4.6 Comparison of the test results with the American (TMS 402-11) and Canadian (CSA Standard S304.1) code provisions

The experimental results for the tensile resistance of the lap spliced bars as presented in Table 4.6 were compared to the theoretical predicted tensile resistances calculated based upon the current provisions for the required development length of deformed bars in tension in CSA S304.1 (CAN/CSA, 2004a) and TMS 402-11 (MSJC, 2011) as discussed in Section 2.2. Lap splice lengths of 504 and 537 mm resulted when calculated in accordance with CSA S304-04 (CAN/CSA, 2004a) for construction Phases I and II, respectively. The resulting lap splice length as calculated in accordance with TMS 402-11 (MSJC, 2011) was equal to 488 mm. The mathematical expressions and input data used in the calculation of the required development lengths in accordance with both code provisions are presented in Appendix 4F. The theoretical proportion of tensile resistance developed by the lap spliced bars in each specimen was then calculated as follows:

$$\%T = A_s f_y \frac{L_s}{l_d} \qquad \text{[Eq. 4.3]}$$

where A_s is the area of a single No. 15 bar and is equal to 200 mm^2, f_y is the nominal yield stress of the reinforcement and is equal to 400 MPa, L_s is the lap splice length provided in each specimen and l_d is the resulting lap splice length calculated in accordance with either CSA S304-04 (CAN/CSA, 2004a) or TMS 402-11 provisions (MSJC, 2011). The linear and proportional increase in bar force with development length, assumed in CSA S304.1-04, was also assumed in this relationship.

Figures 4.29 and 4.30 show the theoretical proportion of tensile resistance developed by the lap spliced bars as calculated using Equation 4.3 in accordance with CSA S304-04 (CAN/CSA, 2004a) and TMS 402-11 (MSJC, 2011), respectively. Also shown in the figures, is the actual tensile resistance for each wall splice specimen as obtained from testing. In general, similar values for the predicted tensile resistance for each replicate were obtained when calculated using both code provisions.

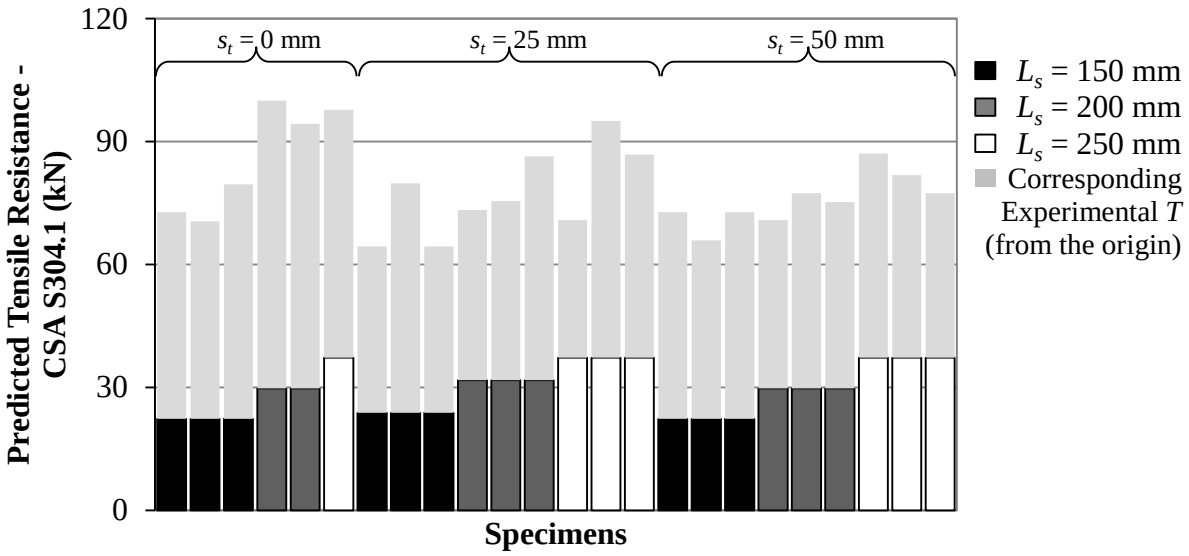

Figure 4.29 Theoretical tensile resistance developed by the lap spliced bars calculated in accordance with CSA S304.1 and corresponding experimental tensile resistance.

Figures 4.31 and 4.32 show the ratio of the test-to-predicted maximum tensile force in the reinforcement based upon CSA S304.1 and TMS 402-11 (CAN/CSA, 2004a, MSJC, 2011), respectively. A review of the data presented in these figures shows that the mean test-to-predicted ratio was 2.74 as calculated in accordance with CSA S304.1, and 2.53 in accordance with TMS 402-11. In general, ratios of the test-to-predicted tensile force greater than 1 represent

cases for which the code predicted values were conservative, whereas ratios less than unity represent cases for which the predicted values were unconservative.

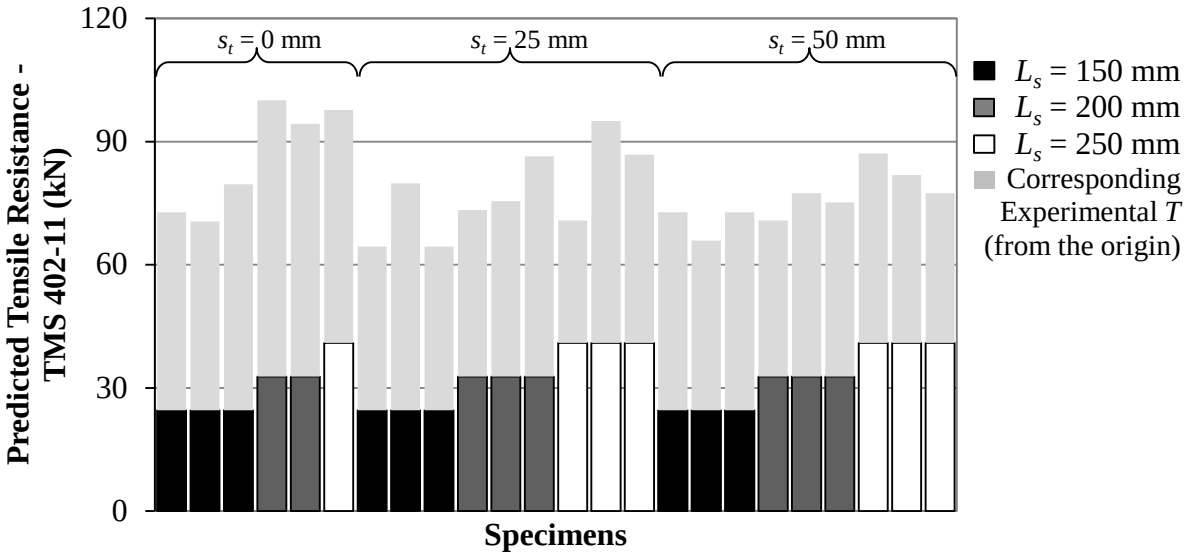

Figure 4.30 Theoretical tensile resistance developed by the lap spliced bars calculated in accordance with TMS 402-11 and corresponding experimental tensile resistance.

The ratio of the test-to-predicted maximum tensile force in the reinforcement generally decreased with increasing lap splice length for any value of transverse spacing provided between the spliced bars. This trend is likely the result of the linear and proportional increase in bar force with increasing lap splice length that was assumed for all the specimens within this investigation, based upon CSA S304.1-04 Clause 12.4.3.1 (CAN/CSA, 2004a), for cases when the development length provided is less than that required to yield the reinforcement. The results of this investigation, as well as recent findings using reinforced concrete specimens (Zuo and Darwin, 2000) suggest that bars with short anchorage lengths may have greater capacities than

those implied by the current design codes. However, the results are based on a limited range of parameters and so a more accurate relationship is yet to be established.

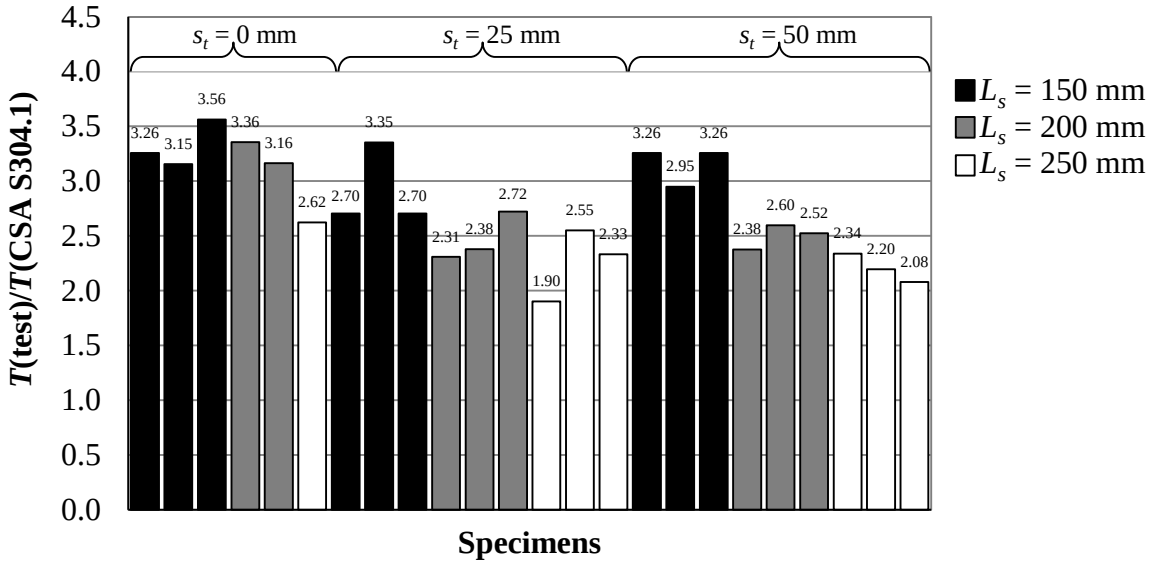

Figure 4.31 Ratio of the test-to-predicted maximum tensile force in the reinforcement with predicted loads based upon CSA S304.1-04.

Figures 4.31 and 4.32 also show that the ratio of the test-to-predicted maximum tensile force for the wall splice specimens also generally decreased with increased transverse bar spacing. It would appear from the results that both codes are appropriate to conservatively predict the tensile resistance of the reinforcement in specimens with both contact and non-contact lap splices (when the bars are located within the same block cell), given the limited test database included in this investigation.

The test-to-predicted tensile force ratios for the specimens with contact lap splices were 0.81 and 0.83 of those for specimens with non-contact lap splices when calculated in accordance

with CSA S304.1 (CAN/CSA, 2004a) and TMS 402-11 (MSJC, 2011), respectively. It therefore appears that a factor of 1.2 applied to Equations 2.3 and 2.5 for cases when the lap spliced bars are not in contact but located within the same block cell would result in similar test-to-predicted tensile force ratios for all wall splice specimens.

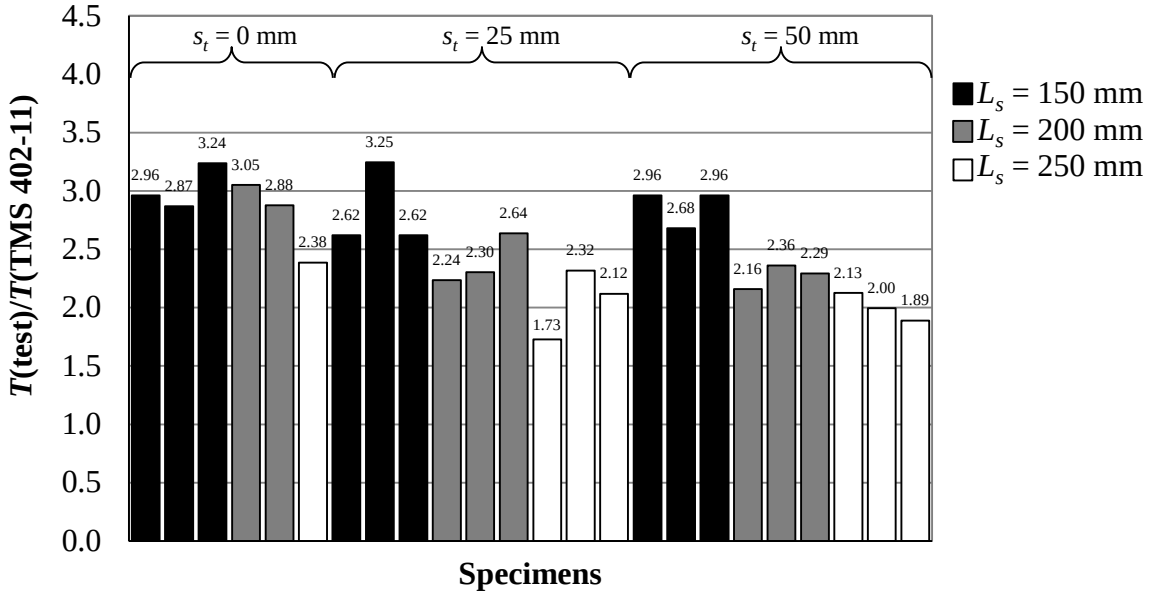

Figure 4.32 Ratio of the test-to-predicted maximum tensile force in the reinforcement with predicted loads based upon TMS 402-11.

4.4.7 Summary of wall splice specimens results

Lap splice failure due to a loss of bond between the reinforcement and the surrounding grout was identified as cause of failure in all wall splice specimens. The lap splice failure generally resulted in the formation of flexural cracks on the tension face that ultimately led to the specimen failure. The flexural cracks were only observed in the mortar joints and typically occurred within the midspan region (i.e. in the bed joints adjacent to the central block course), and up to the third or fourth last joint adjacent to each support.

Regardless of the lap splice length, the tensile resistance of the lap spliced reinforcing bars in contact for the wall splice specimens was higher than that calculated for the non-contact lap splices with the same splice length. The use of tie wire to ensure contact between the lapped bars, which is not a typical practice used in construction, likely caused an increased capacity as a result of the higher stresses developed due to the bar ribs riding over each other with increased slip.

Non-contact lap splices behaved similarly regardless of the lateral bar spacing provided, though a slight decrease in the mean tensile capacity of the lapped bars with 50 mm transverse spacing as compared to the 25 mm-spaced bars was observed, particularly for specimens with 200 and 250 mm lap splice lengths. The reduction in the clear distance between the bars and the webs of the block as the transverse spacing between bars increased likely affected bond performance.

A regression analysis for the experimental results further showed that the tensile resistance of the non-contact lap splices is insensitive to the lateral spacing provided between the lapped bars. Similar to recent findings using reinforced concrete specimens (Zuo and Darwin, 2000), the results of this investigation suggest that bars with short anchorage lengths may have greater capacities than those implied by the current design codes. The results, however, are based on a limited range of parameters and so a more accurate relationship is yet to be established.

A comparison of the experimental results for the tensile resistance of the lap spliced reinforcement with the theoretical predicted tensile resistances calculated based upon the current

provisions for the required development length of deformed bars in tension in CSA S304.1 (CAN/CSA, 2004a) and TMS 402-11 (MSJC, 2011) showed that both code provisions conservatively predicted the tensile resistance for the contact and non-contact lapped bars located within the same block cell. Typical construction practice generally does not allow lapped bars to be tied together and hence some transverse bar spacing commonly results.

CHAPTER 5

CONCLUSIONS

5.1 Overview

The tensile lap splice resistance of Grade 400, No. 15 reinforcing bars with varying transverse spacings and lap splice lengths was evaluated using full-scale concrete block wall splice specimens. The range of the transverse spacing between bars was limited to that which allowed the bars to remain within the same cell, and included the evaluation of tied spliced bars in contact. A total of twenty-seven two-and-a-half block wide by thirteen course tall wall splice specimens reinforced with two sets of lap spliced bars were tested in four-point loading. Three values of lap splice length (150, 200, and 250 mm), and three values of transverse spacing between the lap spliced bars (0, 25, and 50 mm) were tested, with three replicates per configuration. The range of lap splice lengths for the wall splice specimens was selected such that a bond failure of the reinforcement occurred. To do so, the three lap splice lengths were initially tested in two-and-a-half block wide by three courses tall double pullout specimens. The double pullout specimens were reinforced with two tied contact lap splices and tested in direct tension. Six replicates were constructed and tested for each reinforcement configuration in these specimens. Both the double pullout and the wall splice specimens were constructed in running bond with all cells fully grouted.

The tensile capacity of the lap spliced reinforcement, failure modes, crack propagation patterns, and internal damage were critically reviewed for select specimens of each reinforcement configuration for both specimen types. The following section provides a summary of the findings and conclusions derived from this investigation.

5.2 Summary of Findings

5.2.1 Double pullout specimens reinforced with contact lap splices

The double pullout specimens were included in the first stage of the experimental program to determine a reasonable range of lap splice lengths that would ensure a bond failure of the reinforcement in the full-scale wall splice specimens. Three values of lap splice length were tested: 150, 200, and 250 mm. The tensile resistance for these specimens was directly obtained from the load versus displacement relationship as recorded by the data acquisition system throughout testing. The tensile resistance of the lap spliced bars, failure modes, and observed internal damage, were critically reviewed. The following conclusions were noted:

- The contact lap splices with a 150, 200, and 250 mm lap splice length tested in the double pullout specimens developed approximately 38, 35, and 29% of the theoretical yield capacity of the reinforcement, respectively. The mean tensile resistance for the specimens with a 150 mm lap splice length was 33.2 kN with a coefficient of variation of 5.4%. The mean tensile resistances and coefficients of variation for the specimens with 200 and 250 mm lap splice length were 30.3 and 25.2 kN, and 6.5 and 7.7%, respectively. The difference between the mean tensile resistances recorded for each set of replicates was found to be statistically significant.

- Different than expected, the tensile resistance of the contact lap splices in the double pullout specimens was inversely proportional to the lap splice length provided. A detailed analysis of the results did not identify any particular reason for this phenomenon. For the short lap splice lengths used in this investigation, the linear but not proportional

relationship between bond force and lap splice length known from reinforced concrete may provide an explanation for this behaviour (ACI Committee 408, 2003). The load versus splice displacement behaviour, failure modes, and internal damage obtained for the double pullout specimens, were nonetheless comparable to the results of previous investigations and therefore used as the basis for establishing the parameters used in the design of the wall splice specimens.

- Three failure modes were identified for the double pullout specimens: bar pullout, bar pullout followed by longitudinal splitting, and splitting of the masonry assemblage with no visual evidence of bar pullout. Specimens with a 150 mm lap splice length typically failed by bar pullout, whereas the predominant failure mode for the specimens with 200 and 250 mm lap splice lengths was a combined bar pullout with longitudinal splitting.

- Similar observations of internal damage were noted for all reinforcement configurations. Crushing of the grout between bar lugs and consequent bar pullout were identified, further confirming that bond loss between the reinforcement and the surrounding grout led to failure of these specimens.

5.2.2 Wall splice specimens with contact and non-contact lap splices

An iterative sectional approach using moment-curvature response was used to calculate the maximum tensile resistance of the spliced reinforcing bars in the wall splice specimens based upon the ultimate recorded load and the mechanical properties of the masonry assemblage and the reinforcing steel. The following conclusions and observations were noted:

- Lap splice failure due to a loss of bond between the reinforcement and the surrounding grout was identified in all wall splice specimens. The lap splice failure generally resulted in the formation of wide flexural cracks on the tension face that ultimately led to specimen failure. The flexural cracks were only observed in the mortar joints and typically occurred within the midspan region (i.e. in the bed joints adjacent to the central block course), and up to the third or fourth last joint adjacent to each support.

- Regardless of the lap splice length, the tensile resistance of the lap spliced reinforcing bars in contact for the wall splice specimens was higher than that calculated for the non-contact lap splices with the same splice length. The tensile resistance for the contact lap splices in specimens with 150, 200, and 250 mm lap splice length was, on average, 6, 27, and 17% greater than that calculated for the non-contact lap splices (i.e. for transverse spacings equal to 25 and 50 mm), respectively. The use of tie wire to ensure contact between the lapped bars is not a typical practice used in construction and likely caused an increased capacity as a result of the higher stresses developed due to the bar ribs riding over each other with increased slip.

- In general, non-contact lap splices behaved similarly regardless of the lateral bar spacing provided. For the specimens with a 150, 200, and 250 mm lap splice length, the tensile resistance of the lap spliced bars with 25 mm transverse spacing was approximately 1.4, 5.2, and 2.6% higher than that for the spliced bars with a 50 mm transverse spacing, respectively. This minor decrease in the tensile capacity of the lapped bars with 50 mm transverse spacing may have been the result of the reduction in the clear distance between

the bars and the block webs that resulted with increased transverse spacing between bars that likely affected bond performance.

5.2.3 Regression analysis for the resulting wall splice specimen test data

A regression analysis was performed to estimate the relationship between the tensile resistance of the lap spliced reinforcement as a function of the lap splice length, and the transverse bar spacing between the lap spliced bars in the full-scale wall splice specimens. The following conclusions were drawn:

- The regression analysis for the experimental results showed that the tensile resistance of the non-contact lap splices is insensitive to the lateral spacing provided between the bars, given the limited range of parameter included in this investigation.

- The relationship between the calculated and the empirically predicted tensile resistances was found to be linear but not proportional. This is consistent with previous findings related to reinforced concrete research which indicate that a single bar deformation within the lap splice length will develop mechanical interlock between the reinforcement and the surrounding material once slip initiates.

5.2.4 Comparison of the test results with the American and Canadian code provisions

The experimental results for the tensile resistance of the lap spliced reinforcement in the wall splice specimens were compared to the theoretical predicted tensile resistances calculated based upon the current provisions for the required development length of deformed bars in tension in CSA S304.1 and TMS 402-11. The following was noted:

- Both CSA S304.1 and TMS 402-11 code provisions conservatively predict the tensile resistance of the contact and the non-contact lap splices when the lapped bars are located within the same block cell. Typical construction practice generally does not allow lapped bars to be tied together and hence some transverse bar spacing commonly results. Similar to recent findings using reinforce concrete specimens, the results of this investigation suggest that bars with short anchorage lengths may have greater capacities than those implied by the current design codes.

5.3 Recommendations for Future Research

Double pullout and full-scale wall splice specimens were used in this investigation to study the effect of the lap splice length in the in the tensile resistance of contact and non-contact lap splices, when the spliced bars are located within the same block cell. Valuable but limited information was obtained with regards to the bond behaviour of spliced reinforcement in masonry. Further research is therefore required to complete a parametric study of the different factors affecting bond. The following are recommendations for future work:

- In the current study, only one bar size (i.e. No. 15 reinforcing bars) was analyzed. The incorporation of larger bar sizes will provide a better understanding of the effect of this parameter in the force transfer mechanism between the reinforcement, the surrounding grout, and the grout/block interface.

- In the current study, contact lap splices were tied with wire prior to their installation. This may have resulted in an increased splice tensile capacity of the reinforcement, as higher stresses are likely to develop between bar ribs with increasing slip. The use of untied lapped bars when studying contact lap splices is recommended as typical construction practice generally does not permit lap splices to be tied together.

- The use of LVDTs on both sides of the wall splice specimens at the constant moment region during testing is recommended to account for any effect of unsymmetrical cracking in the deflection profiles of the specimens. Also, the use of a single larger LVDT to measure the vertical displacement of the companion masonry prisms is suggested, as the two-LVDT setup used in this investigation resulted in several erratic strain measurements as a result of the uneven rotation of the two devices.

REFERENCES

ACI Committee 408 (1979). “Suggested Development, Splice, and Standard Hook Provisions for Deformed Bars in Tension (ACI 408, IR-79)”, American Concrete Institute, Detroit, USA.

ACI Committee 408, “Bond and Development of Straight Reinforcing Bars in Tension”, American Concrete Institute, Farmington Hills, Mich., 2003.

ACI 530/ASCE 5/ TMS 402, “Building Code Requirements for Masonry Structures”, American Concrete Institute, Farmington Hills, MI, U.S.A.,1999.

Ahmadi, B.H., “Effect of Loss of Bond in Lap Splices of Flexurally Loaded Reinforced Concrete Masonry Walls”, Materials and Structures, Vol. 34, October 2001, pp 475-478.

Ahmed, K., Feldman, L.R. (2012). ‘Evaluation of Contact and Non-Contact Lap Splices in Concrete Block Masonry Construction,” Canadian Journal of Civil Engineering, V. 39, No. 5, pp. 515 – 525.

Ahmed, K., “Evaluation of Contact and Non-Contact Lap Splices in Concrete Block Masonry Specimens”, MSc Thesis, University of Saskatechewan, Saskatoon, SK., Canada., June, 2011.

ASTM (2011a) “ASTM A370-11 Standard Test Methods and Definitions for Mechanical Testing of Steel Products,” ASTM International, West Conshohocken, PA, USA.

ASTM (2011b) “ASTM C1019-11 Standard Test Method for Sampling and Testing Grout,” ASTM International, West Conshohocken, PA, USA.

ASTM (2010) “ASTM C140-10 Standard Test Methods for Sampling and Testing Concrete Masonry Units and Related Units,” ASTM International, West Conshohocken, PA, USA.

Bartlett, F.H., “Pitfalls in Regression Analysis,” University of Western Ontario, London, Ontario. 1999.

Baynit, A. R. “Bond and Development Length in Reinforced Concrete Block Masonry”. M. Eng. Thesis, Carleton University, Ottawa, ON, 1980.

Cheema,T.S., Klingner, R.E., “Tensile Anchorage Behaviour of Deformed Reinforcement in Grouted Concrete Masonry”, ACI Journal, May-June 1985, pp. 372-380.

Cheema, T.S., Klingner, R.E., “Failure Criteria for Deformed Reinforcement Anchored in Grouted Concrete Masonry”, ACI Journal, July-August 1985, pp. 434-442.

Cheema, T.S., Klingner, R.E., “Design Recommendations for Tensile Anchorages of Deformed Reinforcement in Grouted Concrete Masonry”, ACI Journal, September-October, 1985, pp. 616-621.

CSA (2004a) “CAN/CSA S304.1-04 (R2010) Design of Masonry Structures”, Canadian Standards Association, Mississauga, ON, Canada.

CSA (2004b) “CAN/CSA A371-04 (R2009) Masonry Construction for Buildings,” Canadian Standards Association, Rexdale, ON, Canada.

CSA (2004c) “CAN/CSA A165 Series-04 (R2009) CSA Standards on Concrete Masonry Units,” Canadian Standards Association, Rexdale, ON, Canada.

CSA (2004d) “CAN/CSA A179-04 (R2009) Mortar and Grout for Unit Masonry,” Canadian Standards Association, Rexdale, ON, Canada.

CSA (2008) “CAN/CSA A3000-08 Cementitious Materials Compendium (consists of A3001, A3002, A3003, A3004, and A3005),” Canadian Standards Association, Rexdale, ON, Canada.

CSA (2009) “CAN/CSA A23.2-2A-09 Concrete Materials and Methods of Concrete Construction/Test Methods and Standard Practices for Concrete,” Canadian Standards Association, Rexdale, ON, Canada.

De Vial, C., “Performance of Reinforcement Lap Splices in Concrete Masonry”, MSc. Thesis, Thesis, Washington State University, Washington DC. 2009.

Drysdale, R.G., Hamid, A.A., “Masonry Structures: Behaviour and Design”, Canadian Masonry Design Centre, Mississauga, Ontario, 2005.

Hamad, B.S., Mansour, M., “Bond Strength of Non-Contact Tension Lap Splices”, ACI Structural Journal, V.93, No. 3, May-June 1996.

Hamid, A.A., “Design and Construction of Reinforced Masonry in North America”, The 6th Conference of Seismology and Earthquake Engineering, 2004, pp. 179-196.

Hatzinikolas, M.A., Korany,Y., “Masonry Design: for Engineer and Architects”, Canadian Masonry Publications, Edmonton, Alberta, 2005.

ICBO, “Uniform Building Code (UBC)”, International Conference of Building Officials, Whittier, Calif, 1997.

International Code Council (ICC), “International Building Code”, Country Club Hills, IL., 2006.

Masonry Standards Joint Committee: 2005, “Building Code Requirements for Masonry Structures”, ACI 530-05, American Concrete Institute, Farmington Hills, MI, ASCE-05, American Society of Civil Engineers, Reston, VA, TMS 402-052, The Masonry Society, Boulder, CO.

McLean, D., Smith, C., “Noncontact Lap Splices in Bridge Column-Shaft Connections”, Washington State University, Washington D.C., 1997.

Mjelde, J. “Performance of Lap Splices in Concrete Masonry Shear Walls”, MSc. Thesis, Washington State University, Washington DC. 2008.

MSJC (2011). “TMS 402-11/ACI 530-11/ASCE 5-11: Building Code Requirements and Specification for Masonry Structures”, Masonry Standards Joint Committee, Boulder, CO, USA.

MSJC (1992). “ACI 530-92/ASCE 5-92/ TMS 402-92, Building Code Requirements for Masonry Structures”, Masonry Standards Joint Committee, Boulder, CO, USA.

NCMA, “Evaluation of Minimum Reinforcing Bar Splice Criteria for Hollow Clay Brick and Hollow Concrete Block Masonry”, National Concrete Masonry Association, Report No. MR 12, Herndon, Virginia, July, 1999.

Park, R., Priestley, M.J. Nigel, and Gill, W. D., “Ductility of Square Confined Concrete Columns”, ASCE Proceedings, V-108, ST4, Apr. 1982, pp. 929-950.

Sagan, B.E., Gergely, P., White, R.N, “Behavior and Design of Non-Contact Lap Splices Subjected to Repeated Inelastic Tensile Loading”, ACI Structural Journal, V-88, No. 4, July - August, 1991, pp. 420-431.

Sculler, M.P., Hammons, M.I., Atkinson, R.H., “Interim Report on a Study to Determine the Lap Splice Requirements for Reinforced Masonry,” ASTM Special Publication STP 1180: Masonry: Design and Construction Problems and Repairs, eds. J.M. Melander & L.R. Lauersdorf, Philadelphia, PA, 1993, pp.75 – 90.

Soric, Z., Tulin, L. G., “Bond Stress Deformation in Pull-out Masonry Specimen”, ASCE Journal of Structural Engineering, Vol. 115, No. 10, October 1989, pp. 2588-2602.

Uniat, D. B., Lap Splices of Deformed Bars in Reinforced Concrete Block Masonry Walls, M. Eng Thesis, Carleton University, Ottawa, ON, 1983.

Zuo, J., Darwin, D., “Splice Strength of Conventional and High Relative Rib Area Bars in Normal and High-Strength Concrete”, ACI Structural Journal, V. 97, No. 4, pp. 630-641.

APPENDIX 3A

CONSTRUCTION AND TESTING DATES OF THE TEST SPECIMENS

This Appendix provides the details of the construction and testing dates of all the specimens used in this investigation. Table 3A-1 shows the information for the double pullout specimens whereas Table 3A-2 presents the details for the wall splice specimens. The age in days of each specimen at the time of testing is also included in the last column in both tables.

Table 3A-1 Construction and testing dates of the double pullout specimens.

Specimen ID*	Construction Date	Test Date	Age at test (Days)
P150-1	September 12th, 2011	October 24th, 2011	42
P150-2	September 12th, 2011	October 25th, 2011	43
P150-3	September 12th, 2011	October 26th, 2011	44
P150-4	September 12th, 2011	October 27th, 2011	45
P150-5	September 12th, 2011	October 28th, 2011	46
P150-6	September 12th, 2011	October 28th, 2011	46
P200-1	September 12th, 2011	October 31th, 2011	49
P200-2	September 12th, 2011	November 1st, 2011	50
P200-3	September 12th, 2011	November 25th, 2011	74
P200-4	September 7th, 2011	November 28th, 2011	82
P200-5	September 7th, 2011	November 28th, 2011	82
P200-6	September 7th, 2011	November 29th, 2011	83
P250-1	September 6th, 2011	November 29th, 2011	84
P250-2	September 6th, 2011	November 30th, 2011	85
P250-3	September 6th, 2011	November 30th, 2011	85
P250-4	September 6th, 2011	December 1st, 2011	86
P250-5	September 12th, 2011	December 1st, 2011	80
P250-6	September 12th, 2011	December 2st, 2011	81

**Specimen ID is in the form of Paaa-b where 'P' indicates the specimen type (i.e. pullout specimen), aaa is the lap splice length in mm, and b is the specimen number within the construction series.*

Table 3A-2 Construction and testing dates of the wall splice specimens.

Specimen ID*	Construction Phase	Construction Date	Test Date	Age at test (Days)
W150/0-1	II	April 13th, 2012	July 6th, 2012	84
W150/0-2	II	April 13th, 2012	June 29th, 2012	77
W150/0-3	II	April 13th, 2012	July 5th, 2012	83
W150/25-1	I	September 8th, 2011	January 12th, 2012	126
W150/25-2	I	September 8th, 2011	January 13th, 2012	127
W150/25-3	I	September 7th, 2011	January 16th, 2012	131
W150/50-1	II	April 13th, 2012	June 13th, 2012	61
W150/50-2	II	April 13th, 2012	June 20th, 2012	68
W150/50-3	II	April 13th, 2012	June 12th, 2012	60
W200/0-1	II	April 12th, 2012	July 19th, 2012	98
W200/0-2	II	April 12th, 2012	July 17th, 2012	96
W200/0-3	II	April 12th, 2012	July 12th, 2012	91
W200/25-1	I	September 12th, 2011	January 17th, 2012	127
W200/25-2	I	September 7th, 2011	January 18th, 2012	133
W200/25-3	I	September 7th, 2011	January 19th, 2012	134
W200/50-1	II	April 19th, 2012	June 27th, 2012	69
W200/50-2	II	April 19th, 2012	July 13, 2012	85
W200/50-3	II	April 19th, 2012	June 7th, 2012	49
W250/0-1	II	April 12th, 2012	July 25th, 2012	104
W250/0-2	II	April 12th, 2012	July 24th, 2012	103
W250/0-3	II	April 12th, 2012	July 20th, 2012	99
W250/25-1	II	April 13th, 2012	June 26th, 2012	74
W250/25-2	II	April 13th, 2012	June 25th, 2012	73
W250/25-3	II	April 17th, 2012	June 15th, 2012	59
W250/50-1	II	April 17th, 2012	June 14th, 2012	58
W250/50-2	II	April 17th, 2012	July 18th, 2012	62
W250/50-3	II	April 19th, 2012	July 11th, 2012	83

**Specimen ID is in the form of Waaa/bb-c where 'W' indicates the specimen type (i.e. wall splice specimen), aaa is the lap splice length, L_s, in mm, bb is the transverse spacing between the lap spliced bars, s_t, in mm, and c is the specimen number within the construction series.*

APPENDIX 3B

DETAILS OF THE ZAP SCREWLOK MECHANICAL COUPLERS

Type 2 Zap Screwlok mechanical couplers were used in the test setup for the double pullout and the wall splice specimens as described in Chapter 3 Sections 3.6.6 and 3.6.7, respectively. Figure 3B-1 shows the general characteristics of the Type 2 mechanical couplers as provided in the supplier's data sheet. Figure 3B-1 a) shows the front view of a mechanical coupler, while Figure 3B-1 b) the lateral view thereof. Table 3B-1 provides the specifications for the size 16 coupler used in this project that was appropriate for No. 15 reinforcing bars as used. As shown in Table 3B-1, the average twist-off torque for the screws is 68 Nm. However, a 54.2 Nm (40 lb-ft) torque was used in order to prevent damage to the screws, and be able to reuse the couplers for several tests. The applied torque was sufficient to resist the yield strength of Grade 400 steel reinforcing bars (Ahmed, 2011).

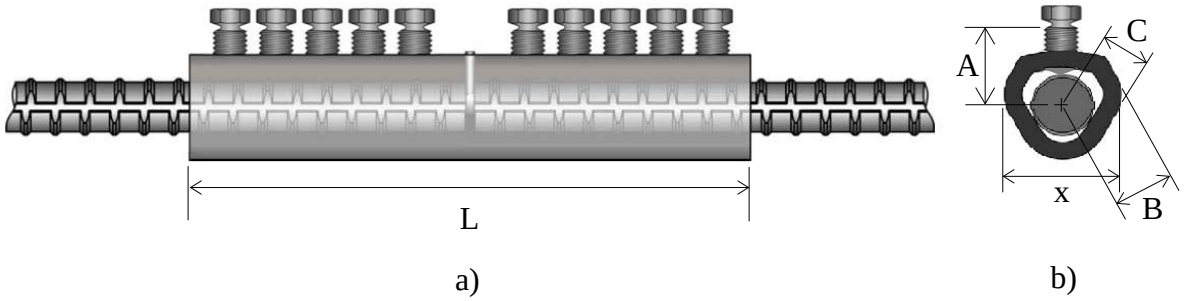

Figure 3B-1 Type 2 Zap Screwlok mechanical coupler – modified from the manufacturer's catalogue in the website: http://www.barsplice.com/Products-Zap.html# (last accessed Jan, 2014): a) front view, and b) lateral view.

Table 3B-1 Size 16 mechanical couplers specifications – retrieved from the manufacturer's catalogue in the website: http://www.barsplice.com/Products-Zap.html#(last accessed Jan, 2014).

Rebar size (metric)	L (mm)	A (mm)	B (mm)	C (mm)	X (mm)	Number screws per bar	Average screw torque (Nm)
16	229	29	19	16	41	4	68

APPENDIX 4A

COMPANION SPECIMEN TEST RESULTS

This appendix presents the individual test results for the material properties of the companion specimens tested in conjunction with the double pullout and the wall splice specimens as reported in Table 4.1. Table 4A-1 shows the results for the absorption test and compressive strength of the masonry blocks for both construction phases, respectively. Table 4A-3 provides the results of the mortar cubes tested along with the double pullout specimens, whereas Table 4A-4 presents the results for the mortar cubes tested in conjunction with the wall splice specimens. Tables 4A-5 and 4A-6 show the results for the non-absorptive grout cylinders tested along with the double pullout and the wall splice specimens, respectively. Table 4A-7 presents the results for the compressive strength of the absorptive grout prisms tested in conjunction with the double pullout specimens, whereas Table 4A-8 shows the results for absorptive grout prisms tested in conjunction with the double pullout specimens during the two construction phases. Tables 4A-9 and 4A-10 show the results for the compressive strength of the masonry prisms tested in conjunction with the double pullout and the wall splice specimens, respectively. Lastly, table 4A-11 presents the results of the mechanical properties of the reinforcing steel used in each of the two construction phases that were representative for both specimen types.

Table 4A-1 Absorption test results for the concrete masonry blocks.

Construction phase	Test no.	Block type	Absorption (%)	Density, D (Kg/m^3)	Net volume, V_n (mm^3)	Average net area, A_n (mm^2)
I	1	Frogged ended	8.6	1963	$7.2x10^6$	$3.8x10^4$
	2		9.1	1936	$7.2x10^6$	$3.8x10^4$
	3		8.9	1880	$7.4x10^6$	$3.9x10^4$
	4		9.3	1868	$7.4x10^6$	$3.9x10^4$
	5		8.7	1881	$7.4x10^6$	$3.9x10^4$
	6		10.1	1846	$7.5x10^6$	$3.9x10^4$
II	1	Frogged ended	9.1	1875	$7.6x10^6$	$4.0x10^4$
	2		5.5	1958	$7.6x10^6$	$4.0x10^4$
	3		6.5	1935	$7.5x10^6$	$4.0x10^4$
	4		5.8	1949	$7.6x10^6$	$4.0x10^4$
	5		6.4	1935	$7.6x10^6$	$4.0x10^4$
	6		9.2	1733	$9.1x10^6$	$4.8x10^4$
	1	Flat ended	9.2	1901	$8.3x10^6$	$4.4x10^4$
	2		5.2	1973	$8.3x10^6$	$4.4x10^4$
	3		5.0	1957	$8.4x10^6$	$4.4x10^4$
	4		5.2	1973	$8.3x10^6$	$4.4x10^4$
	5		5.2	1939	$8.4x10^6$	$4.4x10^4$
	6		5.8	1971	$8.3x10^6$	$4.4x10^4$

Table 4A-2 Compressive strength of the concrete masonry blocks.

Construction phase	Test no.	Compressive strength (MPa)	Average compressive strength (MPa)	C.O.V. (%)
I*	1	25.7	25.4	6.4
	2	25.9		
	3	26.5		
	4	24.3		
	5	23.1		
	6	23.3		
	7	27.2		
	8	27.1		
II	1	22.3	23.4	8.1
	2	25.7		
	3	20.8		
	4	22.1		
	5	22.7		
	6	25.3		
	7	23.2		
	8	24.9		
	9	21.1		
	10	25.8		

** Results represent the material properties for both the double pullout and wall splice specimens.*

Table 4A-3 Compressive strength of the mortar cubes tested in conjunction with the double pullout specimens.

Construction phase	Test no.	Compressive strength (MPa)	Average compressive strength (MPa)	C.O.V. (%)
I	1	17.5	16.6	11.0
	2	18.9		
	3	16.1		
	4	17.7		
	5	16.3		
	6	19.2		
	7	17.7		
	8	16.3		
	9	11.3*		
	10	14.5		
	11	14.6		
	12	13.7		

**Outlier as identified at the 95% confidence level.*

Table 4A-4 Compressive strength of the mortar cubes tested in conjunction with the wall splice specimens.

Construction phase	Test no.	Compressive strength (MPa)	Average compressive strength (MPa)	C.O.V. (%)
I	1	21.1	18.9	12.8
	2	15.9		
	3	20.7		
	4	16.0		
	5	18.8		
	6	20.9		
II	1	13.4	13.5	11.5
	2	16.6		
	3	11.1		
	4	13.5		
	5	14.8		
	6	12.2		
	7	12.5		
	8	14.2		
	9	13.6		
	10	11.3		
	11	14.1		
	12	10.8		
	13	13.1		
	14	12.7		
	15	14.9		
	16	13.7		
	17	14.1		
	18	12.3		
	19	13.0		
	20	16.0		
	21	15.6		

Table 4A-5 Compressive strength of the non-absorptive grout cylinders tested in conjunction with the double pullout specimens.

Construction phase	Test no.	Compressive strength (MPa)	Average compressive strength (MPa)	C.O.V. (%)
I	1	19.8	20.5	10.6
	2	23.2		
	3	21.3		
	4	20.6		
	5	20.8		
	6	21.2		
	7	16.3		
	8	17.3		
	9	22.4		
	10	21.8		

Table 4A-6 Compressive strength of the non-absorptive grout cylinders tested in conjunction with the wall splice specimens.

Construction phase	Test no.	Compressive strength (MPa)	Average compressive strength (MPa)	C.O.V. (%)
I	1	20.3	18.7	10.8
	2	19.4		
	3	17.1		
	4	18.9		
	5	15.0		
	6	20.6		
	7	21.6		
	8	15.9		
	9	19.8		
	10	18.2		
	11	17.3		
	12	20.2		
II	1	12.6	14.1	8.2
	2	9.2*		
	3	16.4		
	4	14.5		
	5	13.8		
	6	14.0		
	7	13.6		
	8	14.6		
	9	14.7		
	10	15.2		
	11	13.7		
	12	11.8		
	13	14.0		
	14	13.0		
	15	12.5		
	16	14.4		
	17	15.2		
	18	12.6		
	19	14.7		
	20	15.3		
	21	15.2		

**Outlier as identified at the 95% confidence level.*

Table 4A-7 Compressive strength of the absorptive grout prisms tested in conjunction with the double pullout specimens.

Construction phase	Test no.	Compressive strength (MPa)	Average compressive strength (MPa)	C.O.V. (%)
I	1	19.2	22.1	10.4
	2	21.4		
	3	22.3		
	4	23.3		
	5	18.4		
	6	20.3		
	7	23.2		
	8	25.4		
	9	24.8		
	10	22.9		

Table 4A-8 Compressive strength of the absorptive grout prisms tested in conjunction with the wall splice specimens.

Construction phase	Test no.	Compressive strength (MPa)	Average compressive strength (MPa)	C.O.V. (%)
I	1	17.5	18.4	12.3
	2	16.1		
	3	20.5		
	4	23.0		
	5	18.4		
	6	20.9		
	7	15.1		
	8	18.0		
	9	15.8		
	10	18.9		
	11	18.8		
	12	18.1		
II	1	12.7	16.2	11.0
	2	13.2		
	3	18.6		
	4	16.6		
	5	17.4		
	6	18.7		
	7	19.0		
	8	14.6		
	9	17.4		
	10	16.6		
	11	14.1		
	12	16.7		
	13	15.0		
	14	13.5		
	15	16.9		
	16	15.6		
	17	17.3		
	18	16.1		
	19	17.0		
	20	16.5		
	21	16.1		

Table 4A-9 Compressive strength of the masonry prisms tested in conjunction with the double pullout specimens.

Construction phase	Specimen ID.[(1)]	Compressive strength (MPa)	Average compressive strength (MPa)	C.O.V. (%)
I	PP-1	12.5	11.0	10.6
	PP-2	11.7		
	PP-3	11.5		
	PP-4	9.8		
	PP-5	10.9		
	PP-6	10.0		
	PP-7	9.8		
	PP-8	10.5		
	PP-9	10.3		
	PP-10	13.2		
	PP-11	11.7		
	PP-12	10.0		
	PP-13	9.8		
	PP-14	9.7		
	PP-15	12.5		
	PP-16	10.6		
	PP-17	14.2*		
	PP-18	12.6		

**Outlier as identified at the 95% confidence level.*

[(1)]Specimen ID is in the form of PP-aa, where PP indicates that the Prism was tested along with a Pullout specimen, and aa is the order within the test series.

Table 4A-10 Compressive strength of the masonry prisms tested in conjunction with the wall splice specimens.

Construction phase	Specimen ID.[(1)]	Compressive strength (MPa)	Average compressive strength (MPa)	C.O.V. (%)
I	PW-1	13.0	12.7	2.8
	PW-2	12.7		
	PW-3	12.4		
	PW-4	13.2		
	PW-5	16.8*		
	PW-6	12.3		
II	PW-7	13.3	12.5	12.5
	PW-8	14.7		
	PW-9	14.6		
	PW-10	12.1		
	PW-11	13.9		
	PW-12	10.1		
	PW-13	11.1		
	PW-14	12.9		
	PW-15	13.2		
	PW-16	14.0		
	PW-17	12.5		
	PW-18	13.0		
	PW-19	10.9		
	PW-20	14.5		
	PW-21	11.3		
	PW-22	11.8		
	PW-23	12.1		
	PW-24	12.7		
	PW-25	14.2		
	PW-26	9.6		
	PW-27	10.1		

**Outlier as identified at the 95% confidence level.*

[(1)]Specimen ID is in the form of PW-aa, where PP indicates that the Prism was tested along with a Wall splice specimen, and aa is the order within the test series.

Table 4A-11 Material properties of the reinforcing steel used in the construction of the double pullout and wall splice specimens.

Construction phase	Test no.	Yield stress, f_y (MPa)	Modulus of elasticity, E_s (GPa)	Strain at initiation of strain hardening, ε_{sh}	Slope at initiation of strain hardening (MPa)	Ultimate stress, f_{ult} (MPa)
I	1	440	158	0.015	4711	585
	2	436	153	0.013	4409	594
	3	432	154	0.010	5157	608
	4	431	239	0.014	7125	645
	5	432	173	0.014	7389	649
	6	433	167	0.015	4784	585
II	1	443	182	0.013	4531	601
	2	412	133	0.011	4158	591
	3	440	192	0.014	4756	655
	4	432	164	0.014	4739	653
	5	441	201	0.013	4308	598
	6	433	209	0.011	3667	593

APPENDIX 4B

LAP SPLICE TENSILE RESISTANCE VERSUS SPLICE DISPLACEMENT CURVES FOR THE DOUBLE PULLOUT SPECIMENS

This section presents the load versus splice displacement curves for all the double pullout specimens replicates tested during the first stage of the project. Figures 4B-1 to 4B-6 show the curves for corresponding to the specimens with a 250 mm lap splice length. Figures 4B-7 to 4B-12, and 4B-13 to 4B-18 present the load-displacement curves for the specimens with a 200 and 150 mm lap splice length, respectively. The theoretical yield load of the reinforcement equal to 86.8 kN as established for the testing of the reinforcing steel bar samples is shown with a dotted line in each of the figures.

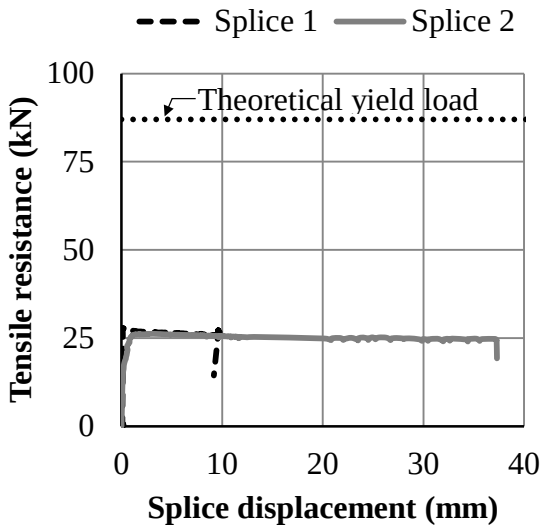

Figure 4B-1 Tensile resistance-displacement curve – Specimen P250-1.

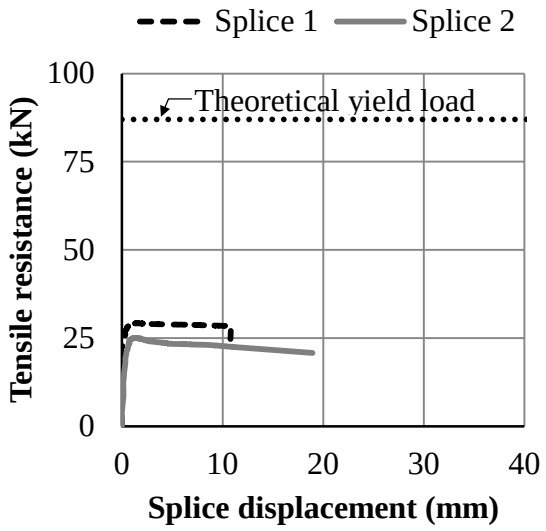

Figure 4B-2 Tensile resistance -displacement curve – Specimen P250-2.

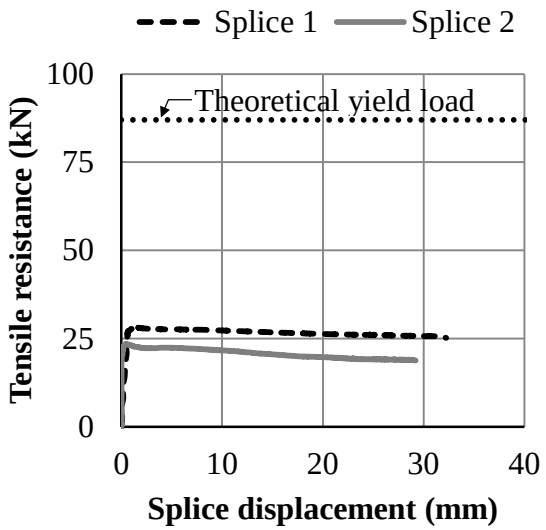

Figure 4B-3 Tensile resistance-displacement curve – Specimen P250-3.

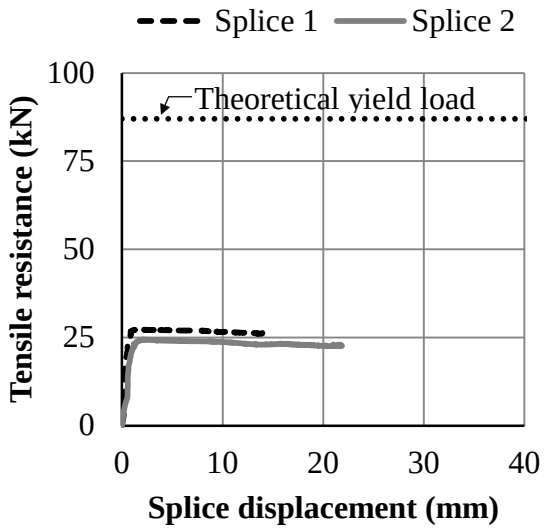

Figure 4B-4 Tensile resistance-displacement curve – Specimen P250-4.

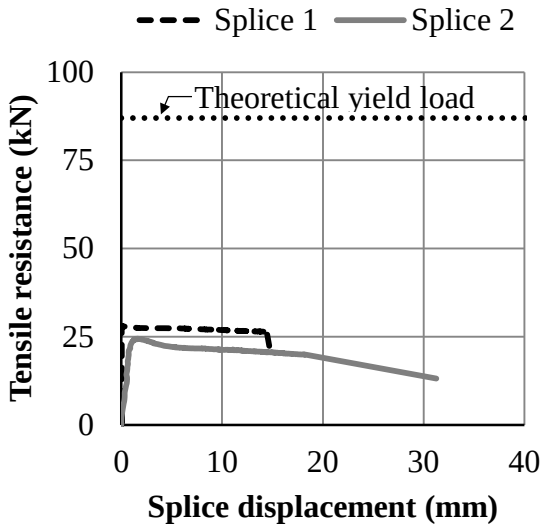

Figure 4B-5 Tensile resistance-displacement curve – Specimen P250-5.

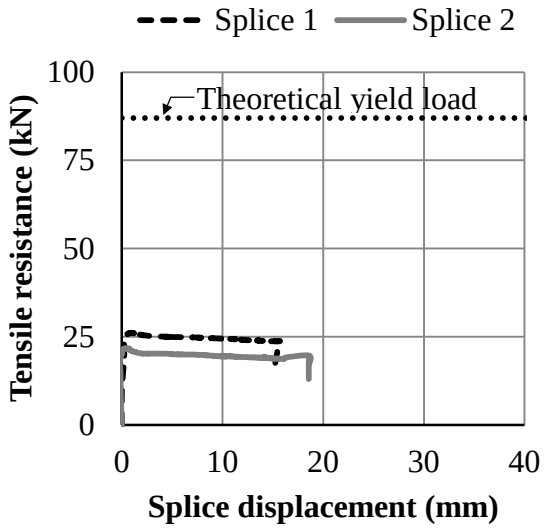

Figure 4B-6 Tensile resistance-displacement curve – Specimen P250-6.

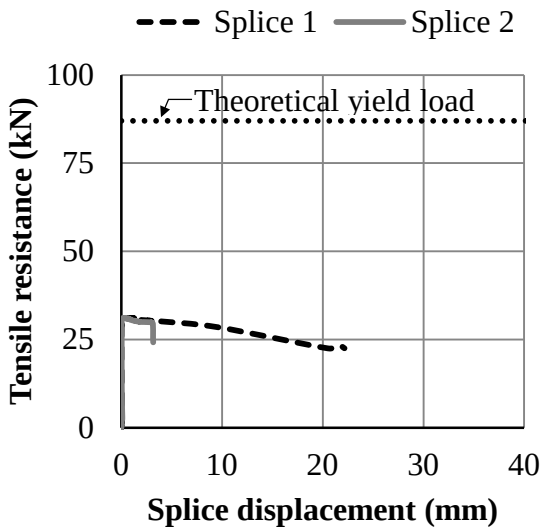

Figure 4B-7 Tensile resistance-displacement curve – Specimen P200-1.

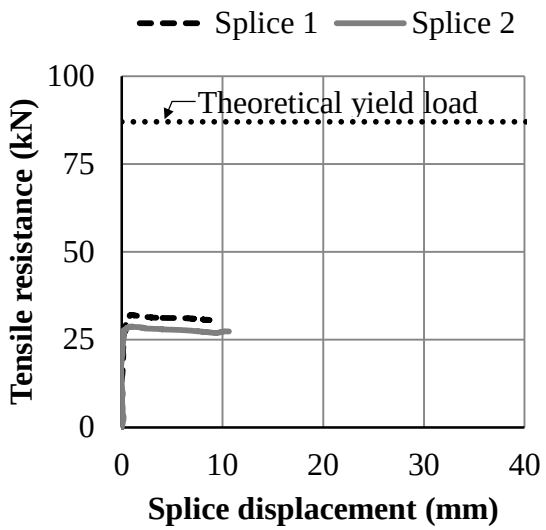

Figure 4B-8 Tensile resistance-displacement curve – Specimen P200-2.

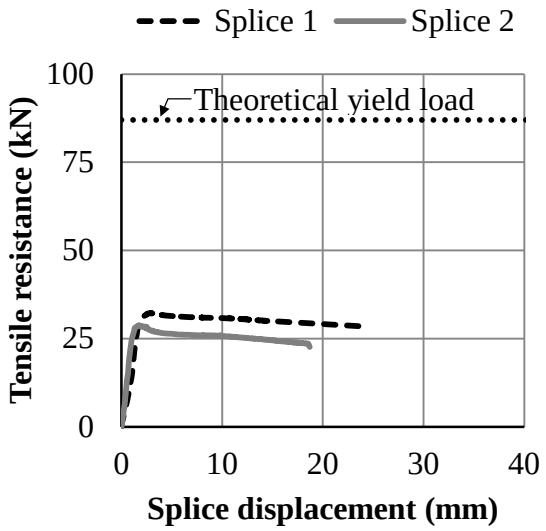

Figure 4B-9 Tensile resistance-displacement curve – Specimen P200-3.

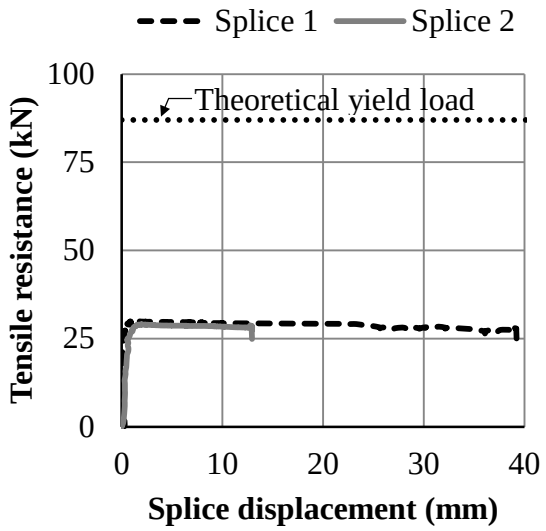

Figure 4B-10 Tensile resistance-displacement curve – Specimen P200-4.

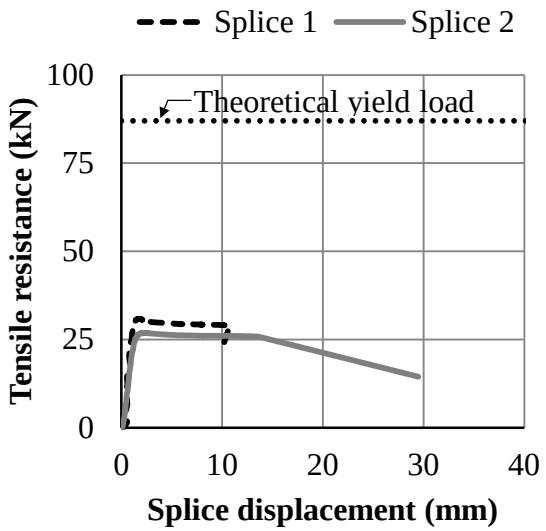

Figure 4B-11 Tensile resistance-displacement curve – Specimen P200-5.

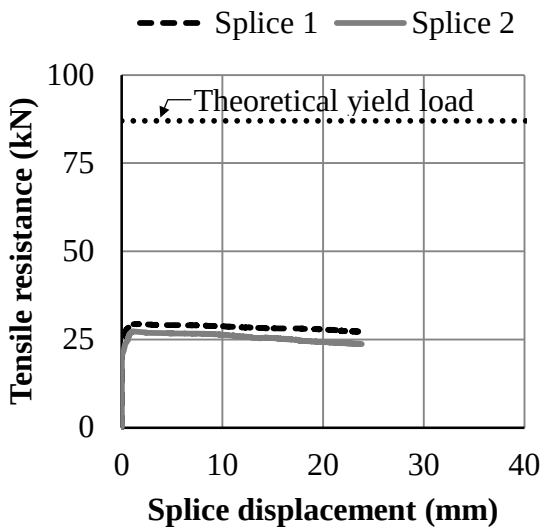

Figure 4B-12 Tensile resistance-displacement curve – Specimen P200-6.

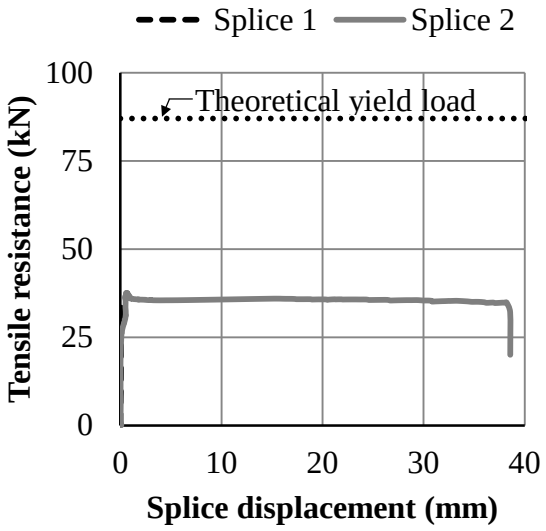

Figure 4B-13 Tensile resistance-displacement curve – Specimen P150-1.

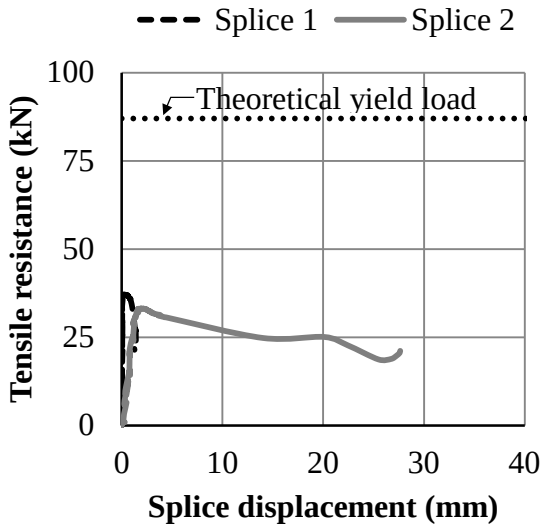

Figure 4B-14 Tensile resistance-displacement curve – Specimen P150-2.

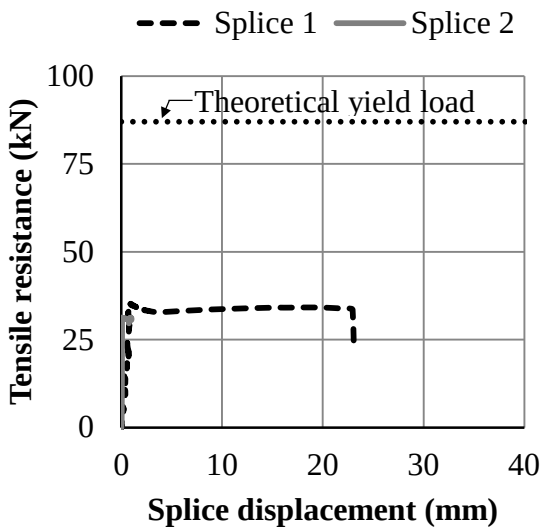

Figure 4B-15 Tensile resistance-displacement curve – Specimen P150-3.

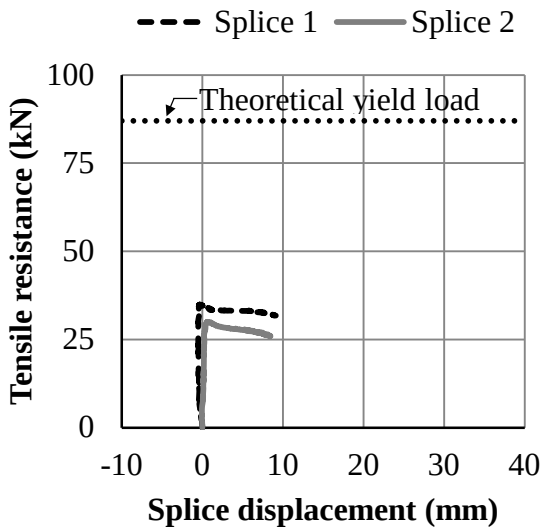

Figure 4B-16 Tensile resistance-displacement curve – Specimen P150-4.

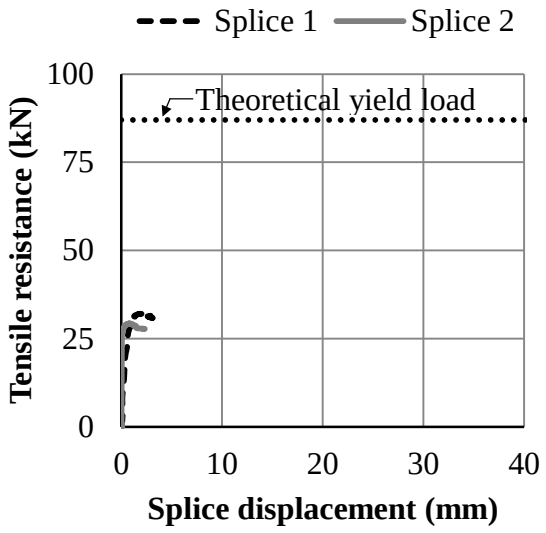

Figure 4B-17 Tensile resistance-displacement curve – Specimen P150-5.

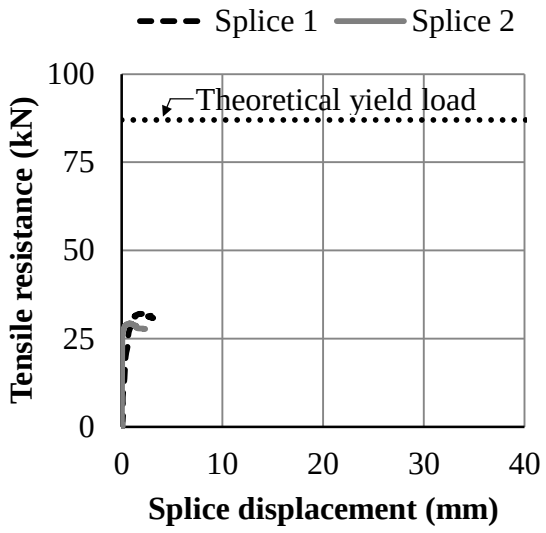

Figure 4B-18 Tensile resistance-displacement curve – Specimen P150-6.

APPENDIX 4C

EXPERIMENTAL LOAD VERSUS MIDSPAN DEFLECTION RESPONSE FOR THE WALL SPLICE SPECIMENS

This section presents the experimental load versus midspan deflection curves for all the wall splice specimen replicates. Figures 4C-1 to 4C-9 show the load versus midspan deflection curves for the specimens with a 150 mm lap splice length, whereas Figures 4C-10 to 4C-18 and 4C-19 to 4C-27 show the curves for the specimens with a 200 and 250 mm lap splice length, respectively. The recorded experimental cracking load, P_{cr}, is indicated with a dotted line in each figure. For specimen W250/0-3, the only specimen that showed yielding of the reinforcement, the load at yielding, P_y, is also indicated in the corresponding figure (i.e. Figure 4C-21).

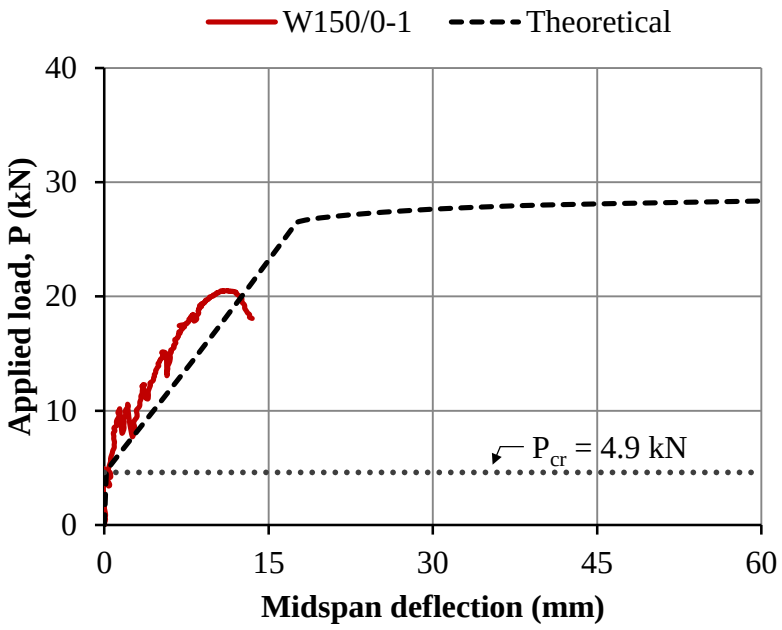

Figure 4C-1 Load versus midspan deflection – Specimen W150/0-1.

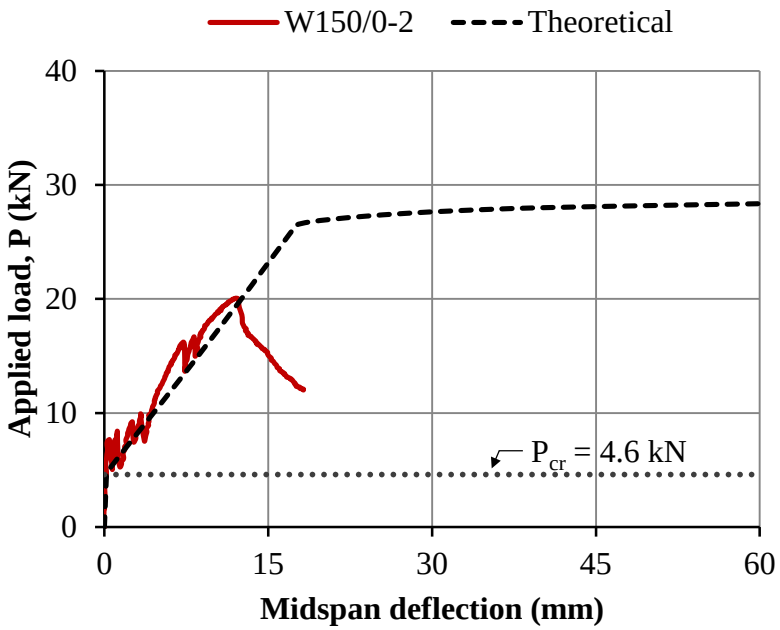

Figure 4C-2 Load versus midspan deflection – Specimen W150/0-2.

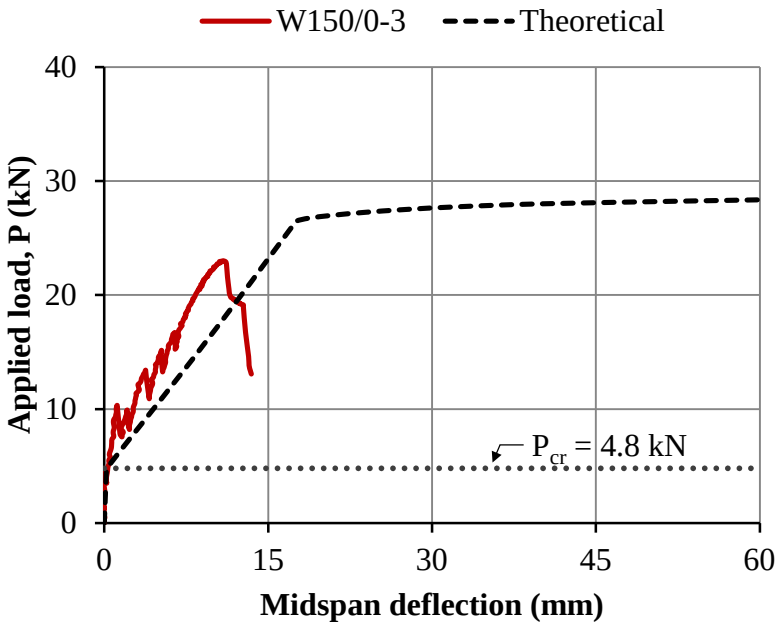

Figure 4C-3 Load versus midspan deflection – Specimen W150/0-3.

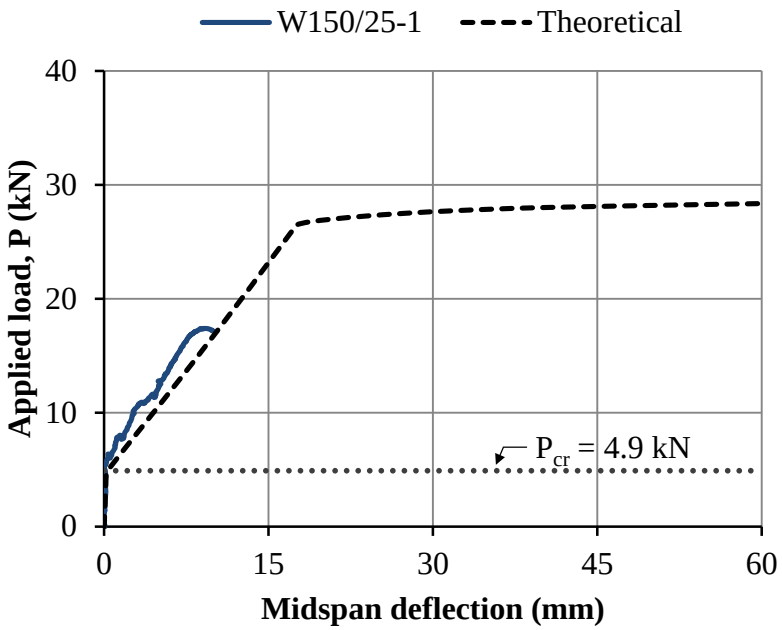

Figure 4C-4 Load versus midspan deflection – Specimen W150/25-1.

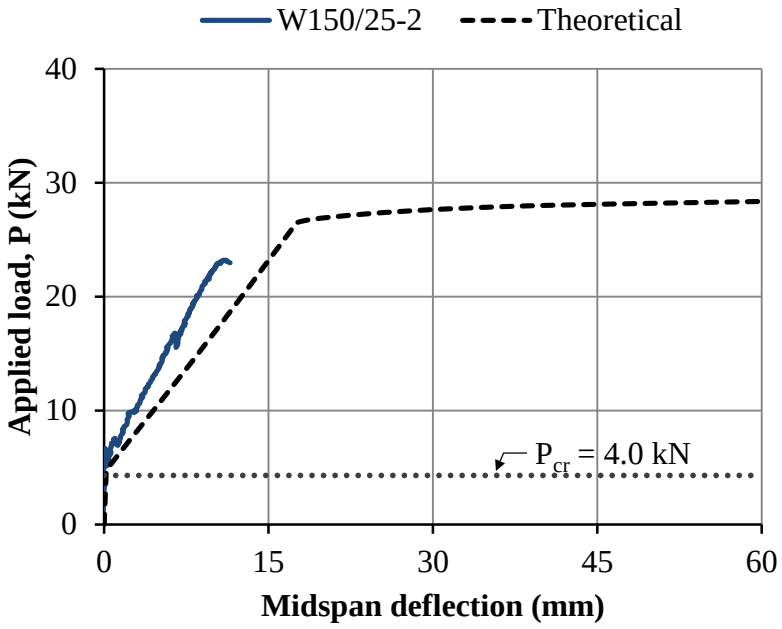

Figure 4C-5 Load versus midspan deflection – Specimen W150/25-2.

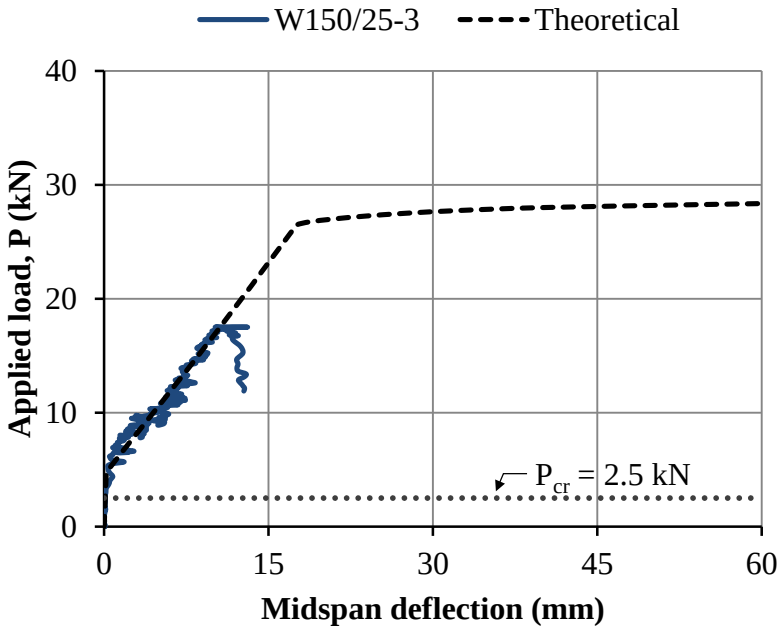

Figure 4C-6 Load versus midspan deflection – Specimen W150/25-3.

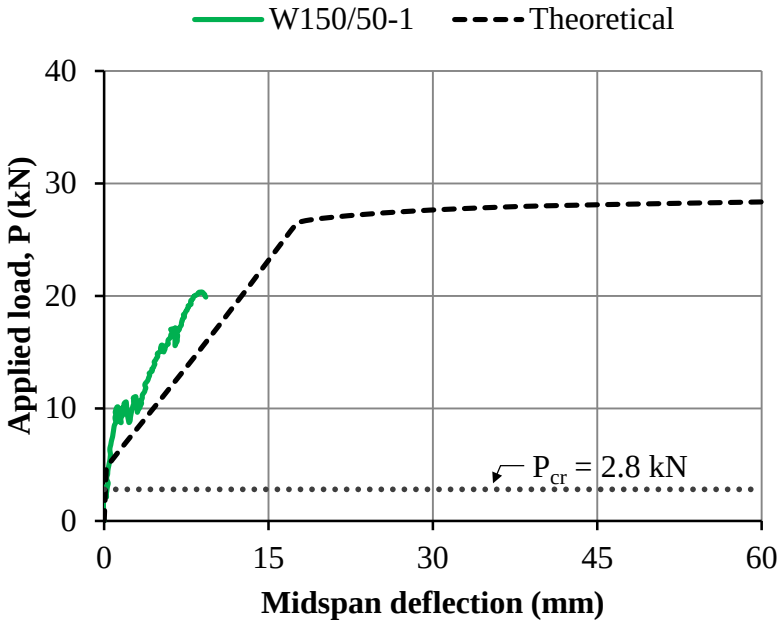

Figure 4C-7 Load versus midspan deflection – Specimen W150/50-1.

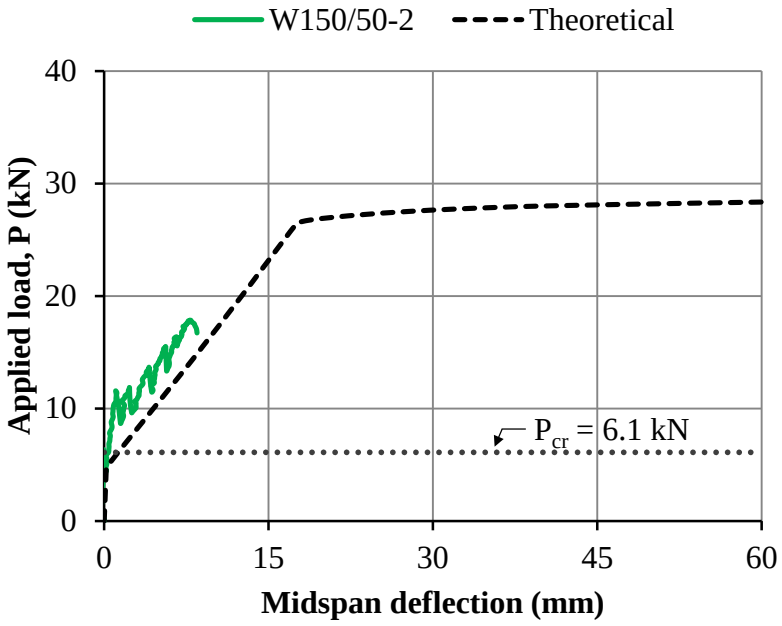

Figure 4C-8 Load versus midspan deflection – Specimen W150/50-2.

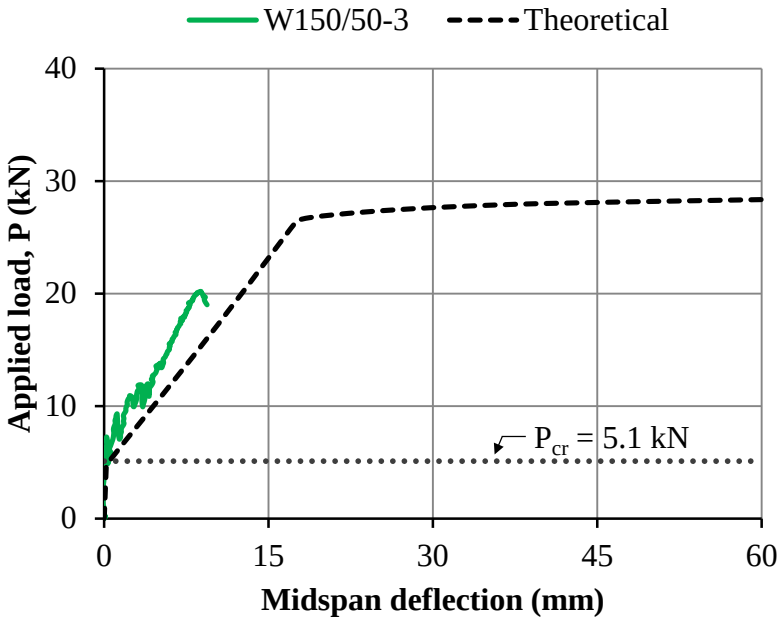

Figure 4C-9 Load versus midspan deflection – Specimen W150/50-3.

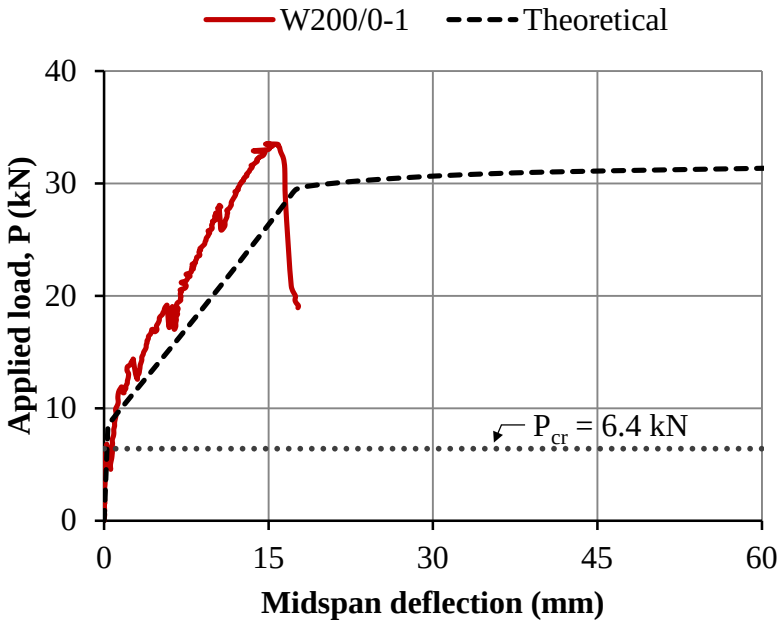

Figure 4C-10 Load versus midspan deflection – Specimen W200/0-1.

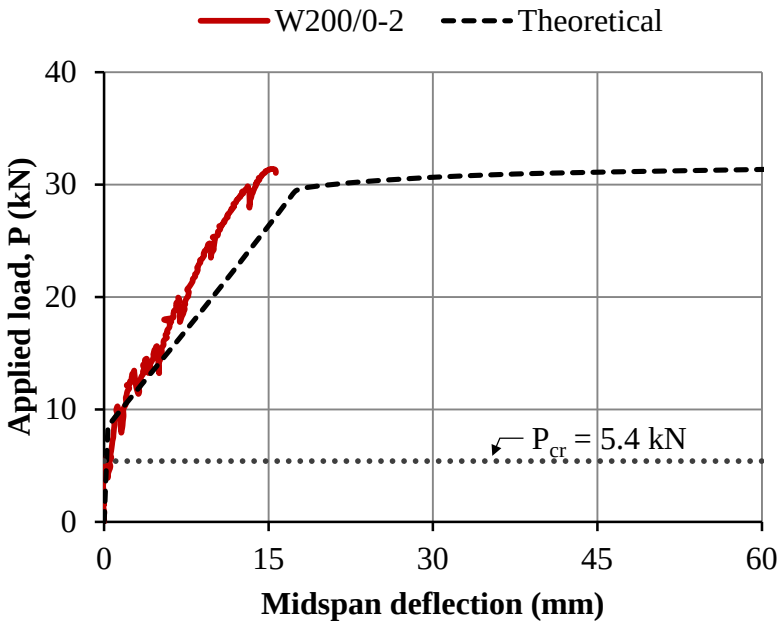

Figure 4C-11 Load versus midspan deflection – Specimen W200/0-2.

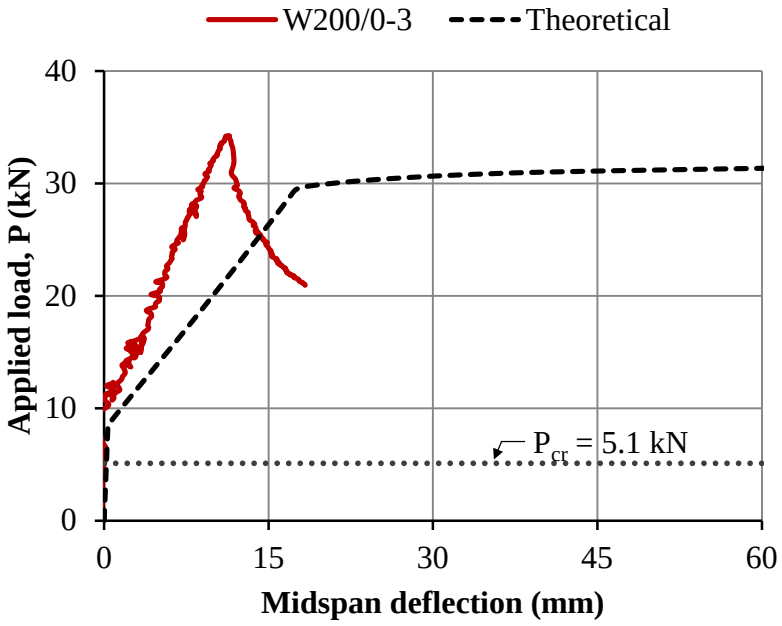

Figure 4C-12 Load versus midspan deflection – Specimen W200/0-3.

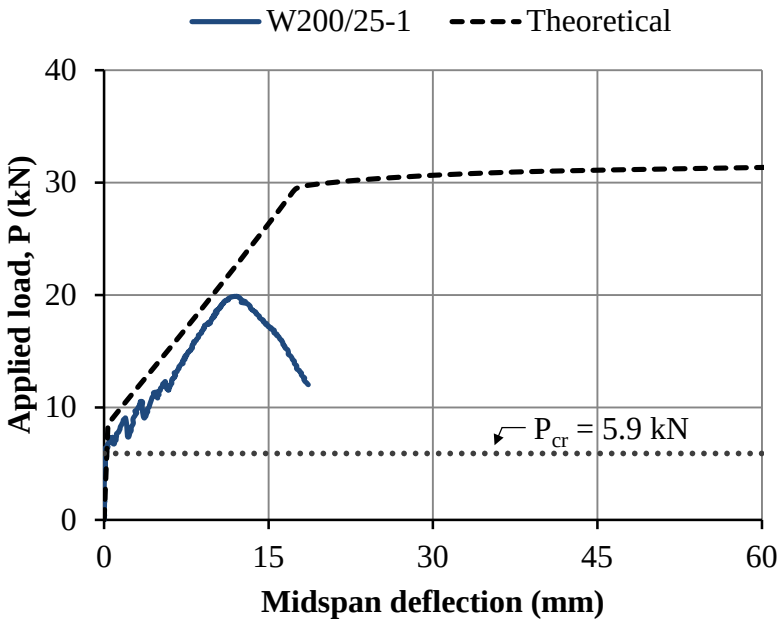

Figure 4C-13 Load versus midspan deflection – Specimen W200/25-1.

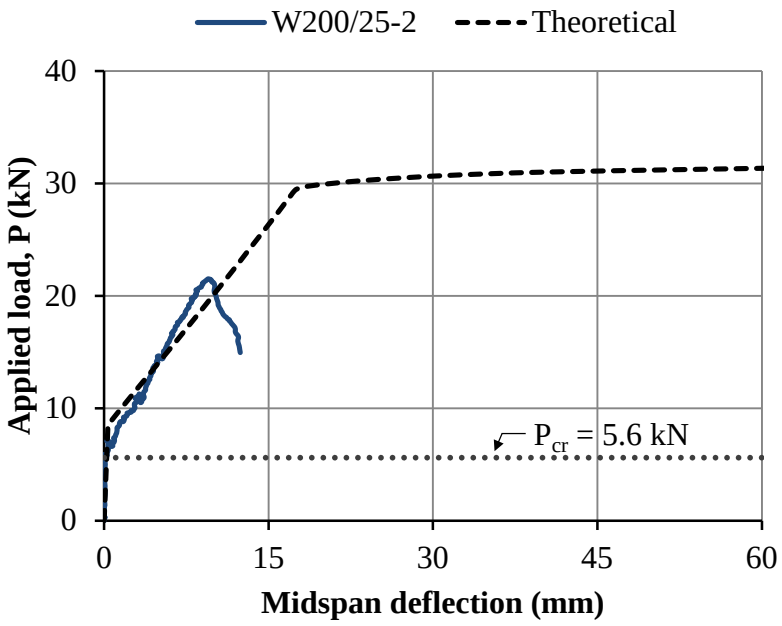

Figure 4C-14 Load versus midspan deflection – Specimen W200/25-2.

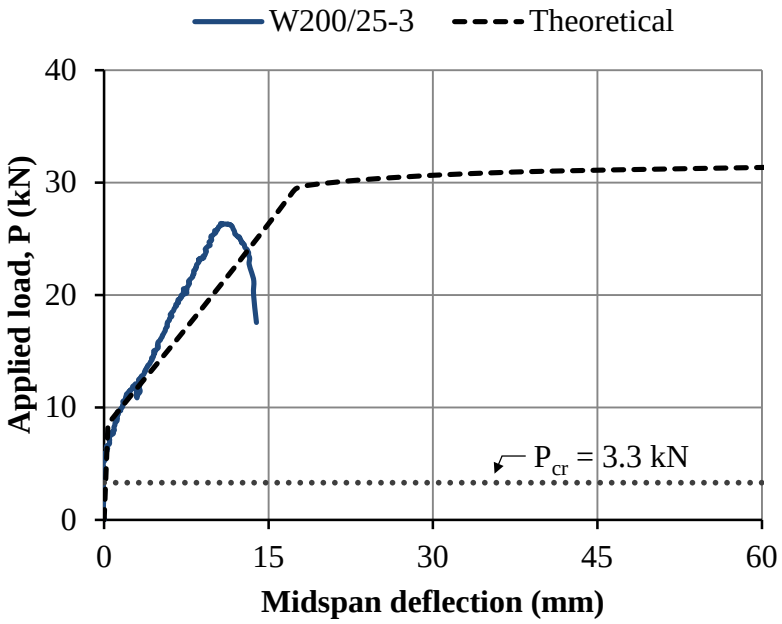

Figure 4C-15 Load versus midspan deflection – Specimen W200/25-3.

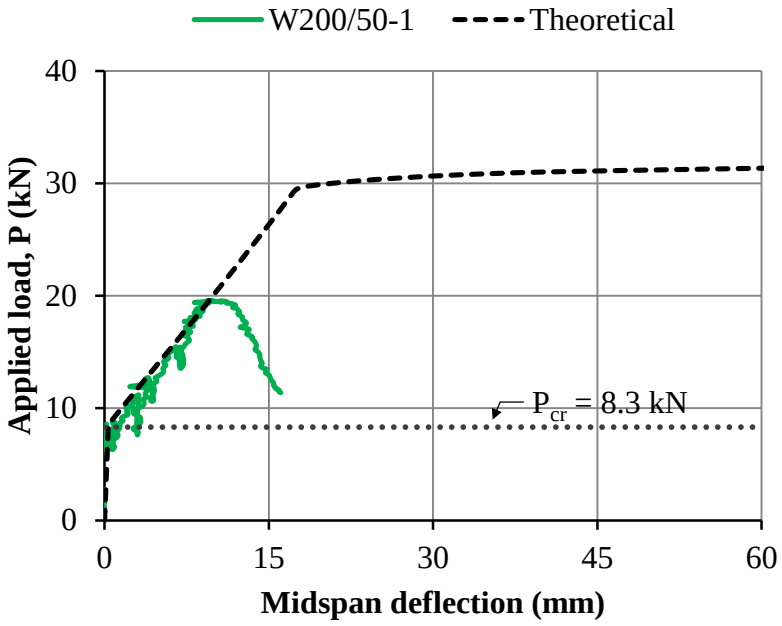

Figure 4C-16 Load versus midspan deflection – Specimen W200/50-1.

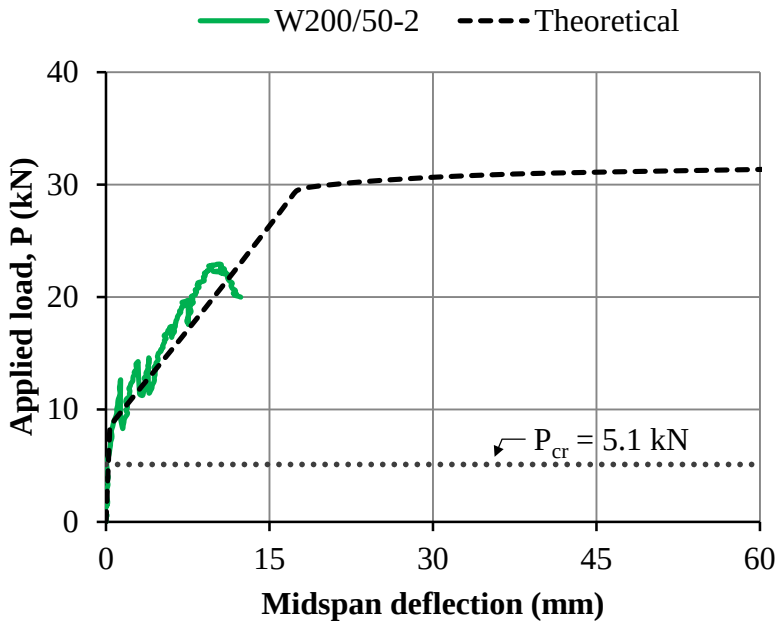

Figure 4C-17 Load versus midspan deflection – Specimen W200/50-2.

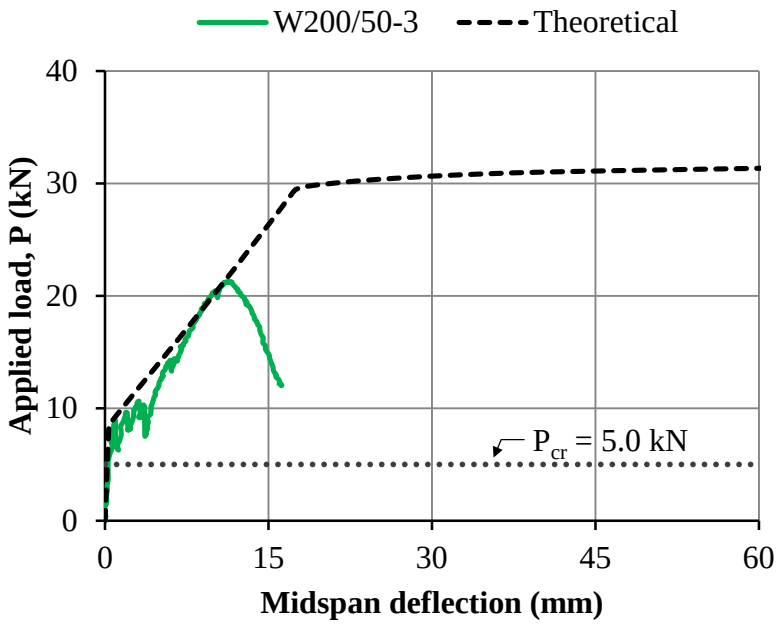

Figure 4C-18 Load versus midspan deflection – Specimen W200/50-3.

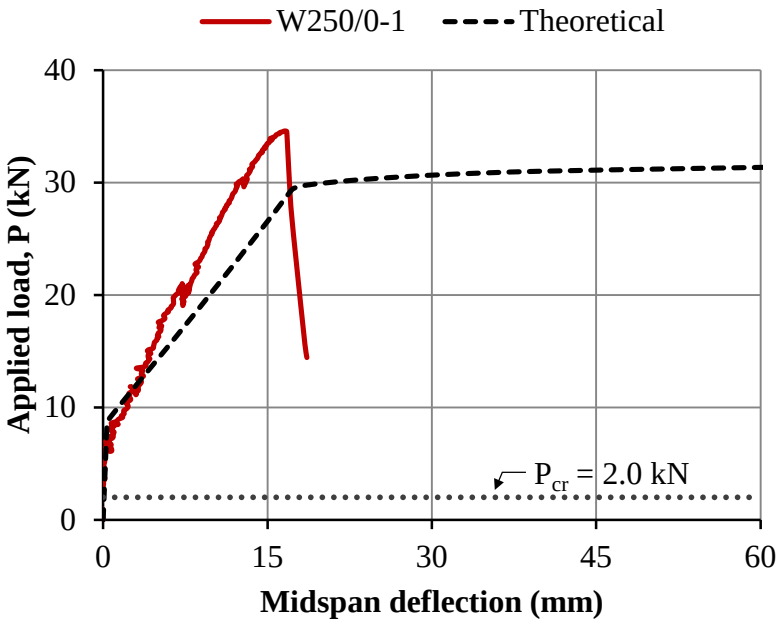

Figure 4C-19 Load versus midspan deflection – Specimen W250/0-1.

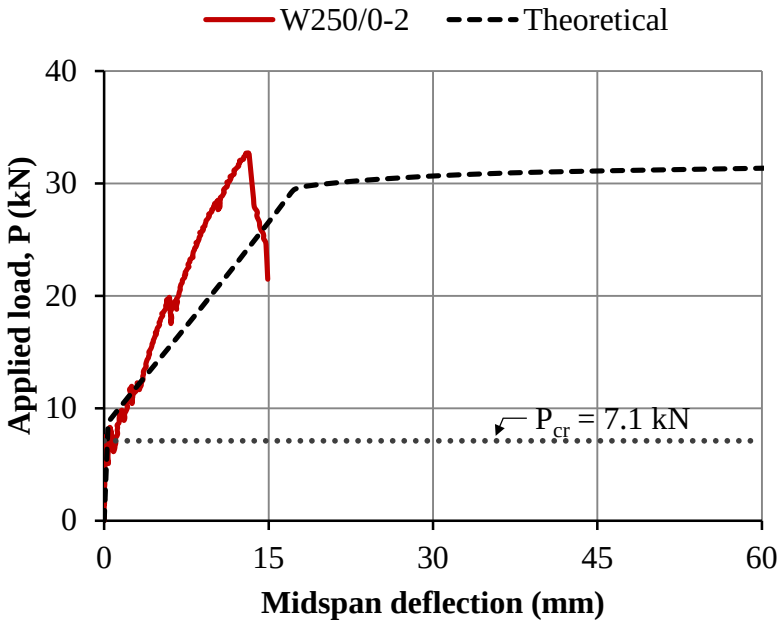

Figure 4C-20 Load versus midspan deflection – Specimen W250/0-2.

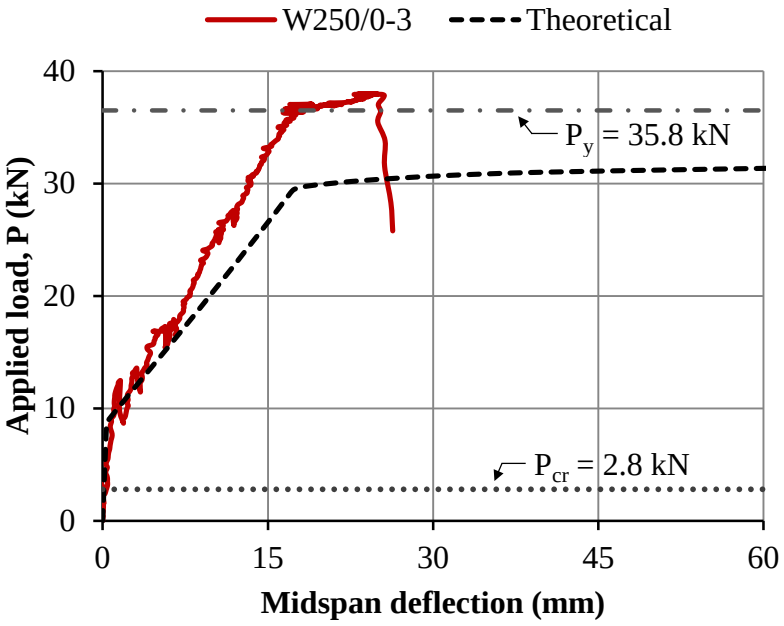

Figure 4C-21 Load versus midspan deflection – Specimen W250/0-3.

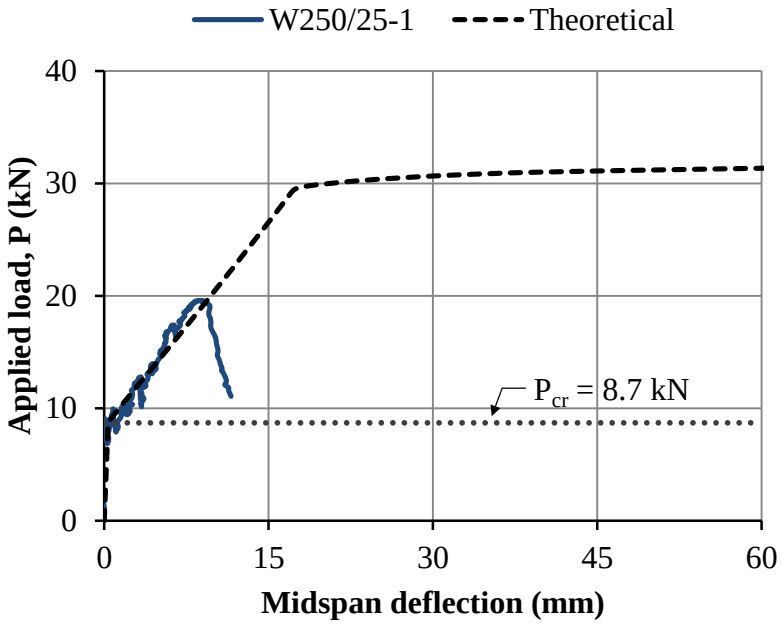

Figure 4C-22 Load versus midspan deflection – Specimen W250/25-1.

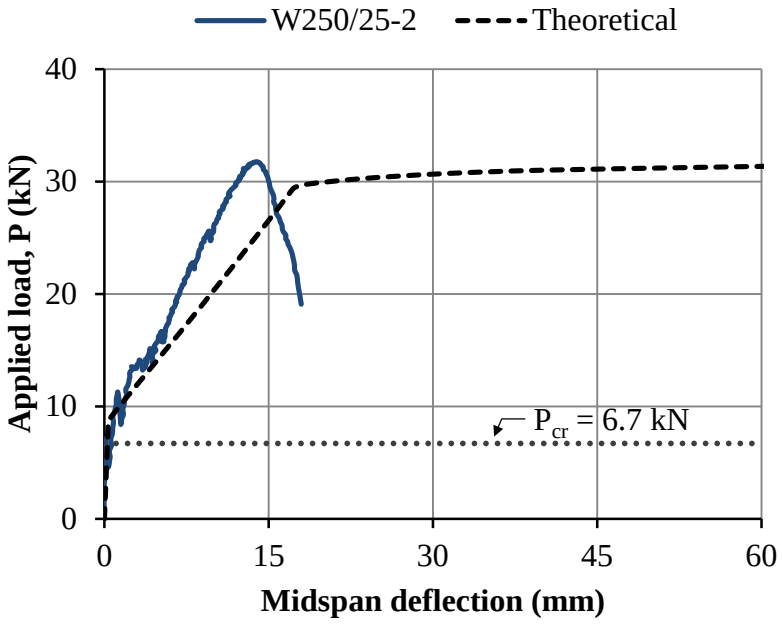

Figure 4C-23 Load versus midspan deflection – Specimen W250/25-2.

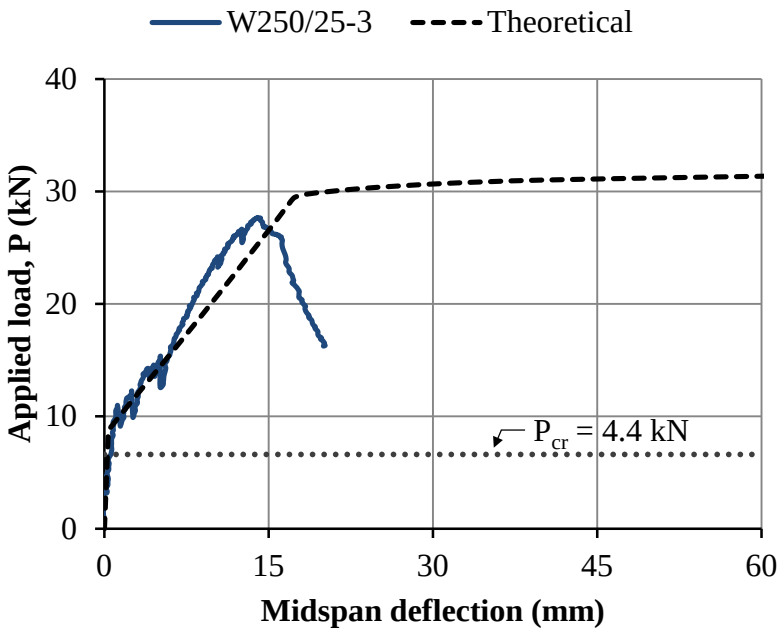

Figure 4C-24 Load versus midspan deflection – Specimen W250/25-3.

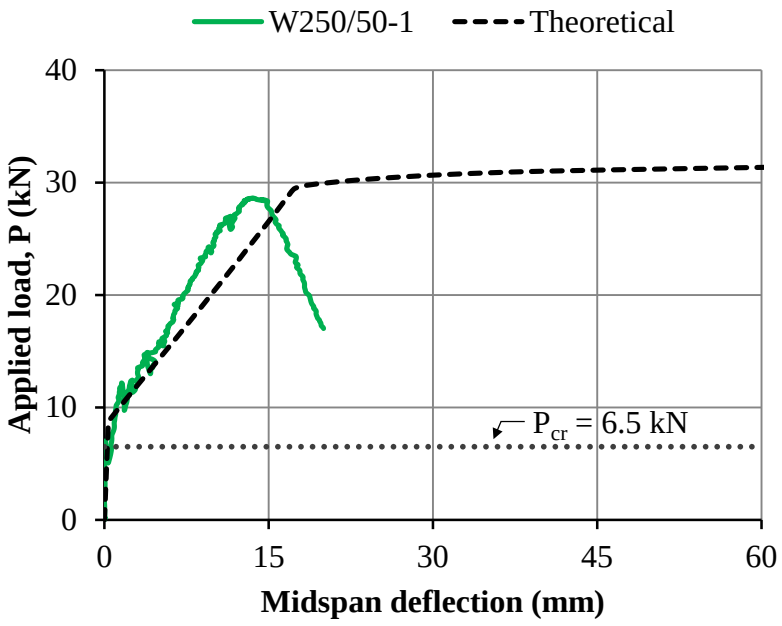

Figure 4C-25 Load versus midspan deflection – Specimen W250/50-1.

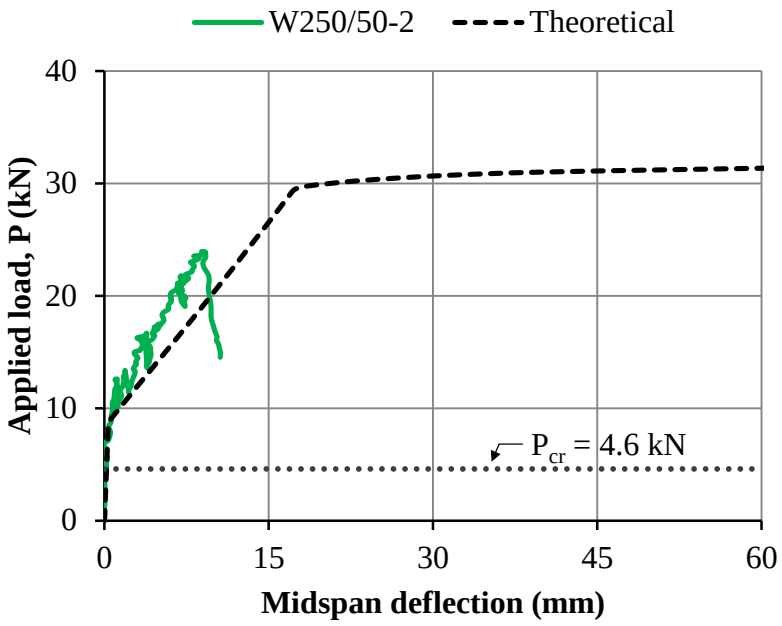

Figure 4C-26 Load versus midspan deflection – Specimen W250/50-2.

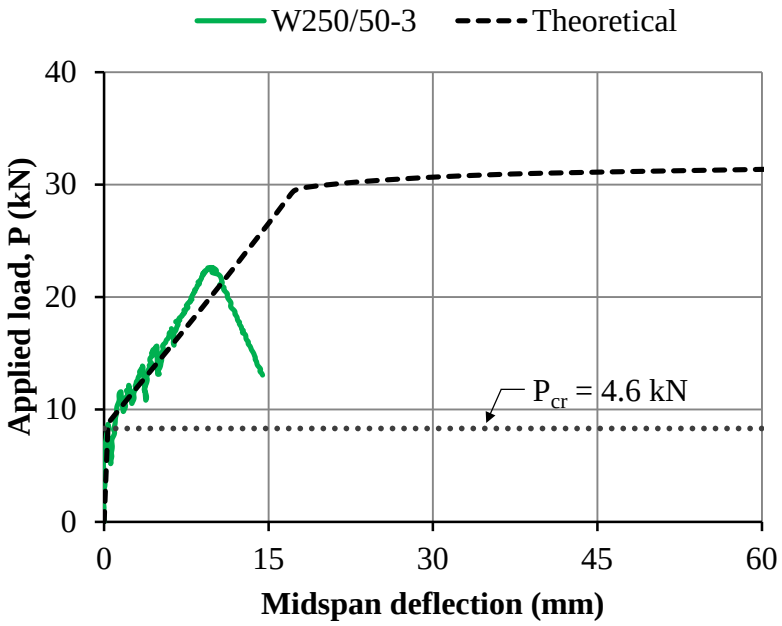

Figure 4C-27 Load versus midspan deflection – Specimen W250/50-3.

APPENDIX 4D

MOMENT – CURVATURE ANALYSIS FOR THE WALL SPLICE SPECIMENS

As described in Section 4.4.4, an iterative sectional analysis based upon the moment-curvature response was performed to calculate the tensile resistance of the reinforcement in the wall splice specimens. This section presents the analytical models and mathematical expressions used in the analysis that are similar to those previously reported by Ahmed (2011), and Ahmed and Feldman (2012).

Theoretical stress-strain relationship for the masonry assemblage

The stress-strain relationship for the masonry assemblage was first obtained by fitting the experimental data for the companion masonry prisms to a modified Park-Kent curve (Park et. al., 1982). The parabolic increasing segment and linear falling curve that form the modified Park-Kent curve were described by the following equations:

Parabolic increasing segment:

$$f_m(\varepsilon_c)=Kf_m\left[\left(\frac{2\varepsilon_c}{0.002K}\right)-\left(\frac{\varepsilon_c}{0.002K}\right)^2\right] \qquad \text{[Eq. 4D-1]}$$

for $\varepsilon_c \leq 0.002$

where f_m = unconfined masonry prism strength (MPa)

ε_c = compressive strength of the masonry

K = strength enhancement factor equal to 1.0 for unconfined masonry with no transverse reinforcement provided.

Linear falling curve:

$$f_m(\varepsilon_c)=Kf_m[1-Z(\varepsilon_c-0.002K)] \quad \text{[Eq. 4D-2]}$$

when $0.002 \leq \varepsilon_c \leq 0.01$

where $Z = \dfrac{0.5}{\left[\dfrac{3+0.29f_m}{145f_m-1000}\right]-0.002K}$

Theoretical stress-strain relationship for the reinforcing steel

The average mechanical properties obtained for the steel bar samples were used to derive the theoretical stress-strain profiles of the reinforcing steel. The three segments comprising the stress, f_s, versus strain, ε_s, curve of the reinforcement were given by the following equations:

Elastic curve – from the origin to the yield point:

$$f_s(\varepsilon_s)=E_s\varepsilon_s \quad \text{[Eq. 4D-3]}$$

for $\varepsilon_s \leq \varepsilon_y$

where E_s = the modulus of elasticity of the reinforcement equal to f_y/ε_y

f_y = the yield stress of the reinforcing bars

ε_y = the yield strain of the reinforcing bars

Yield plateau:

$$f_s(\varepsilon_s)=f_y \quad \text{[Eq. 4D-4]}$$

for $\varepsilon_y < \varepsilon_s \leq \varepsilon_{sh}$

where ε_{sh} = the strain at the initiation of strain hardening

Strain hardening curve:

$f_s(\varepsilon_s) = A + B\varepsilon_s + C\varepsilon_s^2 + D\varepsilon_s^3$ [Eq. 4D-5]

for $\varepsilon_{sh} < \varepsilon_s \leq \varepsilon_{ult}$

where ε_{ult} = strain corresponding to the ultimate stress

A, B, C, and D were calculated using the following boundary conditions:

$f_s(\varepsilon_{sh}) = f_y$

$f_s(\varepsilon_{ult}) = f_{ult}$

$f_s'(\varepsilon_{sh}) = E_{sh}$

$f_s'(\varepsilon_{ult}) = 0$

f_{ult} = ultimate stress of the steel reinforcement

E_{sh} = slope at the initiation of strain hardening

Moment-curvature analysis

The theoretical moment-curvature relationships for the wall splice specimens were calculated based upon the internal moment effect resulting from the applied load level. Prior to first cracking of the specimen, the curvature was given by:

$$\phi_{uc} = \frac{M_{cr}}{E_m I_g}$$ [Eq. 4D-6]

where ϕ_{uc} = curvature of the uncracked section

M_{cr} = applied moment at first cracking calculated from the experimental cracking loads reported in Table 4.5.

E_m = modulus of Elasticity of Masonry equal to 850 f'm as calculated in accordance with CSA S304.1, Clause 6.5.2 (CAN/CSA, 2004a).

I_g = gross moment of inertia of the specimen

After first cracking, a neutral axis depth value, *c*, is assumed. The strain at the extreme compression, ε_x, is then calculated using similar triangles as:

$$\varepsilon_x = \phi c \qquad \text{[Eq. 4D-7]}$$

The distance between the extreme compression fibre and the location of the neutral axis was divided into n equal layers. The strain at mid-height of each layer, ε_i, was then calculated considering a linear strain relationship along the specimen depth as:

$$\varepsilon_i = \frac{\varepsilon_x}{c} d_i \qquad \text{[Eq. 4D-8]}$$

where d_i is equal to the distance from the neutral axis to mid-height of the i^{th} layer.

The compressive stress, f_{mi}, corresponding to the given strain at mid-height of each layer was obtained from the stress-strain response for the masonry prisms (refer to equations 4D-1 and 4D-2), as:

$$f_{mi} = f_m(\varepsilon_i) \qquad \text{[Eq. 4D-9]}$$

The overall compressive force, *C*, was then obtained as the sum of the compressive force developed at each layer, as:

$$C = \sum_{i=1}^{i=n} f_{mi} \frac{c}{n} b \qquad \text{[Eq. 4D-10]}$$

where *b* is equal to the wall splice specimen width.

The strain at the effective depth of the reinforcement, d_{eff}, was calculated from basic mechanics considering a linear strain profile, as:

$$\varepsilon_s = \frac{\varepsilon_x}{c}\left(d_{eff} - c\right) \qquad \text{[Eq. 4D-11]}$$

The tensile resistance of the reinforcement, T, was then calculated from the stress-strain profile for the reinforcing steel (refer to equations 4D-3, 4D-4 and 4D-5) and the cross-sectional area of the steel reinforcement, A_s, as follows:

$$T = A_s f_s(\varepsilon_s) \qquad \text{[Eq. 4D-12]}$$

The iterative program in MathCAD established the neutral axis depth such that a minimum difference of 0.5% existed between the values of C and T. The resisting moment for the cracked section was therefore calculated as:

$$M = \sum_{i=1}^{i=n}\left[f_{mi}\frac{c}{n}bd_i\right] + A_s f_s(\varepsilon_s)\left(d_{eff} - c\right) \qquad \text{[Eq. 4D-13]}$$

Figures 4D-1 to 4D-9 show the theoretical moment-curvature curves derived for each of the reinforcement configurations tested in the wall splice specimens. Figures 4D-1 to 4D-3 show the curves derived for the specimens with a 150 mm lap splice length, whereas Figures 4D-4 to 4D-6, and Figures 4D-7 to 4D-9 show the curves for the specimens with 200 and 250 mm lap splice length, respectively. Also shown in all figures, are the experimental curves for the three specimens within each set of replicates. As discussed in Section 4.4.4, the experimental moment-curvature curves were obtained from the load-deflection profiles of the wall splice specimens. In

general, good agreement was observed between the experimental and theoretically calculated moment-curvature profiles.

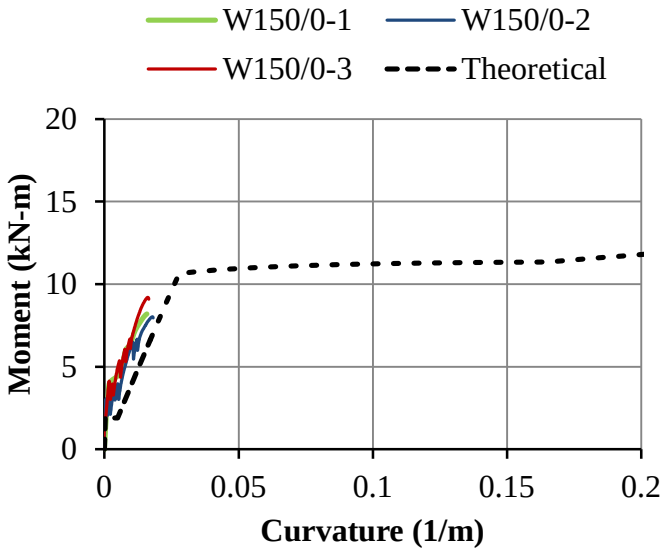

Figure 4D-1 Experimental and theoretical moment-curvature relationship – Specimens W150/0-1, W150/0-2, and W150/0-3.

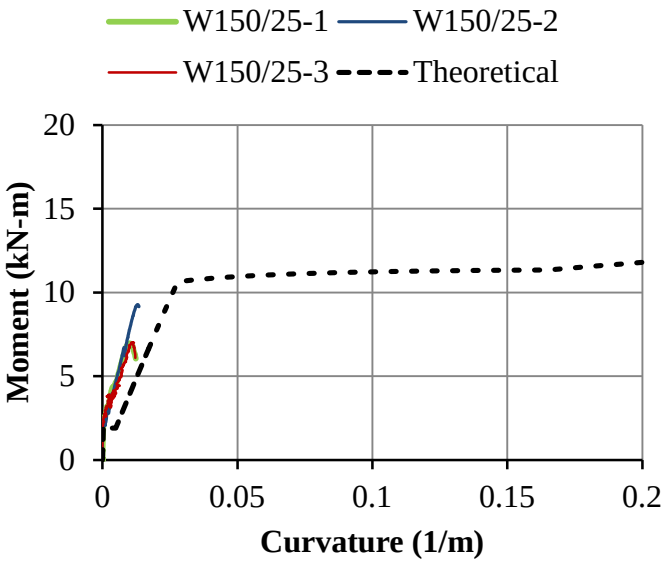

Figure 4D-2 Experimental and theoretical moment-curvature relationship – Specimens W150/25-1, W150/25-2, and W150/25-3.

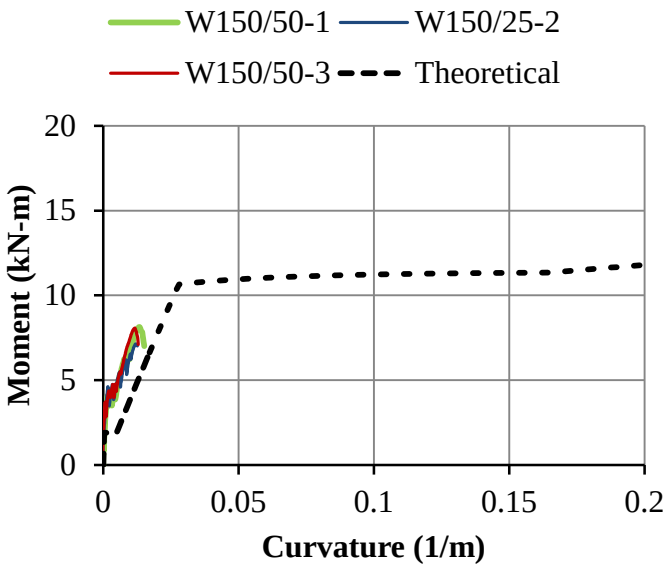

Figure 4D-3 Experimental and theoretical moment-curvature relationship – Specimens W150/50-1, W150/50-2, and W150/50-3.

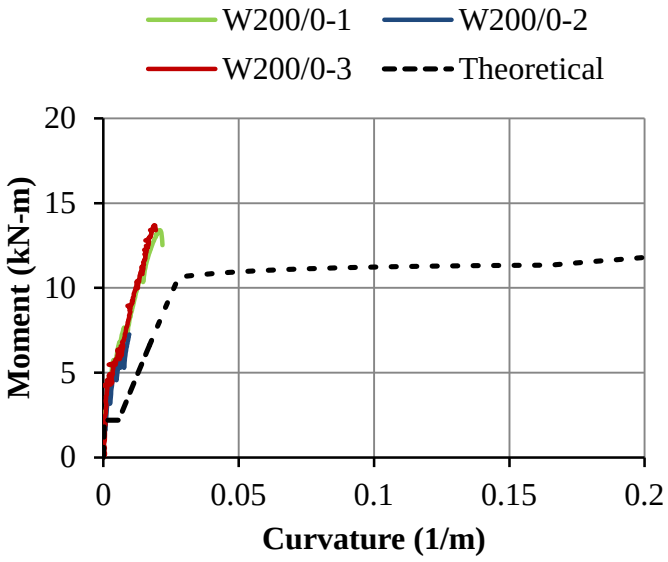

Figure 4D-4 Experimental and theoretical moment-curvature relationship – Specimens W200/0-1, W200/0-2, and W200/0-3.

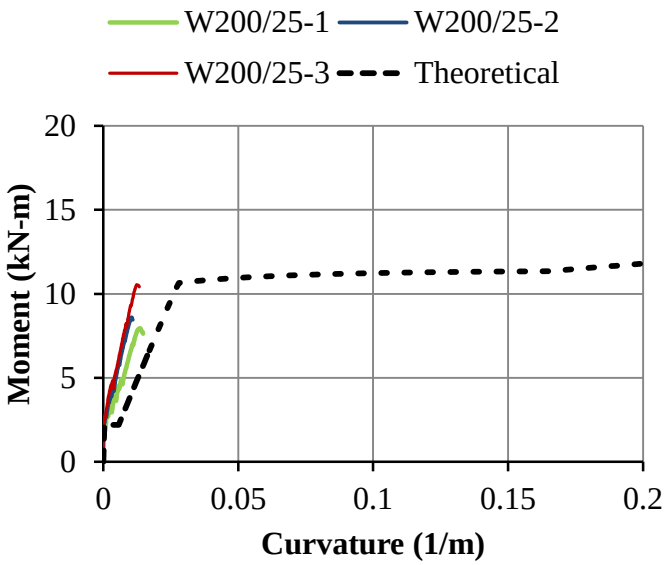

Figure 4D-5 Experimental and theoretical moment-curvature relationship – Specimens W200/25-1, W200/25-2, and W200/25-3.

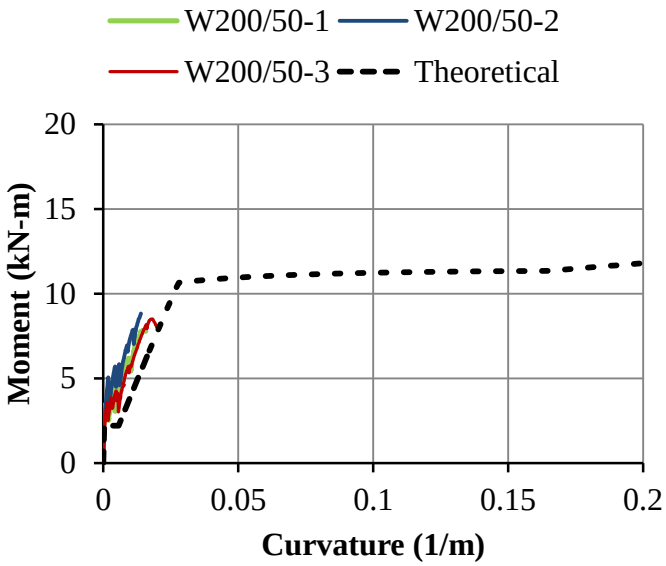

Figure 4D-6 Experimental and theoretical moment-curvature relationship – Specimens W200/50-1, W200/50-2, and W200/50-3.

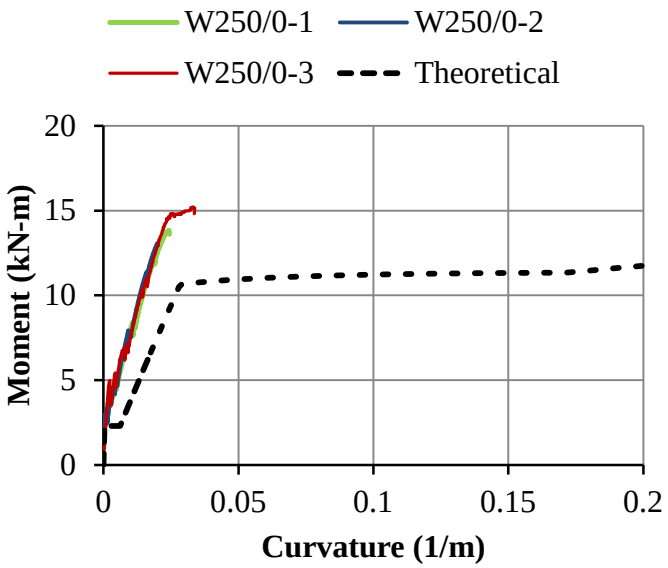

Figure 4D-7 Experimental and theoretical moment-curvature relationship – Specimens W200/0-1, W200/0-2, and W200/0-3.

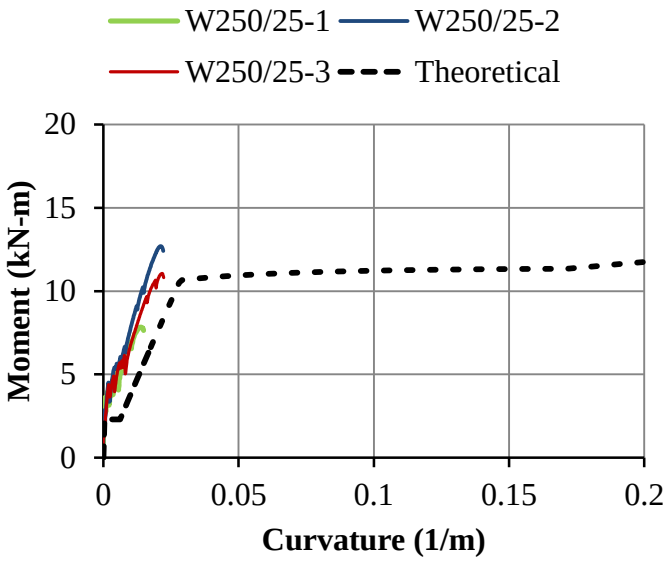

Figure 4D-8 Experimental and theoretical moment-curvature relationship – Specimens W200/25-1, W200/25-2, and W200/25-3.

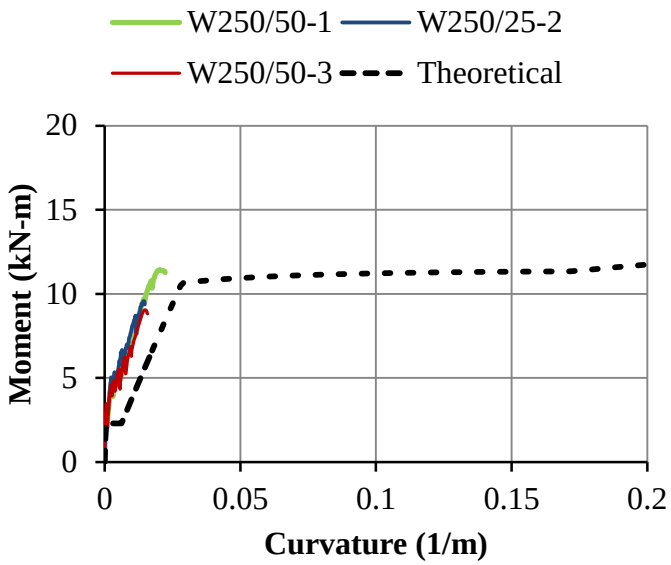

Figure 4D-9 Experimental and theoretical moment-curvature relationship – Specimens W200/50-1, W200/50-2, and W200/50-3.

MathCAD code

This section presents the MathCAD code used to perform the moment-curvature analysis of the wall splice specimens. The code used for the calculation of the tensile resistance of the reinforcement in the wall splice specimens is also presented. As discussed earlier, the tensile resistance of the reinforcement, *T*, was computed from the theoretically calculated curvature at maximum moment using the same sectional analysis. The mathematical expressions and MathCAD code are similar to those reported in Ahmed (2011).

Material properties:

$b := 990 \cdot mm$

$t := 190 \cdot mm$

$d_{eff} := 95 \cdot mm$

$A_s := 400 \cdot mm^2$

$fp_m := 12.5 \cdot \frac{N}{mm^2}$

$E_m := 850 \cdot fp_m$

$M_{cr} := 1.9 \cdot kN \cdot m$

$E_s := 174000 \cdot \frac{N}{mm^2}$

$\varepsilon_y := 0.00249$

$f_y := 434 \cdot MPa$

$\varepsilon_{sh} := 0.014$

$\varepsilon_{ult} := 0.1$

$f_{ult} := 611 \cdot MPa$

$E_{sh} := 5596 \cdot MPa$

Stress-strain relationship for the masonry assemblage:

$$Z := \frac{0.5}{\left(\frac{3 + 0.29 \cdot \frac{fp_m}{\frac{N}{mm^2}}}{145 \cdot \frac{fp_m}{\frac{N}{mm^2}} - 1000} \right) - 0.002} \qquad Z = 81.25$$

$$f_m(\varepsilon c) := \begin{cases} \left[fp_m \cdot \left[\frac{2 \cdot \varepsilon c}{0.002} - \left(\frac{\varepsilon c}{0.002} \right)^2 \right] \right] & \text{if } \varepsilon c \le 0.002 \\ \left[fp_m \cdot \left[1 - Z \cdot (\varepsilon c - 0.002) \right] \right] & \text{if } 0.002 < \varepsilon c \le 0.01 \\ 0 & \text{otherwise} \end{cases}$$

$$\varepsilon c := 0, 0.0001 .. 0.015$$

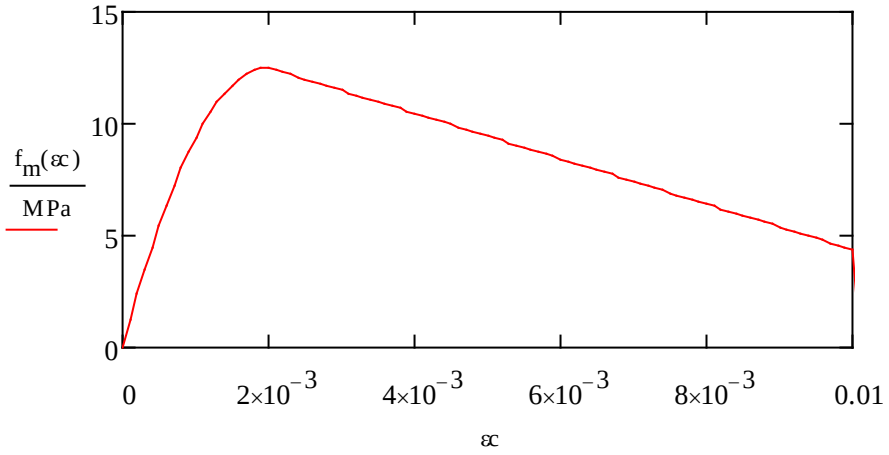

Stress-strain relationship for the reinforcing steel:

$$Cons := \begin{pmatrix} 1 & 0.014 & 0.000196 & 0.000002744 \\ 1 & 0.1 & 0.01 & 0.001 \\ 0 & 1 & 0.028 & 0.000588 \\ 0 & 1 & 0.2 & 0.03 \end{pmatrix}^{-1} \cdot \begin{pmatrix} 434 \\ 611 \\ 5596 \\ 0 \end{pmatrix}$$

$$Cons = \begin{pmatrix} 343.672 \\ 7.347 \times 10^3 \\ -6.675 \times 10^4 \\ 2.001 \times 10^5 \end{pmatrix}$$

$$CA := Cons_1$$
$$CB := Cons_2$$
$$CC := Cons_3$$
$$CD := Cons_4$$

$$f_s(\varepsilon s) := \begin{cases} \varepsilon s \cdot E_s \ \text{ if } \ 0 < \varepsilon s < \varepsilon_y \\ f_y \ \text{ if } \ \varepsilon_y < \varepsilon s \le \varepsilon_{ult} \\ \left[\left(CA + CB \cdot \varepsilon s + CC \cdot \varepsilon s^2 + CD \cdot \varepsilon s^3 \right) \cdot \frac{N}{mm^2} \right] \ \text{ if } \ \varepsilon_{sh} < \varepsilon s \le \varepsilon_{ult} \\ 0 \ \text{ otherwise} \end{cases}$$

$$\varepsilon s := 0, 0.001 .. 0.1$$

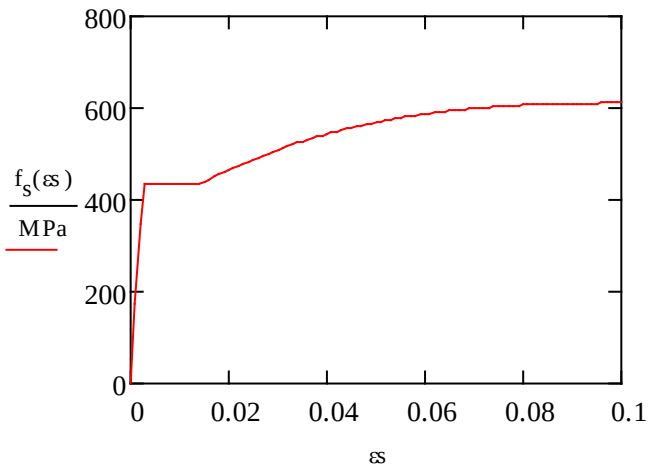

Moment corresponding to any curvature – cracked section:

$$
\begin{aligned}
&\text{MOMENT}(\phi) := \\
&\quad \text{for } p \in 60, 59.9 .. 10 \\
&\qquad c \leftarrow p \cdot 1 \cdot mm \\
&\qquad P \leftarrow 0N \\
&\qquad \varepsilon x \leftarrow c \cdot \phi \\
&\qquad \text{for } i \in 1 .. 100 \\
&\qquad\quad d_i \leftarrow \frac{c}{100} \cdot (i - 0.5) \\
&\qquad\quad \varepsilon_i \leftarrow \frac{\varepsilon x}{c} \cdot d_i \\
&\qquad\quad fm_i \leftarrow f_m(\varepsilon_i) \\
&\qquad \sigma_s \leftarrow f_s\left[\frac{\varepsilon x}{c} \cdot (d_{eff} - c)\right] \\
&\qquad C \leftarrow \left(\sum_{n=1}^{100} fm_n\right) \cdot b \cdot \frac{c}{100} \\
&\qquad T \leftarrow A_s \cdot \sigma_s \\
&\qquad NA \leftarrow c \text{ if } \frac{|C - T|}{T} \leq 0.005 \\
&\quad \varepsilon_{ef1} \leftarrow NA \cdot \phi \\
&\quad \text{for } i \in 1 .. 100 \\
&\qquad d_{ef_i} \leftarrow \frac{NA}{100} \cdot (i - 0.5) \\
&\qquad \varepsilon 1_i \leftarrow \frac{\varepsilon_{ef1}}{NA} \cdot d_{ef_i} \\
&\qquad fmef_i \leftarrow f_s(\varepsilon 1_i) \\
&\quad \varepsilon s \leftarrow \frac{\varepsilon_{ef1}}{NA} \cdot (d_{eff} - NA) \\
&\quad T \leftarrow A_s \cdot f_s(\varepsilon s) \\
&\quad C \leftarrow \left(\sum_{n=1}^{100} fmef_n\right) \cdot b \cdot \frac{NA}{100} \\
&\quad M_{tot} \leftarrow T \cdot \left[d_{eff} - NA + \left[\frac{\left[\sum_{n=1}^{100} \left(n \cdot d_{ef_n}\right)\right] \cdot b \cdot \frac{NA}{100}}{\left(\sum_{n=1}^{100} n\right) \cdot b \cdot \frac{NA}{100}} \right] \right] \\
&\quad M_{tot}
\end{aligned}
$$

Resulting moment database:

$$MOM := \left| \begin{array}{l} \text{for } n \in 1..500 \\ \quad \left| \begin{array}{l} curv \leftarrow (n-1)\cdot 0.001 \\ MOM_n \leftarrow MOMENT\left(\frac{curv}{m}\right) \end{array} \right. \\ MOM \end{array} \right.$$

$MOM =$

	1
1	0
2	0.402
3	0.805
4	1.205
5	1.603
6	2.004
7	…

$\cdot kN \cdot m$

Curvature database:

$$CURV := \left| \begin{array}{l} \text{for } n \in 1..500 \\ \quad curv_n \leftarrow (n-1)\cdot 0.001 \cdot \frac{1}{m} \\ curv \end{array} \right.$$

$CURV =$

	1
1	0
2	$1 \cdot 10^{-3}$
3	$2 \cdot 10^{-3}$
4	$3 \cdot 10^{-3}$
5	$4 \cdot 10^{-3}$
6	$5 \cdot 10^{-3}$
7	…

$\frac{1}{m}$

Curvature corresponding to any moment – cracked section:

$$
\begin{aligned}
&\text{CUR}(M1) := \left| \begin{array}{l}
m1 \leftarrow 0 \quad \text{if} \quad M1 = 0 \cdot kN \cdot m \\
\text{for} \quad n \in 1 .. 500 \\
\quad \text{if} \quad M1 < MOM_n \\
\quad\quad \left| \begin{array}{l}
curv1 \leftarrow CURV_n \\
curv2 \leftarrow CURV_{n-1} \\
mom1 \leftarrow MOM_n \\
mom2 \leftarrow MOM_{n-1} \\
m1 \leftarrow curv2 + \left(\dfrac{curv1 - curv2}{mom1 - mom2} \right) \cdot (M1 - mom2) \\
\text{break}
\end{array} \right. \\
m1 \cdot \dfrac{1}{m}
\end{array} \right.
\end{aligned}
$$

Curvature corresponding to any moment – un-cracked and cracked section:

$$
\begin{aligned}
&\text{cur2}(M) := \left| \begin{array}{l}
k \leftarrow \dfrac{M}{E_m \cdot I_g} \quad \text{if} \quad M < M_{cr} \\
k \leftarrow \text{CUR}\left(\dfrac{M}{kN \cdot m} \right) \quad \text{otherwise} \\
k
\end{array} \right.
\end{aligned}
$$

Calculation of the tensile resistance of the reinforcement corresponding to any curvature:

$$\phi := \frac{0.031}{m}$$

$$X := NA(\phi)$$

$NA(\phi) :=$ for $p \in 60, 59.9 .. 10$

- $P \leftarrow 0N$
- $c \leftarrow p \cdot 1 \cdot mm$
- $\varepsilon x \leftarrow c \cdot \phi$
- for $i \in 1 .. 100$
  - $d_i \leftarrow \frac{c}{100} \cdot (i - 0.5)$
  - $\varepsilon_i \leftarrow \frac{\varepsilon x}{100} \cdot i$
  - $fm_i \leftarrow f_m(\varepsilon_i)$
- $C \leftarrow \left(\sum_{n=1}^{100} fm_n \right) \cdot b \cdot \frac{c}{100}$
- $\varepsilon s \leftarrow \frac{\varepsilon x}{c} \cdot (d_{eff} - c)$
- $T \leftarrow A_s \cdot f_s(\varepsilon s)$
- $NA \leftarrow c \text{ if } \frac{|C - T|}{T} \leq 0.005$

NA

$TR(\phi) :=$

- $\varepsilon eft \leftarrow X \cdot \phi$
- for $i \in 1 .. 100$
  - $dt_i \leftarrow \frac{X}{100} \cdot (i - 0.5)$
  - $\varepsilon t_i \leftarrow \frac{\varepsilon eft}{100} \cdot i$
  - $fmt_i \leftarrow f_s(\varepsilon t_i)$
- $\varepsilon s \leftarrow \frac{\varepsilon eft}{X} \cdot (d_{eff} - X)$
- $T \leftarrow A_s \cdot f_s(\varepsilon s)$
- $TR \leftarrow T$
- TR

$$TREF := TR(\phi) = 141.539 \cdot kN$$

$$Tension := \frac{TREF}{2} = 70.769 \cdot kN$$

APPENDIX 4E

THEORETICAL LOAD VERSUS MIDSPAN DEFLECTION ANALYSIS

The theoretical load versus midspan deflection response for the wall splice specimens was derived using the conjugate beam method. According to this method, the deflection of a beam at any point is equal to the moment at the corresponding point in the conjugate beam. The loading acting on the conjugate beam is equal to the bending moment diagram of the actual beam divided by its flexural rigidity (i.e. equal to the curvature resulting from the actual applied load). An iterative sectional approach, which divided the specimen length into 240 equal segments, was used for the analysis. The resulting moment in each segment was calculated from basic mechanics, whereas an interpolation between the curvatures of the un-cracked and the cracked section was performed to calculate the effective curvature corresponding to each segment.

An equation for the effective curvature of the wall splice specimens was derived by Ahmed (2011) to consider the effect of the transition from the un-cracked to the cracked section properties, based on Bischoff's equation for the effective moment of inertia (Bischoff, 2005). The effective curvature, ϕ_{eff}, is given by:

$$\phi_{eff}=\phi_{cr}\left[1-\left(\frac{M_{cr}}{M_a}\right)^2\right]+\phi_g\left(\frac{M_{cr}}{M_a}\right)^2 \qquad \text{[Eq. 4E-1]}$$

where, ϕ_{cr} = the curvature of the cracked section as calculated from the theoretical moment-curvature relationship described in Appendix 4D

M_{cr} = the applied moment at first cracking calculated from the experimental cracking loads reported in Table 4.5

M_a = the applied moment

Φ_g = the curvature of the gross/uncracked section

The length of the wall, L, was divided into n segments each of a width equal to L/n. The moment M_i at the ith segment was calculated from basic mechanics, whereas the curvature corresponding to M_i was calculated using equation 4E-1. The midspan deflection was then given by:

$$\Delta_{mid} = \sum_{i=1}^{i=n} \frac{1}{4} \phi_i \frac{L^2}{n} - \sum_{i=1}^{i=\frac{n}{2}} \phi_i L_i \frac{L}{n} \qquad \text{[Eq. 4E-2]}$$

MathCAD code

Moment corresponding to any applied load:

$$ML(x,p) := \begin{cases} ML \leftarrow \frac{p}{2} \cdot x & \text{if } x < 800 \cdot mm \\ ML \leftarrow \frac{p}{2} \cdot 800 \cdot mm & \text{if } 800 \cdot mm \le x \le 1600mm \\ ML \leftarrow \frac{p}{2} \cdot 800mm - (x - 1600mm) \cdot \frac{p}{2} & \text{if } x > 1600mm \end{cases}$$

Deflection corresponding to any applied load at midspan:

$$\text{mdef}(x) := \left| \begin{array}{l} P \leftarrow x \\ \text{for } i \in 1..240 \\ \quad \left| \begin{array}{l} L_i \leftarrow i \cdot 10\text{mm} - 5\text{mm} \\ \text{moment} \leftarrow \text{ML}(L_i, P) \\ \phi_i \leftarrow \dfrac{\text{moment}}{E_m \cdot I_g} \quad \text{if} \quad \text{moment} \le M_{cr} \\ \phi_i \leftarrow \text{CUR}\left(\dfrac{\text{moment}}{\text{kN}\cdot\text{m}}\right) \cdot \left[1 - \left(\dfrac{M_{cr}}{\text{moment}}\right)^2\right] + \dfrac{\text{moment}}{E_m \cdot I_g} \cdot \left(\dfrac{M_{cr}}{\text{moment}}\right)^2 \quad \text{otherwise} \end{array} \right. \\ \text{midspandef} \leftarrow 10\text{mm} \cdot \sum_{n=1}^{120} \left(\phi_n \cdot L_n\right) \end{array} \right.$$

$P := 0\text{kN}, .25\text{kN} .. 43\text{kN}$

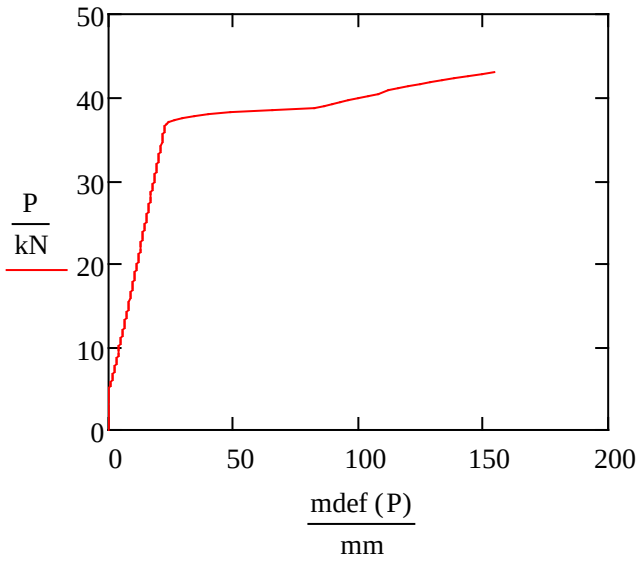

APPENDIX 4F

CALCULATION OF THE RESULTING LAP SPLICE LENGTHS IN ACCORDANCE WITH CSA S304.1 AND TMS 402-11

This section presents the mathematical expressions and input data used in the calculation of the required development length of the reinforcement for the wall splice specimens tested in this investigation in accordance with CSA S304.1 (CAN/CSA, 2004a), and TMS 402-11 (MSJC, 2011). As discussed in Section 4.4.6, the experimental results for the tensile resistance of the lap spliced bars were compared to the theoretically predicted tensile resistances calculated based upon the Canadian and the U.S. code provisions for the required development length of deformed bars in tension. A detailed description of the current provisions in both CSA S304.1 (CAN/CSA, 2004a) and TMS 402-11 (MSJC, 2011) is presented in Section 2.2.

Required lap splice length in accordance with CSA S304.1

The lap splice length, l_d, in accordance with CSA S304.1 provisions was calculated using Equation 2.3, as follows:

$$l_d = 0.45 k_1 k_2 k_3 \frac{f_y}{\sqrt{f'_{gr}}} d_b \qquad \text{[Eq. 2.3]}$$

where, k_1 = 1

k_2 = 1

k_3 = 0.8

f_y = 400 MPa

f'_{gr} = 18.4 and 16.2 MPa for Phases I and II, respectively, as reported in Table 4.6 for the companion absorptive masonry prisms

d_b = 15 mm

The resulting lap splice lengths in accordance with CSA S304.4 (CAN/CSA, 2004a) were therefore equal to 504 mm, and 537 mm for construction phases I and II, respectively.

Required lap splice length in accordance with TMS 402-11

Equation 2.5 was used to calculate the required lap splice length of the reinforcement, l_d, in accordance with TMS 402-11 (MSJC, 2011), as follows:

$$l_d = \frac{1.5 d_b^2 f_y \gamma}{K\sqrt{f'_m}} \qquad \text{[Eq. 2.5]}$$

where, d_b = 15 mm

f_y = 400 MPa

γ = 1

K = the clear cover to the reinforcement, equal to 87.5 mm

f'_m = the specified compressive strength of the masonry, equal to 10 MPa, in accordance with TMS 402-11 Specification for Masonry Structures (MSJC, 2011)

A lap splice length of 488 mm resulted for both construction phases when calculated in accordance with TMS 402-11 (MSJC, 2011).